PRODUCTION AND STABILISATION OF COPPER COLLOIDS

A thesis submitted for the degree of
Doctor of Philosophy of the
University of London and for the
Diploma of Membership of the
Imperial College

by

PAUL ANTHONY FRANCIS

Department of Mineral Resources Engineering
Royal School of Mines
Imperial College of Science, Technology and Medicine
London SW7 2BP

October, 1990

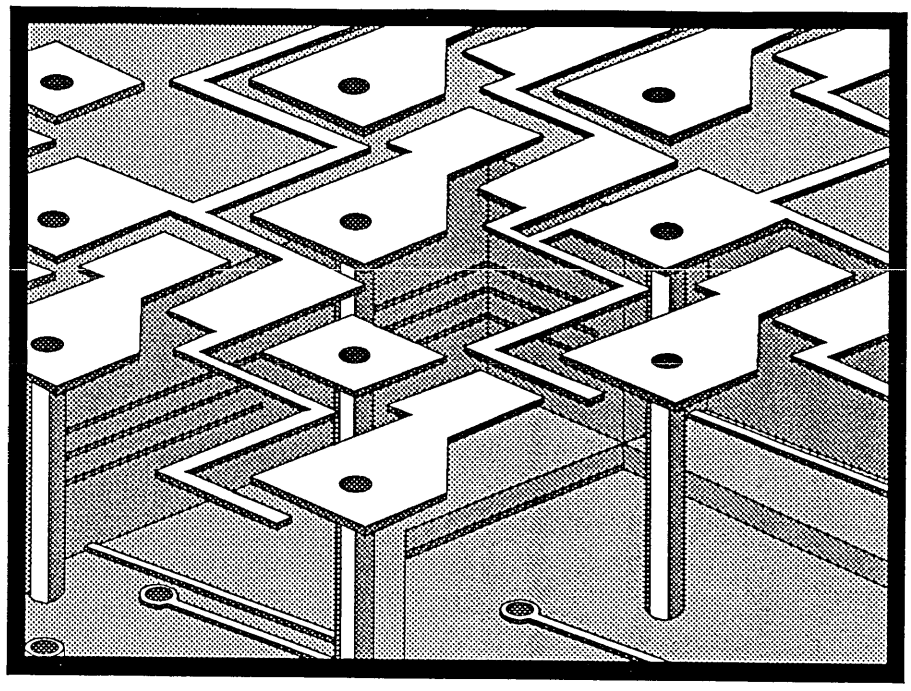

Cross section through a typical multi-layer printed circuit board.

This thesis is dedicated to my wife, Sally,
who encouraged me every step of the way.

"I mean, yes idealism, yes the dignity of pure research, yes the pursuit of truth in all its forms, but there comes a point where you begin to suspect that if there is any *real* truth, its that the entire universe is almost certainly being run by a bunch of maniacs; and if it comes to a choice between spending *another* ten million years finding that out or taking the money and running, then I for one could do with the exercise."

Frankie Mouse,
Hitchiker's Guide to the Galaxy - The Original Radio Scripts
Douglas Adams

ABSTRACT

This thesis contains details of the production and stabilisation of copper colloids as used in the electroplating industry. In their adsorbed form, copper colloidal particles act as nucleation sites and catalytic centres for reductant oxidation in the electroless plating of drill holes in both double-sided and multi-layer printed circuit boards, prior to their being plated electrolytically.

Voltammetry indicated that oxidation of the proprietary reductant was very slow, although production of the initial *ca.* 1 nm palladium particles, which catalysed subsequent copper growth to *ca.* 5 nm particles, was fast. The feasibility was demonstrated of metallising drill hole surfaces directly, i.e. by using an aqueous regenerative reductant such as the Cr(II)/Cr(III) couple to reduce Cu(II). However, the oxidation of such a reductant on the copper surfaces of printed circuit boards would cause copper deposition both there and on the drill hole surfaces. The stability of the colloid, as measured by particle size increase determined by PCS, was found to be sensitive to atmospheric oxygen.

The copper colloid was stabilised by gelatin which completely sheaths the particle so that it responds as a gelatin particle, thus the gelatin structure and stability was found to be one of the most important parameters in stabilising the colloid.

It was found by rotating ring-disc voltammetry that the formation of hydrogen peroxide from the reduction of oxygen at the copper surface was responsible for the destruction of the stabilising power of gelatin, and this was confirmed by the storing of the colloid under nitrogen which prolonged colloid stability.

ACKNOWLEDGEMENTS

I would like to take this opportunity to thank all those who helped me with my thesis over the last three years, especially Dr. G. H. Kelsall, my supervisor, for his invaluable support, and Dr. M. Goodenough, my industrial supervisor and the sponsoring company, Lea Ronal (UK) Ltd for their assistance.

I would also like to thank members of my research group, past and present, including Colin for the diagrams and use of his fax machine, Frank for his philosophical insights and carrot cake, Dave M. and Sam for their cheerful outlook, Paul D. for his infectious enthusiasm, Ying Yang, Li Chun and Liang for the Chinese perspective, Biodun for the removals, Dave R., Nick, Mohammed, Francis and Ian.

Finally I would like to thank other friends and family, for their unfailing love and support.

Oh, yes, and BJ.

NOMENCLATURE

Conventional symbols for the disciplines of electrochemistry and colloid science are used wherever possible. The list below defines the major symbols and their units.

a	Particle radius, nm	U	Velocity, m s^{-1}
A	Area, m^2	U_{ef}	Electrophoretic mobility, $m^2 s^{-1} V^{-1}$
A^*	Effective Hamaker constant, J		
C or c	Concentration, mol m^{-3}	U_Q	Electrophoretic velocity, m s^{-1}
d	Particle diameter, nm	V_A	Attraction energy, J
D	Diffusion coefficient, $cm^2 s^{-1}$	V_m	Molar volume, m^3 mol^{-1}
e	Elementary charge,	V_R	Repulsive energy, J
	1.60219×10^{-19} C	z	Valency
E	Electric field, V m^{-1}	χ	Adsorption/orientation
E	Redox potential, V		potential, V
E^0	Standard redox potential, V	ϕ	Adsorption energy, J
F	Faraday constant, 96485 C mol^{-1}	ν_v	Characteristic frequency, Hz
h	Planck's constant,	σ	Charge density, A m^{-2}
	6.626×10^{-34} J s	$1/\kappa$	Debye length, nm
H_0	Minimum distance of separation	ε	Dielectric constant, $J^{-1} C^2 m^{-1}$
	between two particles, nm	ν	Kinematic viscosity, $cm^2 s^{-1}$
i_L	Diffusion limiting current, A	λ	Wavelength, nm
k	Boltzman constant,	ψ	Potential, V
	1.3805×10^{-23} J K^{-1}	κ	Double layer thickness, nm
MM	Molar mass, g	ω	Rotation rate, s^{-1}
N_I	Particle number concentration	ϕ_β	Self-atmosphere potential, V
N_A	Avagadro's constant,	σ	Surface charge density, C m^{-2}
	6.02205×10^{23} mol^{-1}	ψ	Surface potential, V
pzc	Point of zero charge, pH	γ	Surface tension, J m^{-2}
Q	Charge, C	ε_0	Vacuum permittivity, 8.85419×10^{-12} $J^{-1} C^2 m^{-1}$
R	Gas constant, 8.31441 J K^{-1} mol^{-1}		
S.H.E.	Standard hydrogen electrode	ϕ	van der Waals term for adsorption energy, J
T	Temperature, K		
$t_{1/2}$	Half life, s	η	Viscosity, kg $m^{-1} s^{-1}$
		ζ	Zeta potential, V

CONTENTS

LIST OF TABLES

LIST OF FIGURES

CHAPTER 1. INTRODUCTION

1.1. Background

Double-sided and multilayer printed circuit boards (PCBs) require a continuous conducting layer to connect the sides or layers of the board through holes used to seat components. After laminating of the surface of the board with copper, these through-holes are drilled exposing non-conducting glass fibre/epoxy surfaces that require subsequent plating. In the PCB industry, a catalyst is used to act as a nucleation/copper reduction site in the subsequent electroless plating step. These catalysts are usually colloidal particles of Pd/Sn or copper, the latter being the less expensive option. The copper colloid is sold to PCB manufacturers as a colloidal concentrate that is diluted and pH adjusted for use. As the colloid is not used immediately after it is made, and will usually require a shelf-life whilst held in stock, stability of the colloid is of vital importance. At present, copper colloids have a shelf life of about 3 months, which is insufficient as they are made in Europe and often shipped to the Far East for use.

1.2. Copper Colloid System

Colloids consist of a continuous phase, the *dispersion medium*, containing a *dispersed phase* [1], which has one or more of the components with at least one dimension within the size range 1 nm to 1 μm. Particles of this size are thermodynamically unstable to remaining dispersed due to their high surface energy, but may be rendered kinetically stable by electrostatic and/or steric (i.e. by the use of adsorbed macromolecules) means. Copper colloids used in the PCB industry are aqueous dispersions of copper metal particles with diameters of order 5 nm, equivalent to some 5000 atoms. At high copper concentrations (about 5 g Cu dm^{-3}), the colloids are stabilised by gelatin. However, as mentioned before, gelatin is not sufficiently robust to confer long term stability (> 6 months), particularly at higher ambient temperatures.

1.3. Application of Copper Colloids to Electroless Plating

Electroless copper plating is very important in PCB manufacturing. It is the preferred technique for plating through-holes between the different layers of a multilayer board or

the sides of a double-sided board [2]. In a manufacturing process, colloidal copper particles adsorb onto the surface of the holes and act as nucleation and catalytic centres for reductant oxidation in the electroless copper plating process prior to electrolytic copper plating [3]. Complete and uniform coverage of the drill holes in PCBs by the colloidal copper particles is essential for application of a strong and impermeable electrolytic over-plate to prevent the evolution of gas during soldering; moisture in the epoxy resin of the PCB volatilises when the board is heated during wave-soldering. The high pressures associated with the gas evolved can cause blow-holes in the copper plate, allowing the ingress of gas into the molten solder, which affects its quality and hence the reliability of the electronic assembly [4].

1.4. The Current Process for the Electroplating of Drill Holes

In an existing copper colloid manufacturing process [5], copper sulphate solutions are reduced by dimethylaminoborane (DMAB) in the presence of Pd(II) ions, the more facile reduction of which provides the primary nuclei on which the copper then grows:

$$Pd^{2+} + 2e \rightarrow Pd$$

$$Me_2NHBH_3 + 3H_2O \rightarrow H_3BO_3 + 5H^+ + Me_2NH_2^+ + 6e$$

$$Cu^{2+} + 2e \rightarrow Cu$$

The reaction is carried out in the presence of gelatin, which stabilises the resulting copper particles by forming a sheath around the metal core with a hydrodynamic diameter of about 100 nm. After 24 hours, the less powerful reducing agent hydrazine is added,

$$H_2NNH_2 \rightarrow N_2 + 4H^+ + 4e$$

producing further copper growth, but probably no new nuclei. The pH is then about 8, with a copper concentration of about 5 g Cu dm^{-3}.

In the present process, gelatin has two functions, both of which are achieved only partially; firstly, the gelatin has to stabilise the dispersion over its shelf life (about 12 months minimum), and secondly, it has to deposit the particles onto the surface of the hole which is about 70 % silica. To allow deposition, the pH of the colloid is adjusted to about 3.5, at which the gelatin-coated particle is positively charged, whilst the silica is negatively charged, thus enabling electrostatic adsorption. However, bonding can take place at higher pH values, even above the iso-electric point of the gelatin, suggesting that additional

adsorption mechanisms, e.g., hydrogen bonding, are involved. After deposition, residual gelatin is removed by two cold washes, as residual high molecular weight material causes poor adhesion of copper layers subsequently deposited.

After further treatment with warm hydrazine at pH 6 to reduce adventitious dissolved oxygen and surface oxide, copper is deposited electrolessly from an EDTA solution, using formaldehyde as the reductant [6]:

$$[CuEDTA]^{2-} + 2HCHO + 4OH^{-} \rightarrow Cu + 2HCOO^{-} + H_2 + 2H_2O + EDTA^{4-}$$

After application of a resist mask, 25 μm of copper are electrodeposited from an acid copper sulphate bath, followed by 12 μm of a tin/lead alloy electrodeposited from a fluoroborate solution.

1.5. Objectives

The project had two main objectives:

1) To investigate the current production method of copper colloids in order to research alternatives to the expensive Pd/DMAB route. This objective was carried out in two ways; a) the Pd/DMAB reduction process was examined and b) other alternative reductants were investigated, including regenerative aqueous reductants.
2) To investigate the stability of copper colloids and increase their life-span by a) studying the mechanisms of stabilisation and failure of the presently-used gelatin system, and b) investigating alternative steric stabilisers.

CHAPTER 2. LITERATURE REVIEW

2.1. Production and Stabilisation of Copper Colloids

A solid can be dispersed in a liquid to form a sol or colloid either by *degradation* of the bulk material or *aggregation* of the molecules or ions of the material.

Degradation by grinding does not lead to extensive distribution of solids as the smaller particles tend to reunite under the mechanical forces involved, hence prolonged milling leads to an equilibrium in particle size.

The aggregation method is a better method of particle dispersion that involves either precipitation from a supersaturated solution e.g., cooling or seeding, or chemical reaction, e.g., reduction to form a solid phase.

The first step in the aggregation method is the formation of a new phase, which involves two distinct stages - *nucleation* and *growth*. It is the relative rates of these processes that determine the particle size of the precipitate formed, i.e., smaller, more monodispersed particles are obtained when the rate of nucleation is high and the rate of crystal growth is low.

Monodispersity of the colloid is very important as the probability of collision of particles is enhanced in polydisperse systems, which leads to destabilisation of the system [7]. Production of a monodispersed sol can sometimes be achieved by seeding a supersaturated solution with very small particles or another condition that leads to a short burst of nucleation.

Monodispersions of silver halide sols were formed by cooling hot saturated aqueous solutions of silver halide and by diluting aqueous solutions of the complexes formed in the presence of excess silver or halide ions [8]. In both cases, the concentration of the material of the dispersed phase slowly passed the saturation point and attained a degree of supersaturation at which nucleation became appreciable. After the initial outburst of nucleation and the accompanying relief of supersaturation, very few new nuclei were formed and so the particles then grew uniformly from the nuclei by a diffusion controlled process and a monodispersed sol was formed.

The present Lea Ronal copper colloid batch manufacturing process [9] requires the presence of palladium particles to catalyse the rate of copper reduction and to act as sites for copper particle formation. Palladium ions are used as they are readily reducible [10], but the use

of this material is costly. However, recent Japanese patents [11][12][13][14][15] refer to a process where no catalyst was used, but the reduction rate was enhanced by heating the solution to 70 °C and aging for a certain time. The colloid was supported by gelatin and poly(ethylene)glycol, PEG (MM = 1000 - 100,000). The amount of gelatin added (10 g gelatin dm^{-3}) was five times that used in the Lea Ronal process, and an additional 50 g PEG dm^{-3} was used. Increasing the gelatin concentration is known to increase the stability of copper colloids, but prevents successful deposition. No mention was made of how long it took to form the colloid, the size of the resulting copper particles or the continuity of the subsequent electroless layer after deposition.

Copper colloids produced for the study of surface-enhanced Raman scattering (SERS) were prepared from $CuSO_4$ solutions using sodium borohydride as a reductant and trisodium citrate as a stabiliser [16]. The results of this work and a summary of others are listed in **Appendix A**. Excess borohydride was used to prevent the oxidation of the copper particles and the solution was prepared at high pH to prevent oxidation of the excess borohydride ions by water. The colloids were stable for only about 24 hours in stoppered cells. Measurement of Raman scattering after the addition of pyridine showed the formation of Cu-N bonds and the sol flocculated at concentrations > 0.1 mol m^{-3} pyridine. Samples of the colloids were sized using transmission electron microscopy (TEM) but the images were poor, possibly due to oxidation by air on drying. Dynamic light scattering indicated hydrodynamic particle diameters of about 5 nm, with some aggregated particles of characteristic dimension 25 - 30 nm. The copper concentration of the dispersion was 0.25 g dm^{-3}, and the pH was high, indicating that the zeta potential would be large and negative. This allows an estimate of the potential energy profile of the system, which is plotted below.

Figure 2.1.1. The effect of zeta potential (mV) on the total potential energy of overlapping double layers of two spherical copper colloid particles. T = 298 K, a = 2.5 nm, concentration = 20 mol m^{-3}.

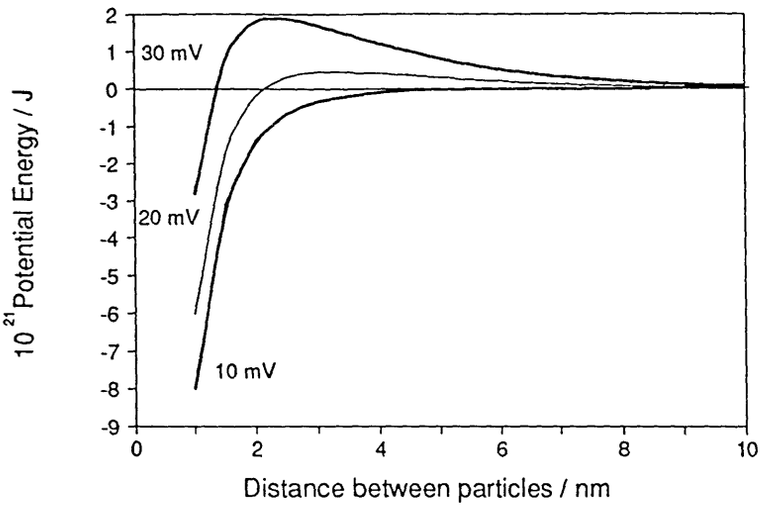

Citrate ions impart stability by adsorbing on the copper to give an increased negative potential. The diagram shows that the colloid is likely to be stabilised electrostatically, even without the presence of citrate.

Hirai *et al.* investigated the formation of stable metal colloids for use as catalysts in the hydrogenation of cyclohexane from several of the transition metals [17]. Rhodium, palladium, osmium, iridium and platinum colloids were prepared successfully by refluxing the metal salts with various alcohols in the presence of vinyl polymers with polar groups, as stabilisers. Reduction did not occur in the presence of polyethyleneimine, gelatin and gum arabic. Poly (vinyl alcohol) was thought to co-ordinate with the Rh(III) ion prior to its reduction with methanol and it is possible that the polymers mentioned above co-ordinate so strongly with Rh(III) via chelation that reduction by alcohols was impossible. Iron(III), cobalt(II), nickel(II) and copper(II) ions were irreducible with methanol, which was thought to be due to the lower standard potential of the first series transition metal ions compared to those of the second and third series.

The production and stabilisation of copper colloids for use as a catalyst in the selective hydration of acrylonitrile to acrylamide was studied by Hirai *et al.* [18][19]. Sodium borohydride was used as a reductant and the sol was stabilised with

poly(*N*-vinyl-2-pyrrolidone). No information on the stability half-life or particle size was given. The sols contained 1.25 g copper dm^{-3}, i.e., 25 % of the copper concentration of the Lea Ronal colloid.

The effect of a large range of protective polymers on the stability of copper colloids was investigated by the same authors in a more recent paper [20]. Stable colloidal copper dispersions were prepared successfully using the following polymers as steric stabilisers; poly(*N*-vinyl-2-pyrrolidone) PVP, poly(vinyl alcohol), poly(methyl vinyl ether), poly(potassium vinyl sulphate), dextrin, amylopectin, methylamylopectin, methylcellulose, ethylcellulose and (2-hydroxyethyl)cellulose. The colloidal dispersion with PVP was stable for over three months provided that it was kept under nitrogen; on contact with air it oxidised in a few minutes. In the absence of any protective polymer, precipitation took place immediately on addition of sodium borohydride to copper sulphate. Copper dispersions were precipitated after a few minutes in the presence of poly(ethylene oxide), PEO and β-cyclodextrin. No reduction occurred in the presence of poly(acrylic acid), poly(2-acrylamido-2-methyl-1-propanesulphonic acid) or the co-polymer of methyl vinyl ether and maleic acid. Poly(aminoethylene) and soluble nylon formed gels in aqueous solutions of copper sulphate.

Most of the polymers used gave stable colloids, but the concentration of copper in these sols was much lower (0.025 g dm^{-3}) than that of commercial copper colloids (5 g dm^{-3}) and it is easier to stabilise colloids at these lower concentrations, due to the increased effect of electrostatic repulsion between particles. The polymers that worked contained *N*-substituted amide, alcoholic, ethereal or sulphate groups in their side chains suggesting the necessity of forming complexes with positively charged Cu(II) ions prior to reduction. Steric factors may be important for the two polymers that gave precipitates. β-cyclodextrin, with a diameter of less than 1 nm, was probably not large enough to prevent the close approach of particles causing agglomeration, and PEO, although large, has its alkoxy groups in the main polymer chain (unlike poly(methyl vinyl ether), which worked) so that steric hindrance may have prevented bond formation. A critical factor that was not examined in any great detail in the paper was the effect of polymer concentration, which, when low, may agglomerate particles by bridging flocculation. A common feature of the polymers in the presence of which no reduction took place was the large proportion of acid groups in side chains. These might form stable bonds with Cu(II) ions that prevent reduction. Hirai *et al.* [20] suggest that no copper is reduced in these cases because sodium

borohydride is mostly involved with oxidation by protons. This seems unlikely as commercial electroless plating baths, using sodium borohydride, are known to operate at low pH.

Besides copper sulphate, copper chloride, copper acetate and copper nitrate were also reduced to form colloidal dispersions. The dispersion formed from copper nitrate was rather unstable and gradually oxidised, even under nitrogen, which was most likely due to the reduction of the nitrate ion to the ammonium ion via a series of intermediates, catalysed by the copper metal.

Several reducing agents were tried by Hirai *et al.* [20], but of these, only the addition of sodium borohydride and hydrazine to copper sulphate formed colloidal copper dispersions. Colloids formed using hydrazine had particles that were generally larger in diameter (20 - 160 nm) than those formed using borohydride (2 - 19 nm). Particle diameters were measured using electron microscopy. Refluxing of copper chloride in an alkaline 1:1 methanol - water mixture formed a small amount of brown precipitate, indicating that Cu(II) was only partially reduced. Formaldehyde added to copper sulphate formed a gel and neither refluxing in ethanol nor the action of hydrogen at 3.7 MPa and 80 °C for 20 hours reduced copper sulphate solutions. It is possible that the formaldehyde had the effect of reducing PVP, opening up the pyrolidone rings, and thus forming the cross-linking that led to gelation. It appears that the main factors in selecting a suitable reducing agent are a suitably low redox potential and the lack of formation of stable intermediates.

Hirai *et al.* [20] found that increasing the relative concentration of PVP to copper sulphate decreased the diameter of the resultant colloid, giving further evidence that PVP acts as a Cu(II) ion ligand prior to reduction. They also suggested that as the viscosity of the solution increased, the mass transport rate of Cu(II) ions to be reduced at the surface of nuclei decreased, which would result in fewer, smaller particles. In addition to this, but not mentioned, was the effect of the viscosity on the agglomeration of particles. The particle diameter was seen to increase as the degree of polymerisation of PVP increased, which would tend to support their former hypothesis, in that a larger molecule would have more Cu(II) ions associated with it which would tend to form the same particle, despite the increased viscosity.

Electron diffraction patterns of the copper particles formed were virtually identical with those obtained for a pure crystal of bulk copper metal, which suggests that a metallic copper particle is a good model of the nature of the dispersed phase in this system, i.e., the particles

are not merely an aggregate of copper atoms but exhibit face-centered cubic packing. Also, clear spectrographic absorbance peaks were observed at 570 nm for the copper colloid solutions, which were attributed to excitation of surface plasmons of copper particles.

'Unprotected' copper sols (1.2 mol m^{-3} Cu) were prepared by Curtis *et al.* [21] by the reduction of copper(II) acetate monohydrate with hydrazine hydrate in methanol, ethanol and propan-2-ol, boiled under reflux for 2 hours under a nitrogen atmosphere. The term 'unprotected' is used by Curtis *et al.* to indicate that no steric stabilisers are used; at the concentration of copper used, and the size of particles observed, it is evident that electrostatic stabilisation takes place. Upon addition of hydrazine, the copper(II) solution turned yellow-orange and eventually darkened to deep red in the space of 10 to 20 s. The red colour persisted until the colloid was exposed to air at which point the colour turns almost immediately brown and then dark green. Prolonged exposure to air resulted in a pale blue-green copper(II) solution with no evidence of particulate matter. Transmission Electron Microscopy (TEM) revealed that the mean particle size of 13.5 nm in the original solution with a range of diameters from 3 to 30 nm. Curtis *et al.* claimed that these figures could be lowered to 7.5, and 3 to 15 nm respectively if smaller volumes of solution were used, which they concluded gave more efficient mixing.

Optical spectroscopy of the colloid showed an absorption peak at 560 nm that shifted to 640 nm, with increased absorption, on exposure of the colloid to air. TEM showed the dark green solution formed on exposure of the colloid to air to consist of aggregates of particles, possibly with some evidence of surface coating of copper(I) oxide. The aggregation of the particles on exposure to air was thought to be due to the depletion of the negative ζ-potential by surface oxidation.

Copper colloids were manufactured and used as catalysts for hydrogen evolution from water by Savinova *et al.* [22]. The colloids were prepared under argon by the reduction of various copper compounds using a variety of reductants and steric stabilisers. The methods used are described below and summarised in **Appendix A.**

The colloids, in decreasing order of stability and monodispersity, were formed by the reduction of a copper-2,9-dimethylphenanthroline complex ($Cu(DMP)_2Cl_2$) > $CuSO_4$ > copper-ethylenediamine complex ($Cu(en)_2SO_4$) > $Cu(HCOO)_2$ > $Cu(CH_3COO)_2$. However, in all these cases, no stable colloid could be made with a concentration > 0.05 g Cu dm^{-3} due to coagulation.

The authors suggest that the size of the resulting particles in a copper colloid was dependent on the starting copper salt in the following way. A copper complex in solution can dissociate to some extent from its ligand, L, and the resultant Cu(II) ion can then hydrolyse and form further polynuclear hydroxy complexes:

$$Cu(II)L_n + nH_2O \Leftrightarrow Cu(II)(H_2O)_n + nL \quad (1)$$

$$Cu(II)(H_2O)_n \Leftrightarrow Cu(II)(OH)(H_2O)_{n-1} + H^+ \quad (2)$$

$$Cu(II)(OH)(H_2O)_{n-1} \rightarrow \text{complete hydrolysis product} \quad (3)$$

The shift of equilibria (1) and (2) to the right is determined both by their stability constants and the acidity of the ligand (due to the equilibrium $L + H^+ \Leftrightarrow LH^+$). The lower the pH of solution, the smaller is the extent of hydrolysis of the copper ions. The degree of hydrolysis increases in the order $CuSO_4 > Cu(HCOO)_2 > Cu(CH_3COO)_2$ and although there was some correlation with the increasing polydispersity of the colloids obtained, it did not correlate exactly with the increasing dissociation constants for these three compounds. The rate of electron transfer, and it was suggested, the rate of nucleation also, are high for complexes with ligands bound to the metal ion via a π-dative bond, such as phenanthroline and aquo complexes, whereas it is low for complexes with relatively inert ligands such as ethylenediamine [23]. This hypothesis was not confirmed convincingly by the result that the particles formed had diameters 3 ± 0.9 nm and 3 ± 1.4 nm when $Cu(DMP)_2Cl_2$ and $CuSO_4$ respectively were used and the particles that formed from the reduction of $Cu(en)_2SO_4$ were 5 ± 0.4 nm, only 2 nm larger. Another possibility during the reduction of $Cu(DMP)_2^{2+}$ ions is the formation of an intermediate complex with Cu(I), with an optical absorption of $\lambda_{MAX} = 455$ nm, which was observed in the colloid solution. It was suggested that the reduction of $Cu(DMP)_2^{2+}$ ions may also form charged copper clusters with DMP molecules co-ordinated on their surface, rather than true metal colloids, but this is unlikely from the evidence of the electron diffraction patterns.

The electric charge on the reductant ion was found to exert a large influence on the subsequent colloid formed. The smaller, monodispersed, stable colloids were formed using reductants of an anionic nature, BH^{4-} and $[SiW_{12}O_{40}]^{5-}$ whereas the cationic reductants, V^{2+} and methylviololgen, $MV^{+\cdot}$ gave polydisperse colloids with particles > 500 nm. These results were linked to the idea of faster electron transfer from anions that are coloumbically attracted to the Cu(II) cation, thus giving a higher nucleation rate. BH_4^- ions gave 2 to 4 nm particles, compared to 8 to 25 nm particles for $[SiW_{12}O_{40}]^{5-}$, which was either the result of the more negative reduction potential of BH_4^- or due to a different reduction mechanism.

It was suggested that slightly smaller colloids of 2 nm could be formed if the mixing rate was increased, although due to the reaction times involved for the formation of copper nuclei, this seems unlikely. Colloids formed were more monodisperse at 0.025 g Cu(II) dm^{-3} when using BH_4^- ions and 0.01 g Cu(II) dm^{-3} when using $[SiW_{12}O_{40}]^{5-}$ ions. At lower concentrations of Cu(II), there was an increase in the fraction of large particles, suggesting there was an optimum concentration for nuclei formation and subsequent growth. The authors do not mention the pH of the solutions used, but presumably the change in ionic concentration might also have some effect on colloid particle size.

The stabilisers used were poly (vinyl alcohol), PVA (MM = 25000) and poly (vinyl pyrrolidone), PVP (MM = 25000), both of which were used successfully by Hirai *et al.* [20]. Poly (acrylamide), PAA (MM = 4×10^7) was also used, but no reduction occurred. A similar result was found with poly(acrylic acid). Poly(ethylene)glycol, PEG (MM = 2000) was tried, but copper was precipitated. Two factors were thought to be important; the type and molar mass of the polymer. It is likely that the PAA forms a stable complex with Cu^{2+} ions that is thermodynamically or kinetically irreducible. The PEG does not have a side group and so it is likely that it is sterically hindered from forming a stable bond with Cu^0, thus not imparting stability, or that as it is not as polar as the other polymers, its stabilising nature is not as effective. The optimal molar ratio of polymer to Cu^{2+} was *ca.* 20. This ratio was used by Hirai *et al.* [20], although they found that increasing the relative concentration of polymer decreased particle size.

The colloids formed were studied by electron microscopy to measure particle size and were shown generally to be ellipsoid to spherical in form. The size of the particles was found to vary with the nature and concentration of reagents in the range 2 - 500 nm. Colloids of particle size < 4 nm were found to have a golden yellow colour that changed to bright purple with increasing size. Colloids with particle sizes > 100 nm were not coloured and scattered light strongly. The change in colour was ascribed to either a change in the diffraction of light or due to the spatial constriction of electrons in smaller particles allowing interband transitions. However, in this range of particle sizes, differences may also be due to the light scattering changing from obeying the Raleigh Law [24] when $r < \lambda/10$ (r = particle radius) to obeying Mie theory [25]. The theory of light scattering by colloids has been extensively described by Kerker [26]. Electron diffraction showed the lattice spacings in all particles were almost identical and corresponded to those in bulk copper crystal, confirming the results of Hirai *et al.* [20].

All colloids were manufactured under an argon atmosphere; exposure to air oxidised the particles within minutes. Oxidation was observed from changes in the optical adsorption spectra of a colloid (particle size 8 to 25 nm), upon contact with air, a peak at $\lambda = 570$ nm gradually disappeared. It was found that all colloids made had a peak in the region 570 - 590 nm. Mie theory predicts a λ_{MAX} of 567 nm for a 40 nm particle and a λ_{MAX} of 586 nm for a 50 nm particle [27]. Clearly, there was no "characteristic" peak, absorption depends on particle size and concentration, but the presence of a peak indicated an unoxidised colloid. These results confirm the work of Hirai *et al.* [20], who found clear spectrophotometric absorbance peaks at 570 nm for copper colloid solutions, which they attributed to excitation of surface plasmons of copper particles. Papavassiliou and Kokkinakis [28] found a clear adsorption peak at 580 nm (2.1 eV) for the optical adsorption spectra of copper particles. Their colloids were produced by the addition of hydrazine to a $CuSO_4$/gelatin solution at 80 °C. The result was a turbid solution that had to be centrifuged to produce a clear solution for absorbance work. They found a slight shift (0.8 to 0.9 nm) to higher absorbance peaks for higher concentrations of gelatin. If the colloid was exposed to air, there was a peak shift to longer wavelengths which was thought to be due to air oxidation of Cu^0 to Cu^{2+} ions. This shift was not as dramatic as the disappearance of the peak observed by Savinova *et al.* [22] and it is likely that there was only slight oxidation of their sample due to the protective action of gelatin.

Although the standard redox potential of bulk metallic copper $E^0_{Cu^{2+}/Cu^0}$ is +0.342 V vs. S.H.E., i.e., it is thermodynamically stable to deoxygenated non-oxidising acids, it was found that an aqueous solution at pH 0.5 containing copper particles with diameters of 3 nm, evolved hydrogen. If a spherical model of a particle with diameter d is assumed, then a change in the redox potential, ΔE_D, can be calculated from [29]:

$$\Delta E_D = -\frac{2\gamma V_m}{dF}$$

where V_m is the molar volume of the metal, γ is its surface tension and F is the Faraday constant. Using $\gamma_{25\,^oC} = 2.19$ J m^{-2}, $V_m = 7.12 \times 10^{-6}$ m^3 mol^{-1} for copper particles with d = 3 nm, gives $\Delta E_D = -0.108$ V and $E^0_{Cu^{2+}/Cu^0} = 0.234$ V. Although this redox potential is still higher than that of E_{H^+/H_2} at pH 0.5, the authors claim that 10^{-7} mol of hydrogen was evolved from 10 cm^3 of a colloid containing 5×10^{-7} g of copper. No attempt to measure the change

in Cu^{2+} concentration in solution was made and it is more likely that the hydrogen was evolved from the oxidation of excess BH_4^- ions in solution, possibly catalysed at the surface of the copper particles.

2.2. Oxidation of Dimethylaminoborane (DMAB)

Borohydride is a popular choice of reductant in electroless metal plating systems, together with hypophosphite, hydrazine and formaldehyde. However, using borohydride can leave a deposit with between 3 to 8 % boron. This is useful in some circumstances, especially where wear resistance is necessary, but borohydride and hypophosphite are impractical when a low level of impurity is required. However, boron-nitrogen compounds, especially the alkyl-substituted amine boranes, are more suitable. The use of amine boranes as reductants in the electroless plating of nickel were first patented in 1962 [30][31]. Of the three compounds obtainable where the methyl group is a substituent, dimethylaminoborane, $(CH_3)_2HNBH_3$, DMAB, is the one that is sufficiently stable and yet has a high reaction rate with metal ions. Another advantage of DMAB is that it is readily soluble in water, whereas diethylaminoborane requires a short chain aliphatic alcohol, e.g., ethanol, to enhance its solubility.

Mallory [32] suggested the following reactions for the electroless plating of Ni using DMAB:

$$(CH_3)_2NHBH_3 + 3Ni^{2+} + 3H_2O \rightarrow 3Ni^0 + (CH_3)_2NH_2^+ + H_3BO_3 + 5H^+ \quad (4)$$

$$2(CH_3)_2NHBH_3 + 4Ni^{2+} + 3H_2O \rightarrow$$

$$Ni_2B + 2Ni^0 + 2(CH_3)_2NH_2^+ + H_3BO_3 + 1/2H_2 + 6H^+ \quad (5)$$

He also mentioned that DMAB can be consumed by acid-catalysed hydrolysis:

$$(CH_3)_2NHBH_3 + 3H_2O + HCl \rightarrow (CH_3)_2NH_2Cl + H_3BO_3 + 3H_2 \quad (6)$$

and showed that this reaction becomes predominant below pH 5 or above 71 °C. This reaction must be balanced against the Ni^{2+} reduction rate that increased at low pH and high temperature. Equation (5) was found to predominate at lower pH and higher temperature.

The mechanism of DMAB oxidation was studied by Lelental [33] on a vacuum-deposited palladium film. X-ray Photoelectron Spectroscopy (XPS) indicated that there were no B-H groups on the surface of the film, and X-ray diffraction found only crystalline boron

and yet hydrogen, boric acid and dimethylamine are also produced by the oxidation of DMAB. Using this evidence he suggested the following reactions for the catalytic decomposition of DMAB on palladium:

$$(CH_3)_2NH - BH_3 + Pd^0 \rightarrow (CH_3)_2NH + BH_3 \cdots Pd \quad (7)$$

$$Pd \cdots B + 3/2H_2 \quad (8)$$

$$BH_3 \cdots Pd + 3H_2O \rightarrow Pd + H_3BO_3 + 3H_2 \quad (9)$$

The relative rates of reactions (8) and (9) depend on both pH and temperature. The lower pH and higher the temperature, the more likely equation (8) will predominate. More than a monolayer of boron formed on the surface of the film, but even when it had, there was no change in the reaction kinetics, indicating that there was no passivation effect. No evidence of oxidation was found on vacuum-deposited nickel or bismuth films, which was surprising as nickel plating with DMAB is known to be autocatalytic. It was suggested by Lelental that the formation of oxides, even under vacuum deposition conditions, had passivated the surface.

As the oxidation of DMAB appeared to involve the cleavage of the N-B bond, Lelental [34] further investigated the energy of the N-B bond in the series of amine boranes and the ability of the various catalysts to bring about its cleavage. In order of catalytic effectiveness, he found that Pd > Au > Ag > Cu, and that for the series $(CH_3)_{3-n}H_nBH_3$, the strength of the donor-acceptor bond decreased monotonically with decreasing n. He found no oxidation wave for any of the amine boranes when platinum, pyrolytic graphite or gold anodes were used and thus deduced that the chemical redox reaction was different from the electrochemical redox reaction, in that specific redox mechanisms were operative at the catalyst. He did not try cyclic voltammetry at a Pd electrode as a function of time. Therefore, it appears that in amine boranes, the strength of the B-N bond is determined to a considerable extent by its polarity, i.e., by the degree of transfer of the unshared electron pair of the nitrogen atom to the boron atom. The inductive effect of the methyl groups increases the electron density on the nitrogen atom, thus increasing the facility of

electron-pair donation to BH_3, producing a stronger bond. This idea is confirmed by the relative enthalpy of gas phase association [35] and the rate of acid-catalysed hydrolysis [36][37] for this series, suggesting a similar N-B cleavage occurs for these reactions.

The mechanism of the reducing action of DMAB in alkali solutions was investigated using cyclic voltammetry by Sazonova and Gorbonova [38]. They suggested the following overall reaction equation in alkaline solution:

$$(CH_3)_2NHBH_3 + 3H_2O \rightarrow (CH_3)_2NH + H_3BO_3 + 3H_2 \qquad (10)$$

and the following reaction scheme for oxidation of BH_3:

$$BH_3 + OH^- \rightarrow BH_3OH^- \qquad (11)$$

$$BH_3OH^- + OH^- \rightarrow BH_2(OH)_2^- + H^+ + 2e^- \qquad (12)$$

$$BH_2(OH)_2^- + OH^- \rightarrow BH(OH)_3^- + H^+ + 2e^- \qquad (13)$$

$$BH(OH)_3^- \rightarrow H_2BO_3^- + 2H^+ + 2e^- \qquad (14)$$

with reactions (15) and (16) in parallel with reactions (12) and (13):

$$BH_3OH^- \rightarrow BH_2OH + H^+ + 2e^- \qquad (15)$$

$$BH_2OH + OH^- \rightarrow BH_2(OH)_2^- \qquad (16)$$

Reaction (12) was found to be the overall rate determining step in the oxidation process.

A summary of the oxidation of 0.17 mol m^{-3} DMAB at 70 °C at a platinised-platinum electrode involves:

i) The weakest bond in the molecule, the N-B bond, breaks first and the borane (BH_3) part adsorbs on the platinum surface.

ii) In the potential range 0 to 1.6 V, two oxidation peaks were observed, corresponding to:

$$Pt\text{--}BH_3 + OH^- \Rightarrow Pt\text{--}BH_3OH^-$$

$$Pt\text{--}BH_3OH^- + OH^- \Rightarrow Pt\text{--}BH_2(OH)_2^- + H^+ + 2e$$

$$Pt\text{--}BH_2(OH)_2^- + OH^- \Rightarrow Pt\text{--}BH(OH)_3^- + H^+ + 2e \qquad 1st\ Peak$$

$$Pt\text{--}BH(OH)_3^- + OH^- \Rightarrow Pt + BO_2^-.2H_2O + H^+ + 2e \qquad 2nd\ Peak$$

Oxidation of DMAB occurred with the release of six electrons, two lost in the initial adsorption stage and the remaining four, as shown above, leading to the production of boric acid. Oxidation of dimethylamine, formed by reaction 10, did not occur, as indicated from measurements of the charge consumed in the first and second oxidation steps compared with the degree of coverage.

2.3. Stabilisation

Stabilisation of a colloidal dispersion requires the summation of the inter-particle forces of attraction (due to van der Waals interactions) and repulsion (due to electrostatic and/or steric forces) to produce a potential barrier opposing aggregation.

2.3.1. Attraction

If uncharged, a monodispersion of spherical copper colloidal particles would undergo rapid coagulation (<1 s) according to the theoretical Smoluchowski rapid coagulation rate constant $k_2 = 4kT/3\eta$, (where η = viscosity of the dispersion medium) that relates the half life ($t_{1/2}$) to the particle number concentration (N_1) by:

$$t_{1/2} = (N_1 k_2)^{-1} \tag{17}$$

Equation (17) shows that increasing the concentration of a colloidal solution increases its rate of coagulation. The reason for this coagulation is that colloidal particles are constantly undergoing Brownian encounters and the particles may adhere when they collide because of a combination of the van der Waals attraction between atoms, originating from permanent dipole/permanent dipole, and transitory dipole/transitory dipole (London [39]) forces.

The van der Waals attraction between two atoms or molecules is relatively short range, extending only over a few tenths of a nanometre. For colloidal particles containing many atoms, the net effect of summing all possible permutations of inter-atomic interactions is the generation of a long range, strong attraction force between the particles.

Hamaker [40] extended London's treatment of the dispersion forces between atoms to calculate those between colloid particles. The result for the attraction between two spheres, V_A, each of radius a, is:

$$V_A = -(A^*/6)G \tag{18}$$

where A^* is the effective Hamaker constant and the geometrical term G is given by $2/(s^2-4)+(2/s^2)+\ln(s^2-4/s^2)$. The parameter $s=(H_0+2a)/a$, where H_0 is the minimum distance of separation between the surfaces of the particles. If H_0 is small compared with the particle radius, then the expression for G is dominant and (18) reduces to:

$$V_A \approx -A^* a/12H_0 \tag{19}$$

A^* is difficult to obtain experimentally and was derived from the static dielectric constant by Gregory [41] and Tabor and Winterton [42]:

$$A^* = 0.422\frac{h\nu_v}{\varepsilon_{30}}(X_1 - X_2)^2 \tag{20}$$

where $$X_1 = \frac{\varepsilon_{10}-1}{\varepsilon_{10}+2}, \quad X_2 = \frac{\varepsilon_{10}-1}{\varepsilon_{10}+2}$$

and $h\nu_v$ can be thought of as the ionisation energy; h = Planck's constant, ν_v = the characteristic frequency of the atom, ε_{10} = dielectric constant of disperse phase and ε_{30} = dielectric constant of dispersion medium.

Another way of calculating A^* is from the Lifshitz-van der Waals constant obtained from optical properties of condensed bodies over a frequency range from visible light to the X-ray region [43]. Numerical examples quoted in this reference give A^* as 17.5 x 10^{-19} J for copper metal in aqueous media.

A plot of V_A against H_0 for two 5 nm spherical copper particles in aqueous media gives a characteristic potential well at close inter-particle distances (**Figure 2.3.1.1**).

Figure 2.3.1.1. van der Waals energy of attraction of two copper metal spherical colloidal particles of diameter 5 nm in aqueous media *vs* their separation distance.

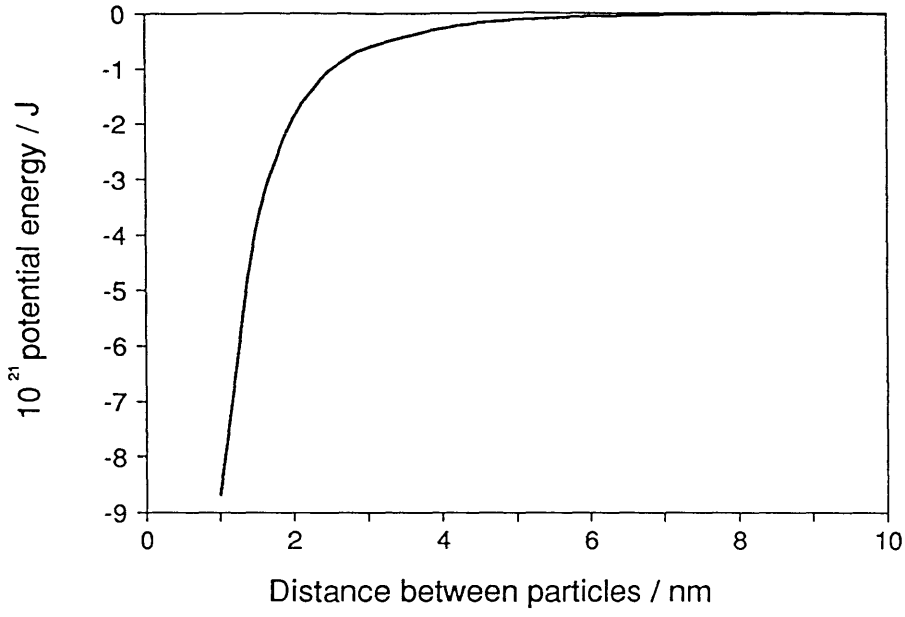

The treatments devised to provide alternative routes for calculating the Hamaker constants are necessarily approximate because they separate the geometric and electromagnetic components of the attraction that are inextricably interwoven [44]. The Hamaker constant is not really a constant but a function of the distance between particles and the temperature [45]. However, **Figure 2.3.1.1** indicates the strength and range of the attractive energy.

Given that strong, long range attractive forces exist between colloidal particles, it follows that to impart colloid stability, it is necessary to provide a repulsion between the particles that must be at least as strong as, and comparable in range to the attractive interaction; this involves *electrostatic stabilisation* and/or *polymeric stabilisation.*

2.3.2. Electrostatic Stabilisation

In aqueous media, colloidal copper particles acquire a potential-dependent charge due to copper ion dissolution and/or specific adsorption of ions from solution. Electroneutrality demands that the net charge in the dispersion medium be equal, but

opposite in sign, to that on the solid side of the solid/liquid interface. It is the mutual repulsion of these charge layers formed around the particles that provide electrostatic stabilisation.

The charge on the dispersed phase is in equilibrium with the electrolyte and increasing the electrolyte concentration will decrease the effective width of the diffuse double layer (the Debye length, $1/\kappa$ [46]).

The double-layer model proposed by Grahame [47] distinguishes between two layers (or planes) of charge. The Outer Helmholtz Plane (the Stern Plane) indicates the closest approach of hydrated ions (which are not necessarily adsorbed) and the Inner Helmholtz Plane indicates the locus of centres of ions that are dehydrated on adsorption. When an ion is adsorbed into the inner Helmholtz plane it rearranges the neighbouring surface charges and in doing so imposes a self-atmosphere potential ϕ_β on itself. The expression for the charge density in the Stern Plane, σ_1, is:

$$\sigma_1 = \frac{\sigma_m}{1 + \frac{N_A}{n_0 V_m} \exp\left(\frac{ze(\psi_\delta + \phi_\beta) + \phi}{kT}\right)}$$

where σ_m = surface charge density corresponding to a monolayer of counter ions,

$n_0 = N_A c$,

N_A = Avagadro's constant,

c = concentration of electrolyte,

V_m = molar volume of solvent,

z = valency of electrolyte,

e = elementary charge,

ψ_δ = potential at the Stern layer and

ϕ = van der Waals term for adsorption energy.

As two of these quantities are unknown, information has to be derived from other sources about them.

1. *Stern Potential*

   The Stern potential can be estimated from electrokinetic measurements. Electrokinetic behaviour depends on the potential of the surface of shear between the charged surface and the electrolyte when in relative motion. This potential is called the zeta potential (ζ). It is reasonable to assume that the shear plane is located a small distance further out from the interface than the Stern plane [48] and therefore

ζ is marginally smaller than ψ_δ. The bulk of experimental evidence suggests that errors introduced by the assumption of $\psi_\delta = \zeta$ are generally small, especially for lyophobic surfaces. ζ may be measured by electrophoresis.

2. *Surface Potential*

ϕ is made up of two terms ψ_0 and χ. Changes in the χ potential arise from the adsorption and/or orientation of solvent molecules at the surface. It is assumed that χ remains constant during variations of ψ_0 and therefore, from the Nernst equation

$$\frac{d\psi_0}{d(\text{pdi})} = \frac{-2.303RT}{zF}$$

where pdi = concentration of potential determining ions.

At the iso-electric point, which is obtainable from electrokinetic measurements, $\psi_0 = 0$ if it is assumed that there is no specific adsorption of non-potential determining ions. Therefore, χ can be calculated from the equation above and hence ϕ.

Double layers form spontaneously when any two phases involving exchangeable species are contacted and therefore the overall Gibbs free energy of formation is negative. When two similar double layers overlap due to the approach of two colloidal particles, then this can be regarded as the effective destruction of the double layer leading to a positive Gibbs free energy change that is manifest as repulsion.

For spheres of radius a at a minimum surface separation H_0, the repulsive energy V_R is given by [49]:

$$V_R = \frac{32\pi\varepsilon k^2 T^2 a\gamma^2}{e^2 z^2}\exp(-\kappa H_0)$$

where $$\gamma = \frac{\exp(ze\psi_\delta/2kT) - 1}{\exp(ze\psi_\delta/2kT) + 1}$$

The total potential energy of the system is obtained by adding the contributions of V_A and V_R, which is shown in **Figures 2.3.2.1** and **2.3.2.2.** These diagrams indicate the zeta potentials and concentrations required to maintain colloid stability electrostatically.

Figure 2.3.2.1. *The effect of zeta potential (mV) on the total potential energy of overlapping double layers of two spherical copper colloid particles. T = 298 K, a = 2.5 nm, concentration = 10 mol m^{-3}.*

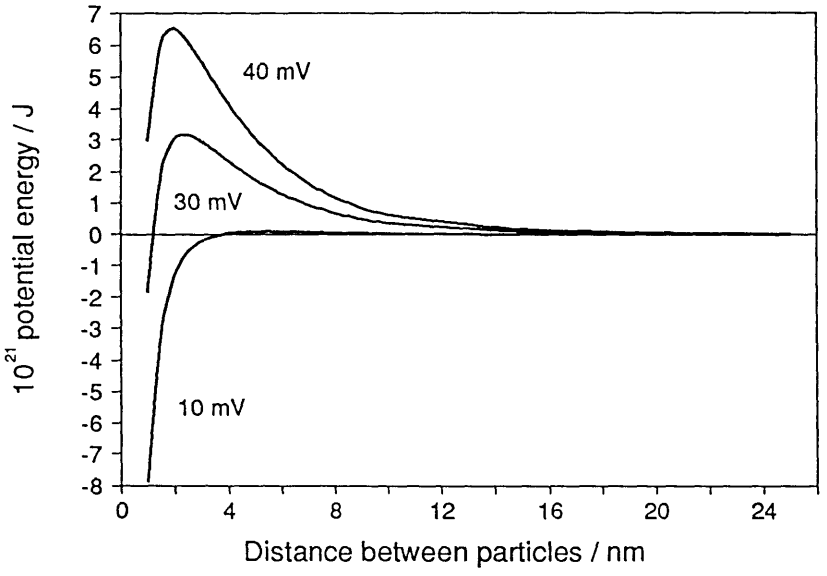

Figure 2.3.2.2. *The effect of concentration (mol m^{-3}) on the total potential energy of overlapping double layers of two spherical copper colloid particles. T = 298 K, a = 2.5 nm, ζ = 30 mV.*

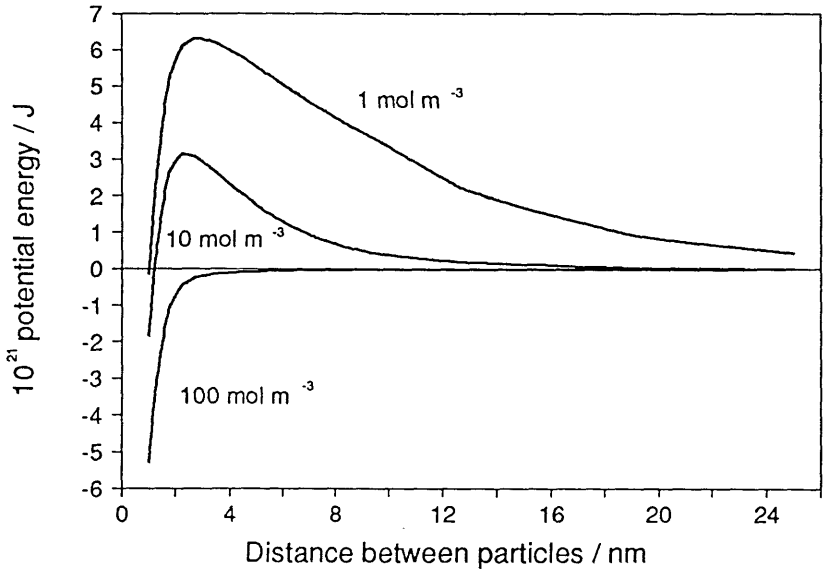

2.3.3. *Electrokinetic Measurement of Particles - Electrophoresis*

The mechanisms of migration of a colloid particle and an ion in an electric field are similar in many respects. In both cases there is a force due to the electric field E on the charge Q,

$$k_1 = QE$$

and a force due to the resistance of the liquid to the movement of a spherical particle at velocity U, expressed by Stoke's formula:

$$k_2 = -6\pi\eta a U$$

From the condition:

$$k_1 + k_2 = 0 \tag{21}$$

it follows that the electrophoretic velocity of the particle is:

$$U_Q = \frac{Q}{6\pi\eta a} E \tag{22}$$

However, electrophoresis occurs as a result of the electric field acting on the double layer as a whole, not just on the inner layer with charge Q. The force applied to the diffuse layer is in the opposite direction to k_1, since the charge of this layer is opposite to that of Q. This force is designated k_3 and is called the electrophoretic retardation force [50]. Although k_3 does not act directly on the particle, it is transmitted partially and produces a decrease in its velocity that is not taken account of in (21). Thus it follows that:

$$k_1 + k_2 + k_3 = 0$$

and (22) now becomes:

$$U_{ef} = \frac{1}{6\pi\eta a}(k_1 + k_3)$$

where U_{ef}= electrophoretic velocity per unit field strength. Since ζ is related to U_{ef} by the Smoluchowski equation [51],

$$U_{ef} = \frac{\varepsilon\zeta E}{4\pi\eta} \tag{23}$$

and as $\zeta = Q/4\pi a^2\kappa\varepsilon$, it follows that:

$$\frac{|k_1 + k_3|}{|k_1|} = \frac{1}{\kappa a}$$

This indicates that if $\kappa a \gg 1$, the electrophoretic retardation force compensates to a very considerable degree for the force applied to the particle. This can be thought of as the double layer becoming thinner and the mean point of the application of k_3 approaching the surface and thus transmitting its force increasingly to the particle, so decreasing its velocity.

Debye and Hückel corroborated (3) but obtained the factor $1/6\pi$. Henry examined this problem critically and found that the difference lay in the allowance that was made for the geometry of the electric field in the vicinity of the particle [52]. Smoluchowski had considered that the field flowed around the particle and Hückel had considered the field to be homogeneous in the vicinity of the particle. It would be expected that the field homogeneity near the particle will be affected by both κa and the conductivity of the particle. This factor was considered by Henry who developed a formula to account for the relationship between the electric conductance of the particle K' and the surrounding liquid K,

$$U_{ef} = \frac{\varepsilon \zeta E}{6\pi\eta} f\left(\kappa a, \frac{K'}{K}\right)$$

where

$$f\left(\kappa a, \frac{K'}{K}\right) = 1 + \lambda(2f_1(\kappa a) - 2)$$

and

$$\lambda = \frac{K - K'}{2K + K'}$$

In the limiting case $\kappa a \rightarrow \infty$, $f_1(\kappa a) = 3/2$, and for a non conducting sphere ($K' = 0$) then Henry's and Smoluchowski's formulae are equivalent. If $\kappa a \rightarrow 0$, then $f_1(\kappa a) = 1$ and for any type of particle Hückel's formula is followed. In fact, electrophoretic mobility has been shown to be independent of particle dielectric constant [53] and so only the thickness of the double layer will affect mobility.

2.3.4. *Polymeric Stabilisation*

There are two methods by which polymer chains can impart colloid stability; *steric stabilisation* and *depletion stabilisation.*

Steric stabilisation of colloidal particles is imparted by macromolecules that are physically adsorbed onto the surface of the particles. The lengths of the adsorbed polymers, typically 20 nm for a polymer chain of molar mass 100,000, prevent the particles coming within range of the van der Waals forces. There are many reviews of the use of steric stabilisation [54].

Depletion stabilisation differs from steric stabilisation in that stability is imparted not by attached polymer, but by macromolecules that are free in solution. One theory for this observation is based on two colloidal particles approaching each other in a solution containing free polymers [55]. If the interparticle distance becomes less than the mean diameter of the free polymer, then the polymer is forced out of this interparticle region. This creates a pressure difference between the side of the particle facing the contact zone and the side of the particle facing the bulk solution. Since some polymers in solution can take up different conformations, only partial depletion of the polymer from the contact zone may occur. The energy of attraction between the two particles is then balanced by the energy required to change the natural conformation of the polymer molecule and remove it from the contact zone into the bulk solution.

Amphipathic polymers of the block or graft type are presumed to be good steric stabilisers. A polymer with a head group that is insoluble in a dispersion medium would be expected to attach itself to a particle, whereas the soluble part of the polymer would stretch out into the solution and stabilise the particle. Stresses induced in the soluble polymer by Brownian collision would not result in desorption, but slipping in the stress zone since the polymer would be firmly bonded on the particle.

Adsorption of amphipathic polymers with hydrophilic and lipophilic parts is simpler when either the medium or the dispersion is nonpolar and the other polar [56]. Crowl and Malati [57] studied the stability of 0.2 to 0.3 μm rutile and iron oxide particles in benzene using a polyester of adipic acid and neopentyl glycol with carboxyl and/or hydroxyl substituted end-groups (MM 2000 to 5000). By comparing the data for maximum adsorption of the polyester on the particles with monolayer formation of the polymer in a Langmuir trough, they found that the polymers adsorbed as close-packed monolayers on the particles. The polyesters ending in carboxyl groups gave better stabilisation than those ending in hydroxyl groups, and although the adsorption of those ending in hydroxyl groups was lower, this

did not account fully for the difference. The charge on the particles was found to be zero by micro-electrophoresis and therefore all stabilisation must have been by steric means. Infra-red analysis of the particles with adsorbed polymers showed that an absorption band occurred at 1580 cm^{-1} that was not present for the free polyester. This frequency is characteristic of the carboxylate ion and indicates that adsorption of the carboxyl containing ions occurred via ionic means. This band was also present, although less intense, for hydroxyl terminated polymers, indicating that strong adsorption of the carboxylate ion occurred despite the excess of hydroxyl ions.

A more theoretical approach to the subject of steric stabilization was undertaken by Napper [58] who investigated organic colloids in both aqueous and non-aqueous solvents. He found that the point of incipient flocculation for colloids stabilized using amphipathic polymers was essentially independent of the anchor polymer used, the dispersed phase, the particle size (< 250 nm) and the molar mass of the stabilizing chain (> 10^3). The most important factor was the θ-solvency condition (the conditions for a θ-solvent is discussed in **Appendix B**). In a non-aqueous system (*n*-heptane), there was a net decrease in entropy, calculated from the Flory equation [59], when two stabilizing chains, poly(12-hydroxystearic acid), PSA, interpenetrated, which arose from the increased segmental concentration in the overlap volume. This decrease in entropy generates a repulsive potential energy that will give rise to stability if it outweighs the combined attractive potential energy resulting from the enthalpy of interpenetration and the London attraction forces. Napper called this entropic stabilization. In the aqueous system the configurational entropy of the stabilizing chain, polyethylene oxide, PEO, was found to increase. This was thought to arise from the fact that water molecules are orientated by the ether oxygen of the PEO, and when interpenetration occurs, this structuring is destroyed and the increase in the water entropy outweighs the decrease in the PEO entropy. The positive enthalpy generated on the release of the water molecules generates the repulsive force necessary to offset the flocculating influence of the entropic effects and attraction forces. Napper terms this enthalpic stabilization, and points out that either or both forms may occur in aqueous or non-aqueous systems. Using the aqueous system, Napper then investigated the effect of ions on the flocculation of this system [60]. He found that although the flocculation effectiveness for anions ($SO_4^{2+} > Cl^- > NO_3^- > CNS^- > Br^- > I^-$) mirrored the Hofmeister series [61], the order for cations ($Rb^+ = K^+ = Na^+ = Cs^+ > NH_4^+ = Sr^{2+} > Li^+ = Ca^{2+} = Ba^{2+} = Mg^{2+}$) was in direct conflict with the postulate that the more highly hydrated ions are the more effective flocculants. Using Franks model [62], he suggested that flocculation is not due to preferential

solvation of the ion at the expense of the polymer as suggested by Hofmeister, but the influence exerted by the structure of the water in the immediate neighbourhood of the hydrated ion, which affects the enthalpy and entropy of the system.

Direct measurement of the forces between polymers were first recorded by Lyklema and van Vliet [63] who used an apparatus which could measure the force on two mica plates, coated in adsorbed polymer, as they approached each other. Klein [64] used this apparatus to show that for polystyrene (MM 600,0000) in cyclohexane, the onset of steric interaction took place at a surface separation comparable with the polymer dimensions (< 60 nm).

2.3.5. Gelatin as a Steric Stabilizer

When organic tissues which contain the protein collagen are subjected to mildly degradative processes, usually involving treatment with alkali or acid followed or accompanied by some degree of heating in the presence of water, the systematic fibrous structure of the collagen is broken down irreversibly. The product of this process is termed gelatin. Fibrils of collagen may be regarded as comprising three protein chains, connected via covalent inter-molecular cross-links. The mild acid or alkali treatment breaks down these covalent bonds and frees gelatin molecules. As no individual bond in the collagen molecule is known to be so labile that it specifically breaks first during gelatin manufacture, the resulting gelatin molecules can be quite random in molar mass, composition and structure. All molecules derived from collagen can be considered as gelatin provided they pass an arbitrary minimum molar mass of 30,000 [65]. The means of manufacture can also affect the composition of gelatin obtained. Generally, the gelatin will contain the same amino acids as the parent collagen, a degree of moisture and a certain amount of inorganic impurity as well. Despite the variety of sources, there is a remarkable similarity in the proportions of amino acids present in all gelatins. All the amino acids commonly found in proteins occur in gelatin with the exceptions of tryptophan and cystine, the sulphur-containing amino acids. The main raw materials for edible and technical gelatin are bones and hides.

There are two main types of manufacturing process, the first involves soaking the collagen in dilute acid, and the second involves soaking the collagen in alkaline solution. The amino acids prepared by the alkaline process differ from those produced by the acid process. The alkali-processed gelatins possess higher hydroxyproline and lower tyrosine contents than the acid-processed gelatin, which appears to be due to the alkali-processed gelatin losing peptides with lower hydroxyproline content. During acid processing, some amide groups

are lost and the iso-electric point of the material can fall from 9-10 to 8-9. The removal of impurities during the acid processing results in the gelatin increasing the proportion of those amino acids present in large quantities, i.e., glycine, proline, hydroxyproline and alanine. Alkaline processing results in a massive loss of amide nitrogen, especially from asparagine and glutamine, and as a result the pI can fall to 5-6. Differences in the relative proportions of end groups also depends on the process route. Alanine end groups predominate in acid-processed gelatin, and serine, threonine, aspartic and glutamic acid end groups predominate in alkali-processed ones. See **Appendix C** for a description of the amino acids and the relative proportions of each in acid-processed and alkali-processed gelatins. The other main difference between the two types of gelatin is that shorter chain lengths predominate in acid-processed kind.

Gelatin consists of a polypeptide backbone, with side-chain groups attached to these, as illustrated in **Figure 2.3.5.1.**

Figure 2.3.5.1. *Molecular structure of gelatin.*

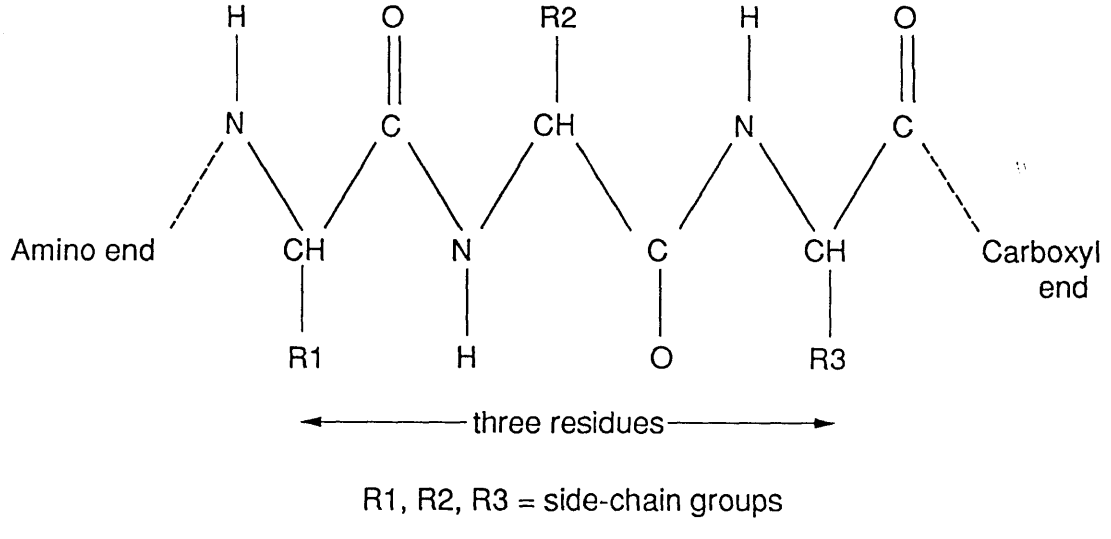

Typical molar masses are in the range 50,000 to 200,000, with individual polypeptide chains ranging in molar mass from 50,000 to 80,000. This means that there is about one α-amino group per 750 to 800 residues, i.e., one α-amino group per approximately 25 ε-amino groups. Therefore, the involvement of the α-amino group in the overall chemistry of gelatin is relatively minor.

Gelatin is employed commercially for one or more of the following properties: gel formation, emulsion stabilization, foam stabilization, flocculation, film formation, adhesion and as a protective colloid. Gelatin has the advantage of being cheap, non-toxic and biodegradable. The first use of the ability of gelatin to stabilise dilute sols was reported by Zsigmondy [66] who established a "gold number" which was an arbitrary unit based on the minimum amount of stabiliser necessary to prevent a gold sol being flocculated by a NaCl solution. He found that gelatin had the lowest gold number of several naturally occurring macromolecules. At high levels of addition, gelatin has the property of being able to adsorb on particles and prevent them from approaching within the range of electrostatic attraction of each other, thus preventing precipitation. Several other workers have established gelatin as the most efficient of colloid protectors.

Due to the polyampholyte nature of gelatin, it can carry a net negative or positive charge depending on the pH of the solution and the pI of the gelatin. In general it has been found that gelatin adsorbs better on a negatively charged surface below its pI [67], which is what would be expected theoretically from consideration of the electrostatic forces. However, increasing the charge on the gelatin also means that the chains repulse each other and thus the adsorption layer density is decreased.

Kragh and Langston [68] studied the flocculation of quartz using gelatin. They found that the best flocculation occurred at a gelatin adsorption density corresponding to one third of a monolayer and that the efficiency of flocculation, but not adsorption, was pH dependent. With a negatively charged suspension, the best flocculation occurred when the gelatin carried a slightly positive charge, and once adsorbed, the gelatin affected the electrophoretic mobility, U_{ef}, of the suspension. If excess gelatin was present then it was found that the pI of the suspension became that of the gelatin, although the U_{ef} was not entirely governed by the adsorbed layer. The fact that the U_{ef} did not correspond quantitatively to the net charge on the gelatin molecule in solution may be due to the effect of the change in the surface of shear as the conformation of the adsorbed layer changes with pH. Flocculation occurred only over a narrow pH range and was easily disrupted by agitation. It was postulated that the gelatin was not adsorbed in ordered monolayers and that a disordered structure in which molecular chains project from the particles was formed first. At low concentrations these enable polymer bridges that span between particles to be formed on collision. When these bonds are broken by agitation then a slow rearrangement of the surface layer involving adsorption of free chains leads to poorer

flocculation. The pH dependence was thought to be due primarily to the influence of molecular charge on the configuration of the adsorbed layer rather than its effect on the net charge of the particle.

2.4. Adsorption on Silica

Silica, as glass fibres, is a main component of PCBs and is composed of silicon atoms in a tetrahedral co-ordination with oxygen atoms. An ideal silica surface would be composed of siloxane bridges (Si-O-Si); however, real silica surfaces have been shown to contain silanol (Si-OH) groups on their surfaces which have been recorded as being stable up to 900 °C [69]. These silanol sites have been shown to be capable of forming co-ordination or hydrogen-type bonds with molecular water [70]. NMR studies have shown that other surface sites on silica are also capable of forming similar bonds [71].

Lange [72] identified two types of adsorbed water by thermogravimetric analysis. His observations suggested the presence of strongly chemisorbed molecular water and the more weakly physisorbed water, which can removed by heating to 120 ^{0}C or evacuation at room temperature. Three types of surface for pure silica were suggested by Lussow [73] under various conditions: type 1 surfaces have strongly adsorbed molecular water, type 2 surfaces have a significant number of silanol groups, but no adsorbed molecular water and type 3 surfaces consist of predominantly siloxane groups with no adsorbed molecular water. However, Hockey [74] has pointed out that it is very difficult to distinguish between physisorbed water and pairs of hydroxyl groups bonded to the same surface site.

Basila [75] has shown, using spectroscopic methods, that the silanol groups on the solid are more reactive than those of aliphatic silanols. Also, impurities (mostly alkali metal oxides) that occur in commercial silica are well known to increase the affinity for the solid to both physisorbed and chemisorbed water and electron donating molecules. The heats of adsorption of amines are greater for silica-aluminas and impure silicas compared to pure silica [76].

A variety of small molecules that are capable of adsorption by hydrogen bonding to silica were found to have little or no effect on the flocculation of dispersed silica [77]. However, it was found that polyacrylamide, $(H_2C{=}CHCONH_2)_n$, could adsorb on and flocculate dispersed silica, presumably by a bridging mechanism, which was different from normal electrolyte coagulation. Prolonged contact of the silica with water led to a loss of the flocculation power of the polyacrylamide, which suggests an ageing process deactivating the silica surface. The ageing process was observed to be enhanced by hydroxyl ions [78].

The process was reversed by cleaning the surface in alcohol and nitric acid, as well as high temperature treatment. The streaming potential method was employed by Eremenko *et al.* [79] in finding that only high molar mass polymers (MM >1000) decrease the zeta potential of silica dramatically.

During an investigation into the hydrophilation of glass surfaces, several polymers were studied [80]. They all had the general form $B(CH_2)_nP$, where B is a functional group chosen to form a strong bond with the silica surface and P is a functional polar group chosen to render the surface hydrophilic. Changes in the contact angle of water on glass following periods of steaming, showed that the relative strengths of the bonds formed by the following functional groups were (in decreasing order): polymethylsiloxane $(Me_2SiO)_n$ > trichlorosilane $\equiv SiCl$ > quaternary ammonium group $-N^+(R_3)R^1X^-$ > dichlorosilane $=SiCl_2$ > monochlorosilane $-SiCl_3$ > ethoxysilane $-Si(OEt)_n$. Infra-red spectroscopic analysis of the residual coating confirmed this order.

Although polysiloxane coatings were found to form the strongest bonds, the coatings obtained were too thick for the required use, i.e., for high optical transmission glasses (e.g., windscreens). The chlorosilane compounds bonded strongly to glass by forming a siloxane link, formed via hydrolysis of the -SiCl bonds by surface hydroxyl groups. Attempts to synthesize a chlorosilane compound with a polar group at the other end of the chain failed due to chemical interaction between the end groups leading to polymerization. The quaternary ammonium group was compatible with polar groups such as -COOH and -OH and bonded strongly with silica. As the chain length of trimethylammonium bromides was increased from 4 to 20, there was an increase in strength of the bond to silica. This illustrates the importance of the polar to non-polar group ratio in the protection of the surface bond and the fact that increased hydration of the quaternary ammonium ion occurs at the surface with shorter chains. The longer the chain, the more it is able to produce closely packed orientated monolayers. The stability of the bond was also dependent on the hydrophilic character of the surface-active group, i.e., the more hydrophilic, the less stable the bond.

Evidence suggests that cationic exchange to form a surface complex does not take place between the surface silanol groups and quaternary ammonium ions, but that the bond is of a charge-transfer type. This view was supported by infra-red analysis of the surface which showed that O-H bonds had been weakened by stretching but not broken.

Other workers consider that long-chain organic cations are attracted by electrostatic force at the glass surface and combine with the negatively charged silanol ions to form a surface compound [81][82]. Experimental evidence [83] shows that silanol groups on the surface are important for the formation of chemical bonds such as:

$$\equiv SiOH + Cl\text{-}Si \rightarrow \equiv Si\text{-}O\text{-}Si \equiv + HCl$$

and in the presence of excess alcohol, a similar reaction can occur to form surface estersils [84]:

$$\equiv SiOH + ROH \rightarrow \equiv SiOR + H_2O$$

Steric factors play an important role and high molar mass alcohols are too large to react with the available surface sites.

Surface adsorption can also occur via chemical bonds that do not involve complete bond rupture, e.g., aliphatic alcohols of shorter chain length can form hydrogen bonds [85][86]. The existence of a negative charge on the surface of silica supports the view that the surface silanol groups are acidic in nature and dissociate as follows:

$$\equiv SiOH \rightarrow \equiv SiO^- + H^+$$

Aromatic and unsaturated organic compounds are more strongly adsorbed on a hydrated surface than the corresponding saturated molecules. The greater affinity for unsaturated molecules has been attributed to the interaction between the π-electrons of the adsorbate and the surface silanols [87]. Dehydration of the surface causes a sharp decrease in the adsorption of unsaturated molecules but conversely, causes a slight increase in the adsorption of saturated organics. This slight increase can be explained by the fact that the molecule is able to approach closer to the surface, and hence there is an increase in the attraction forces.

2.5. Alternative Means of Colloidal Particle Formation

An alternative means of producing fine metal particles is by the technique called *gas evaporation.* The technique involves heating a small amount of metal in an inert gas until it evaporates. On collision with the gas particles it the condenses like mist or snow to form particles. This method was first used by Beek *et al.* [88] to produce evaporated metal films. Kimoto *et al.* [89] developed this technique to form particles by heating various metals in argon with a tungsten wire heater. These were then deposited on SEM specimen grids for

further examination. By changing the pressure of the gas, they could vary the size of particles formed, from 10 nm at 1mm Hg to about 300 nm at 30 mm Hg. The theory of metal particle formation was not explained, but it was suggested that impurities in the metal formed the nuclei on which the condensing metal atoms grew. The particles were mostly spherical, suggesting the cooling of condensed liquid drops. Examination of the copper particles formed by electron diffraction showed that above 20 nm, they were single crystals having a f.c.c. lattice. On exposure to air, a 5 nm layer of Cu_2O had formed. Wada [90] replaced the tungsten element, which was found to evaporate itself, with a plasma flame, and this was replaced by Iwama *et al.* [91] with electron beam heating as the plasma flame could not work at low pressures. Yatsuya *et al.* [92] went back to the method of vacuum evaporation first used by Pfund [93] to form thin metal films, but instead of a depositing the particles on a solid surface, used a running silicon oil substrate so that particles would remain dispersed. Vacuum evaporation has the advantage over gas evaporation in that the process is faster and smaller, more uniformly sized particles are formed. Silver particles were formed of diameters in the order 2-5 nm depending on the distance between the evaporation source and the running oil surface. However, no means of extraction of particles from the high viscosity oil was given, and it was reported in further work [94] that iron particles agglomerated in the oil after a few days. Other metal particles formed were found by electron diffraction to be mainly oxides, but this was thought to be due to the fact that the particles had been exposed to the air.

In an extension of the technique used to produce noble metals by radiation, Marignier *et al.* [95] have formed Co, Ni, Zn, Pb and bimetallic Cu-Pd aggregates. The technique uses the fact that on irradiation of water, the following ions and radicals are produced:

$$H_2O \xrightarrow{\text{radiation}} e_s^-, H_3O^+, H^\cdot, OH^\cdot, H_2O_2 \tag{24}$$

Solvated electrons, e_s^-, can then reduce metal ions in solution in the following way:

$$e_s^- + M^{m+} \rightarrow M^{(m-1)+} \tag{25}$$

$$e_s^- + M^+ \rightarrow M^0 \tag{26}$$

$$nM^0 \rightarrow M_2 \rightarrow \ldots M_n \ldots \rightarrow M_{agg} \tag{27}$$

The rate constants of reactions (24) to (26) are high for most metals, favouring reduction in this way, but oxidation of the transient lower valency states of the metal, or even of the metal itself, can occur by either H_3O^+ or by radiolytic radicals such as $OH^\cdot$ and $H^\cdot$, producing hydrogen.

$$M_n + H_3O^+ \rightarrow M_{n-1} + M^+ + \frac{1}{2}H_2 + H_2O \qquad (28)$$

To prevent reoxidation and favour the reduction of metal, a combination of the following procedures were used; (1) alkanization to lower H_3O^+ and $H^\cdot$ concentrations, (2) addition of an $OH^\cdot$ scavenger such as isopropanol, (3) addition of Pd to start heterogeneous nucleation of M, (4) increase metal ion concentration and (5) limit aggregate size by addition of a surfactant such as poly(vinyl alcohol), PVA (this also acts as an $OH^\cdot$ scavenger).

Using these methods, sols were produced that were stable for several months unless they came into contact with air.

A Pd-Cu colloid was made using a ^{60}Co source with a dose rate of 2×10^{19} eV $cm^{-3} h^{-1}$. The concentrations of reactants were 1 mol m^{-3} Cu, 10 mol m^{-3} Pd, 0.56 mol dm^{-3} isopropanol and 0.1 mol dm^{-3} PVA and the reduction was carried out at pH 10.2. The sample was irradiated up to 5×10^{19} eV cm^{-3}. The colloid formed was dark green (pure Cu colloids were described as pink) with particle sizes from 20 to 1000 nm observed by TEM. Electron diffraction studies of particles showed a regular lattice structure with formula Cu_3Pd.

2.6. Alternative Means of Deposition

An alternative way of depositing copper onto a silica surface, other than using metallic copper colloids, is by adsorbing hydroxylated copper solution species, such as $Cu(OH)_2$ (aq) or positively charged copper hydrous oxide colloid particles on to the silica surface [96] followed by *in-situ* reduction. Silica has a pH_{pzc} of about 2 [97] and is negatively charged at higher pH values. The pzc of $Cu(OH)_2$ is about 9 and so in the pH range 2-9, is available for the bonding to the silica surface by electrostatic adsorption.

The adsorption mechanism of the hydroxylated metal cation on the silica could involve both electrostatic and hydrogen bonding [98], but it has been suggested that the cations may be too hydrated to adsorb and the hydroxides form on the surface as the conditions there are different from those of the bulk solution [99][100]. The dielectric constant of water changes

from around 80 to about 6 near the surface, due to the ordering of water molecules in the double layer [101], hence the solubility of metal salts is decreased and pH conditions change in this region making it possible for metal ions to form metal hydroxides.

Once the hydroxide is adsorbed on the surface it may then be possible to reduce the copper *in-situ* by use of an aqueous reductant. Use of a complexant to complex the reductant (e.g., V(II) picolinate) would relax constraints on the pH range required to ensure the solubility of the reductant. The complexant would have to be chosen to ensure that it was specific to the reductant. If it were able to complex Cu(II) ions, it could lead to desorption of copper from the surface of the silica.

A common method used to initiate electroless copper plating on a dielectric substrate is by immersion into an aqueous colloidal dispersion of palladium in order to deposit 1 - 2 nm diameter particles on the substrate surface. Although simple, this process is flawed. SnCl shells form on Pd particles when Pd^{2+} is reduced by $SnCl_2$, which inhibit the activity of the Pd particles [102]. The shells can be dissolved away in an "acceleration" step, which typically involves the use of HCl or NaOH. Acceleration must be carried out soon after applying the colloid to avoid oxidation of the shell in air to tin oxides that are very difficult to remove. The acceleration step has also been found to cause agglomeration of the Pd particles on the substrate surface [103].

A new method of initiating electroless deposition of copper onto dielectric substrates such as PCBs has been described by Jackson [104]. The process employs a thin film of poly(acrylic acid) (PAA) (MM 250000), applied to the substrate by dip-coating, to bind Pd^{2+} upon immersion of the substrate in aqueous $PdSO_4$. The Pd^{2+} is reduced to Pd^0 upon introduction to an electroless copper plating bath and acts as a catalyst for subsequent copper growth. This method avoids the need for an "acceleration" step used in the preparation of Pd colloids.

Jackson suggests that the Pd^{2+} ion complexes with the carboxyl group of the PAA. X-ray Photoelectron Spectroscopy (XPS) performed on a quartz crystal dipped in PAA and $PdSO_4$ detected only C, O and Pd, no S, suggesting that $PdSO_4$ is not adsorbed, but Pd^{2+} is somehow ion exchanged with H^- at the COOH site. The number of Pd atoms per PAA monomer unit was found to be 0.46, which is within error limits of the theoretical 0.5 expected. High resolution spectra revealed that the Pd($3d_{5/2}$) peak was at 336.2 eV before copper plating, i.e., close to the literature value of 336.1 eV given for Pd^{2+} in a predominantly covalently bonded species (PdO), whereas after plating it was at 335.3 eV, which is given in the literature as the value for Pd^0. The surface concentration of Pd was found to be 90 ± 7 mg

m^{-2} for PCB substrates by removing the film with aqua regia and using AA. (The Lea Ronal copper catalyst, using 20 to 50 cm^3 catalyst concentrate m^{-2} [105] at 0.25 g Pd dm^{-3} only uses 5 to 13 mg Pd m^{-2}). There is no mention of how the PAA film affects the strength of adherence of the electroless copper plating.

2.7. Regenerative Aqueous Reductants

One of the cheapest and easiest forms of reduction is by electrons that are obtained from non-chemical means. However, electrons transmitted to a solution via electrodes are only useful in homogeneous systems and are unable to produce highly dispersed colloids. This being the case, it may be possible to use a regenerative chemical couple as an intermediary between electrode and copper colloid formation.

The initial choice of a reductant for the reduction of Cu(II) to copper metal can be made from values of standard reduction potentials [106]. The chosen reductant must have a sufficiently low enough redox potential to produce copper with the combined ability to be regenerated. Most thermodynamically powerful reducing agents are metals, but the use of these has disadvantages. To make efficient electrochemical contact for the formation of colloids, the metal must be introduced to the solution in a finely powdered form. The metal can only be regenerated by electrodeposition and in this form it must be removed from the cathode and extensively comminuted prior to re-introduction to the reactor.

The suitability of an aqueous reductant depends not only on its reduction potential, but also on kinetic factors and the electrochemical engineering required for the system. Since engineering difficulties arise when the oxidation products are solid or gaseous, only aqueous reductants with aqueous products will be considered.

Two powerful reducing agents, Cr(II) and V(II), may be suitable for the reduction of Cu^{2+} and/or $Cu(OH)_2$ to copper metal. The solution and electrochemistry of these species with relation to copper is therefore discussed below.

2.7.1 Copper

Aqueous solutions contain two ionic species of copper, Cu^+ and Cu^{2+}, which, in the presence of copper metal, are connected by the equilibrium:

$$Cu + Cu^{2+} \Leftrightarrow 2Cu^+ \qquad K = 5.6 \times 10^{-7}$$

Three equilibrium potentials are therefore pertinent to the electrode reactions:

$$Cu^{+} + e \Leftrightarrow Cu \qquad E^{0} = +0.521V$$

$$Cu^{2+} + 2e \Leftrightarrow Cu \qquad E^{0} = +0.342V$$

$$Cu^{2+} + e \Leftrightarrow Cu^{+} \qquad E^{0} = +0.153V$$

Equilibrium potentials used for the Cu_2O/CuO system are listed below:

$$Cu_2O + 2H^{+} + 2e \Leftrightarrow 2Cu + H_2O \qquad E^{0} = +0.471V$$

$$CuO + 2H^{+} + 2e \Leftrightarrow Cu + H_2O \qquad E^{0} = +0.570V$$

$$CuO_2^{2-} + 4H^{+} + 2e \Leftrightarrow Cu + 2H_2O \qquad E^{0} = +1.515V$$

$$2Cu^{2+} + H_2O + 2e \Leftrightarrow Cu_2O + 2H^{+} \qquad E^{0} = +0.203V$$

$$2CuO_2^{2-} + 6H^{+} + 2e \Leftrightarrow Cu_2O + 3H_2O \qquad E^{0} = +2.560V$$

A potential - pH diagram of the Cu - H_2O system is shown in **Figure 2.7.1.1.**

Figure 2.7.1.1. *Potential - pH diagram of the Cu - H_2O system at 25 °C and activity = 0.01.*

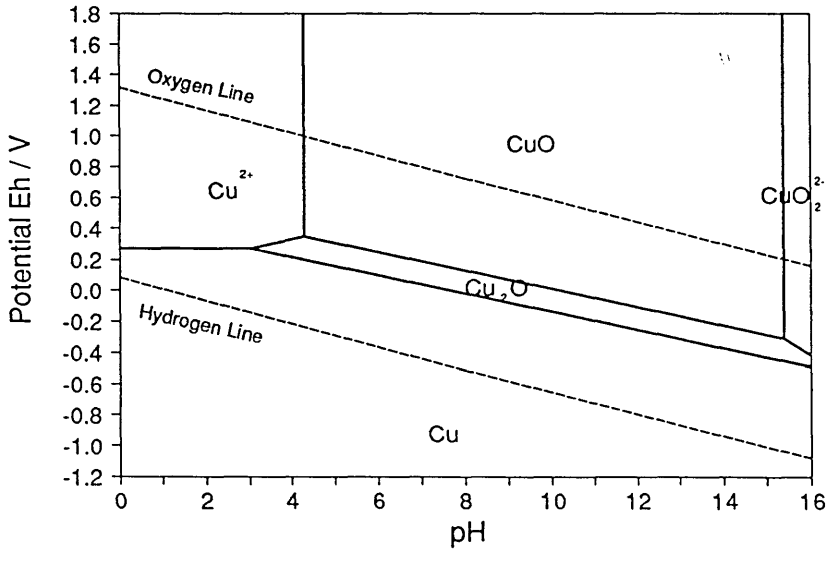

The addition of complexing agents to a solution containing Cu^{+} and Cu^{2+} ions will affect the activity of the two ions to a different extent [107]. If the stability constants $ß_1$ and $ß_2$ for the cuprous and cupric complexes respectively are known, a standard potential E^{0}_{C} for the reaction $Cu^{2+} + e \Leftrightarrow Cu^{+}$ in a solution containing the complexing agent can be calculated from:

$$E_C^0 = E_{Cu^+/Cu^{2+}}^0 + \frac{RT}{F} \ln \frac{\beta_1}{\beta_2}$$

Therefore, an increase in the redox potential as a result of complex formation indicates preferential stabilisation of the Cu^+ ion, while a decrease shows that the Cu(II) complexes are more stable.

2.7.2 The Chromium(II)/Chromium(III) Couple

In common with most of the first series transition metals, chromium exhibits a wide range of oxidation states. The ground state electron configuration is $3d^5\,4s^1$, with the highest +6 oxidation state corresponding to a loss of all the outer electrons. Oxidation states down to -2 have been suggested but the +2, +3 and +6 states are by far the most common.

Chromium is a light silvery grey metal that is reasonably unreactive. It is not soluble in nitric and phosphoric acids, or aqua regia at room temperature, but dissolves in non-oxidising acids such as dilute HCl or H_2SO_4. Since many oxidising agents passivate the metal to some extent, the reactivity of chromium is difficult to predict. The equilibrium potentials of the Cr^{2+}/Cr and Cr^{3+}/Cr^{2+} redox couples are:

$$Cr^{2+} + 2e \Leftrightarrow Cr \qquad E^0 = -0.91V$$

$$Cr^{3+} + e \Leftrightarrow Cr^{2+} \qquad E^0 = -0.41V$$

The domains of Cr^0 and Cr^{2+} stability, plotted on a potential/pH diagram, lie below that of water, thus indicating their thermodynamic capability to decompose water with the evolution of hydrogen. In neutral or alkaline conditions, chromic oxide or hydroxide coatings passivate the metal surface (**Figures 2.7.2.1** and **2.7.2.2**).

Figure 2.7.2.1. Potential - pH diagram for the Cr - H_2O system at 25 °C and activity = 0.01, considering Cr_2O_3.

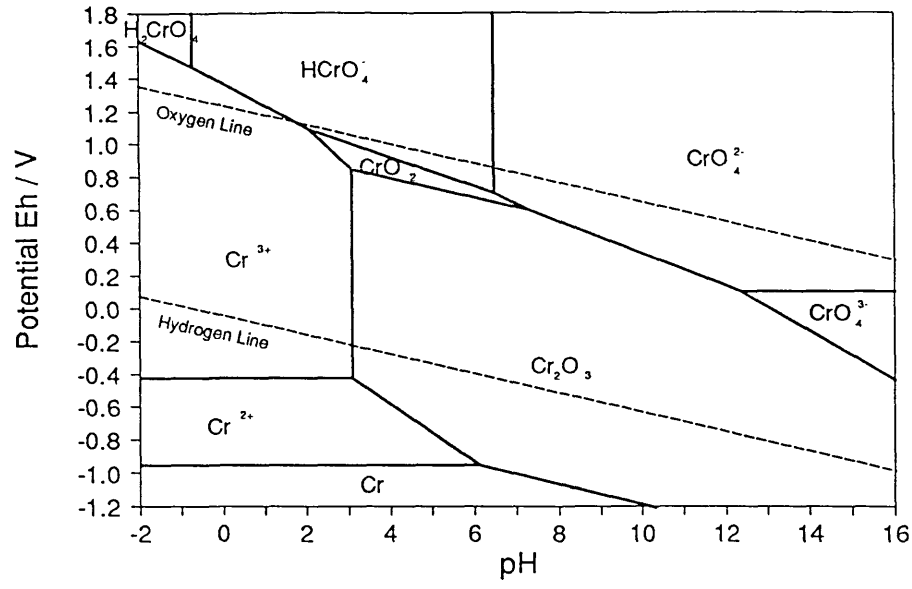

Figure 2.7.2.2. Potential - pH diagram for the Cr - H_2O system at 25 °C and activity = 0.01, considering $Cr(OH)_3$.

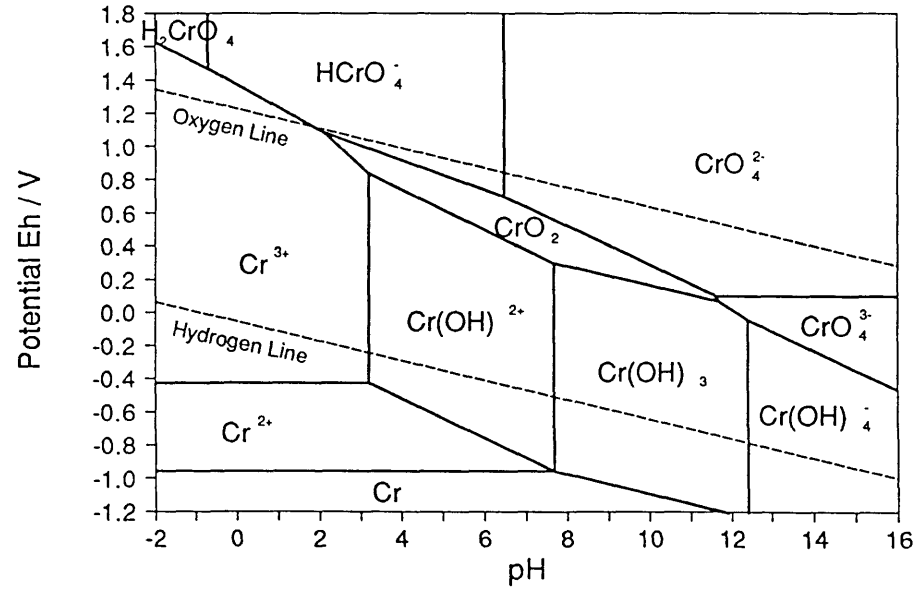

Aqueous solutions of Cr^{2+} can be prepared either by dissolving pure chromium in dilute non-oxidising acids such as HCl, or by reducing chromium salts of higher oxidation state, either electrolytically or chemically, by using a metal that is sufficiently base. Preparation techniques are complicated by the need to prevent oxidation from atmospheric oxygen and this usually results in incomplete reduction.

The Cr^{2+} ion is unstable in water, little is known of its solution chemistry and no hydrolysis data was found. Chromium(II)hydroxide is thought to precipitate at approximately pH 6 but is easily oxidised.

Chromium(II) salts are thermodynamically unstable in water, which they decompose liberating hydrogen.

Chromium(II) is readily oxidised to Cr(III) species. The stability of solutions is considerably increased by protection from atmospheric and dissolved oxygen.

The most stable oxidation state of chromium in aqueous solution is +3. Chromium(III) complexes have a d^3 configuration and are characteristically inert, undergoing slow ligand substitution reactions, enabling Cr(III) species to be present in solution even when they are thermodynamically unstable. This lack of reactivity has allowed extensive study of many Cr(III) complexes, most of which posses octahedral co-ordination, requiring great changes in ionic geometry for redox reactions to occur. Since there is only one way to arrange the three electrons, each in a low energy d_ϵ orbital, in the orbitals available of $Cr(H_2O)_6$, the Jahn-Teller effect does not operate to distort the regular octahedral structure. Hence substitution reactions involving Cr^{3+} must involve less symmetrical species. This difference often results in large activation energy barriers and accounts for the relative stability of Cr(III) species.

In non-complexing, e.g., F^- or ClO_4^-, strongly acidic media, electron transfer for the Cr(II)/Cr(III) couple is a simple, irreversible, one electron process. The reaction is so slow that in the potential range where the forward reaction is measurable, the reverse reaction rate is negligible. The Cr(III)/Cr(II) couple becomes more reversible if the ions are complexed, e.g., $Cr(CN)_6^{3-}/Cr(CN)_6^{4-}$, or when charge transfer assisting ligands, such as Cl^- or Br^- are present.

The standard rate constants have been found to increase in the order Cr^{3+}/Cr^{2+}, $CrCl^{2+}/Cr^{2+}$ and $CrBr^{2+}/Cr^{2+}$, with the latter couple being quasi-reversible [108]. The rate constant of the Cr^{3+}/Cr^{2+} couple at -0.41 V was 1.1×10^{-7} m s^{-1} over a wide range of halide and perchlorate media. Both the $CrCl^{2+}/Cr^{2+}$ and $CrBr^{2+}/Cr^{2+}$ couples had first order standard rate constants

that showed a weak dependency on bulk halide concentration. The $CrCl^{2+}/Cr^{2+}$ couple had a second order rate constant, obtained by accounting for surface chloride adsorption, with no bulk chloride concentration dependence.

Polarographic studies have suggested that the reduction of $CrCl^{2+}$ and Cr^{3+} occurred by two concurrent electron transfer processes, i.e., the electron transfer directly to the Cr^{3+} ion and electron transfer to Cr(II) from a Cr^{2+} ion produced at the electrode surface [109].

The $Cr(H_2O)_6^{2+}$ ion may exchange the labile water molecules for ions/molecules in its inner co-ordination sphere, hence its oxidation is sensitive to the composition of the supporting electrolyte [110]. The higher the dipole moment and polarisibility of the ion, the more likely it is to enter the inner co-ordination sphere of Cr^{2+}, presenting a lower energy barrier for electron transfer.

2.7.3 Vanadium

Vanadium exhibits oxidation states between +2 and +5 in aqueous solution. V(IV) is most common and is dominated by the formation of oxo-species and compounds with VO^{2+} groups. A potential - pH diagram is shown in **Figure 2.7.3.1** to summarise the predominant chemical and electrochemical equilibria in the V/H_2O system.

Figure 2.7.3.1. Potential - pH diagram for the V - H_2O system at 25 °C and activity = 0.01.

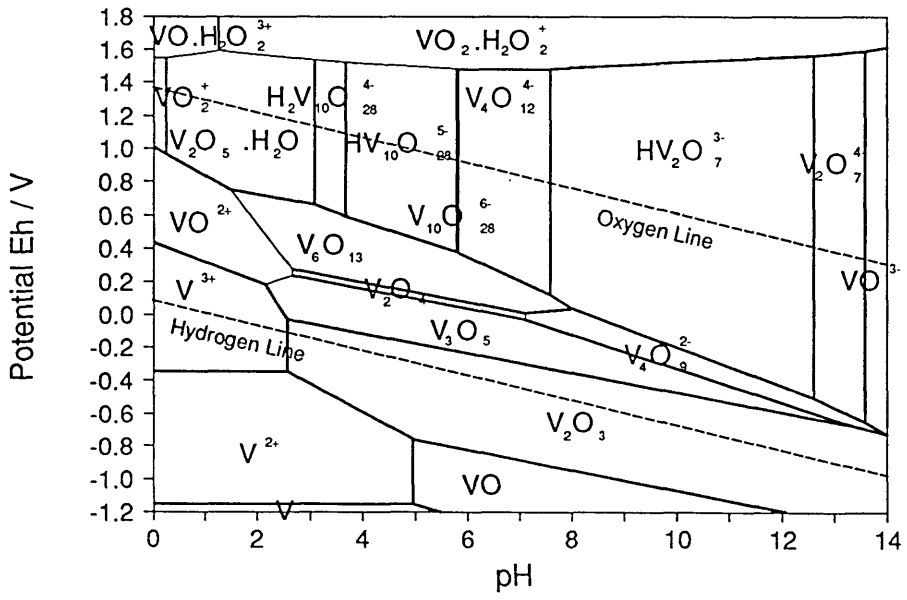

V(II) species are strong reducing agents that may be oxidised by water with concomitant hydrogen evolution. The violet V^{2+} ion can be prepared by dissolving the basic oxides VO or V_2O_2, or by reducing higher oxidation species, in acidic solutions. The hydrated cation $V(H_2O)_6^{2+}$ is kinetically inert, characteristic of its d^3 configuration, like the Cr^{3+} ion, producing slow substitution reactions. There are no thermodynamic data for V(II) complexes with SO_4^{2-}, Cl^-, Br^- or I^-, and due to its instability, very little is known of V^{2+} hydrolysis.

The blue V^{3+} cation is obtained by dissolving V_2O_3 in non-complexing acids or by the oxidation of V^{2+}. Above pH 1.5, significant hydrolysis occurs as follows:

$$V^{3+} + H_2O \Leftrightarrow VOH^{2+} + H^+ \qquad K = 8.7 \times 10^{-4}$$

$$VOH^{2+} + H_2O \Leftrightarrow V(OH)_2^+ + H^+ \qquad K = 1.4 \times 10^{-4}$$

$$2V^{3+} + 2H_2O \Leftrightarrow V_2(OH)_2^{4+} + 2H^+ \qquad K = 1.15 \times 10^{-4}$$

There is reasonable evidence for further hydrolysis although the identity of the species involved, e.g., $V_2(OH)_3^{3+}$, have not been established with certainty [111].

Little is known of V(III) complexes and the thermodynamic data is limited. The association constant of V^{3+} with SO_4^{2-} was measured spectrophotometrically:

$$V^{3+} + SO_4^{2-} \Leftrightarrow VSO_4^+ \qquad K = 29$$

This value agrees with potentiometric results that show that in 0.5 kmol m^{-3} H_2SO_4 that VSO_4 and V^{3+} are present in the ratio 5:1 [112]. Potential measurements suggest that in 1 kmol m^{-3} HCl, 82.3% of V(III) was present as V^{3+} and 17.7% present as VCl^+, assuming no further complexation.

The blue dioxide VO_2 is amphoteric, forming VO^{2+} and $HV_2O_5^{2-}$ in acidic and alkaline solutions respectively. Near neutral solutions contain complex species that are poorly characterised. Above pH 4, a grey hydrous oxide $VO_2.nH_2O$ is formed that dissolves without further OH^- addition to give $V_4O_9^{2-}$ [113], $V_{18}O_{42}^{12-}$ or $HV_2O_5^-$. Hydrolysis of VO^{2+} to $(VOOH)_2^{2+}$ has also been suggested [114]. VO^{2+} reacts with H_2S to precipitate VS_2 [115]. V(IV) also forms a series of hydrated sulphates [116].

V(IV) can be formed from the pH dependent reactions of V(III) and V(V) [117]. The most likely reactions are:

$$V^{3+} + VO_2^+ + H_2O \Rightarrow (VO)_2O^{2+} + 2H^+$$

V(IV) forms only weak halide complexes, decreasing in strength in the order $F^- > Cl^- > Br^- > I^-$.

$$VO^{2+} + Cl^- \Leftrightarrow VOCl^+ \qquad K = 0.04$$

Anionic V(IV) chloride complexes have been proposed in 12 kmol m^{-3} HCl.

VO_2^+ predominates when yellow V_2O_5 dissolves in strong acid. V(V) hydrolysis is complicated and the resulting species ill-characterised. $H_3V_2O_7^-$, $H_2VO_4^-$, HVO_4^{2-} and VO_4^{3-} were thought to form with increasing pH, but it is now evident that decanuclear species occur, i.e., $H_2V_{10}O_{28}^{4-}$, $HV_{10}O_{28}^{5-}$, $V_{10}O_{28}^{6-}$, together with $V_2O_7^{4-}$ and VO_4^{3-}.

In strongly acidic solutions each oxidation state, i.e. V^{2+}, V^{3+}, VO^{2+} and VO_2^+, can be produced by controlled potential electrolysis. Although V(V) can be reduced, through V(IV) and V(III) to V(II), it is convenient to consider each couple individually.

The standard reduction potential for the V(V)/V(IV) is given by:

$$VO_2^+ + 2H^+ + e \Leftrightarrow VO^{2+} + H_2O \qquad E^0 = 1.00V$$

Polarography of V(V) solutions is complicated by mercury oxidation, requiring quantitative prereduction of the oxidised mercury salt before the solution can be reduced itself. The reduction of V(V) to V(IV) is irreversible in most electro-inactive media.

The reactions of V(V) or V(IV) at platinum electrodes are influenced by the formation of platinum oxides and therefore require consistent pretreatment. There is chronopotentiometric evidence that the reduction of V(V) to V(IV) proceeds reversibly only at pre-reduced, clean Pt electrodes [118]. At pyrolytic graphite electrodes, a reasonably well defined irreversible double reduction wave, having a calculated formal potential of 0.159 V, was produced in 1 kmol m^{-3} H_2SO_4 and 1 kmol m^{-3} H_3PO_4 solutions, possibly reflecting a metastable intermediate or a non-equilibrated solution [119][120].

The oxidation of V(IV) and the reduction of V(V) were found to be diffusion controlled at a platinised Pt electrode in 1.0 and 1.8 mol m^{-3} $HClO_4$ [121]. The oxidation of V(IV) has not been attempted on mercury due to electrode instability at the required potential.

The V(III)/V(II) couple has been of special interest as the standard reduction rate constant is 10^{-5} m s^{-1} and is therefore polarographically quasi-reversible, i.e., the rate is controlled by both mass and charge transfer.

$$V^{3+} + e \Leftrightarrow V^{2+} \qquad E^0 = -0.255V$$

No sulphate or chloride complexes form, except at high anion concentrations, and therefore in acidic solution the behaviour is apparently straightforward, though irreversibility has been observed in non-equilibrated solutions. The low value of the rate constant is evident by the irreversible reduction of V^{3+} at a rotating mercury drop electrode [122].

Potentiocoulometric studies indicated a formal potential of -0.537 V for the V(III)/V(II) couple in 3 M H_2SO_4 [123]. Below pH 0, oxidations proceed at 100 % current efficiency on mercury, though at higher pH, irreversibility occurs due to the formation of metastable polynuclear species:

$$x\mathrm{V}^{2+} - ye \Leftrightarrow (x-y)\mathrm{V(II)}.y\mathrm{V(III)}$$

$$(x-y)\mathrm{V(II)}.y\mathrm{V(III)} \Leftrightarrow (x-y)\mathrm{V(II)} + y\mathrm{V(III)}$$

$$(x-y)\mathrm{V(II)} + y\mathrm{V(III)} - (x-y)e \Leftrightarrow (x-y)\mathrm{V(III)}.y\mathrm{V(III)}$$

The reaction above occurs in two steps forming monomeric and/or lower polymerised species [124]. The predominant polymeric species may be tetrameric. A second wave is produced at -0.95 V in solutions of pH 1 or more attributed to the reduction of VOH^{2+}, VO^{+}, $V_2(OH)_2^{4+}$ or higher polymeric species. It has been proposed that dimeric V(II) and V(III) are present in 5 mol m^{-3} vanadium solutions [125].

In acidic media, a potential dependent background current may be present due to the reduction of H^{+} to H_2. In 1 kmol m^{-3} H_2SO_4 and 2 kmol m^{-3} HSO_4^{-} media, a background current was thought to be due to the reduction of H^{+} which serves as a bridge between a V(II) bisulphate complex and the electrode, followed by chemical reprotonation of the resulting sulphate complex.

The reduction of V(IV) at a dropping mercury electrode (DME) is totally irreversible and appears to proceed directly to V(II). The reduction of V(IV) to V(III) is so slow that to achieve a detectable current, the applied overpotential must be increased to a value at which reduction of V(III) to V(II) can occur.

$$\mathrm{V(IV)} \xrightarrow{k_1} \mathrm{V(III)} \xrightarrow{k_2} \mathrm{V(II)} \qquad k_2 \gg k_1$$

V(III) is then formed by the homogeneous reaction between V(II) and V(IV) [126].

$$\mathrm{VO}^{2+} + \mathrm{V}^{2+} + 2\mathrm{H}^{+} = 2\mathrm{V}^{3+} + \mathrm{H_2O}$$

There is also evidence for the formation and reaction of dinuclear V(III) species according to [127]:

$$V^{2+} + VO^{2+} \Rightarrow VOV^{4+}$$

$$VOV^{4+} + H^{+} \Rightarrow V^{3+} + VOH^{2+}$$

$$VOH^{2+} + H^{+} \Rightarrow V^{3+} + H_2O$$

The relationship between current and potential for the reduction of V(IV) at a DME had two parallel sections of about equal gradient, differing by a factor of 2 in current. At potentials less than -0.4 V, V(IV) was reduced to V(III), but at -0.6 V, V(II) was produced. The mechanisms for the two sections are thought to be due to the reactions:

$$VO^{2+} + H^{+} + 2e \rightarrow VOH^{+} \qquad \text{Rate Determinig}$$

at -0.4 V and,

$$VO^{2+} + H^{+} + 2e \rightarrow VOH^{2+} \qquad \text{Rate Determining}$$

$$VOH^{2+} + H^{+} \rightarrow V^{3+} + H_2O \qquad \text{Fast}$$

$$V^{3+} + e \rightarrow V^{2+} \qquad \text{Fast}$$

at -0.6 V, although the rate determining reactions above may represent reprotonation of VO^{2+} to VOH^{3+} and subsequent reduction.

Therefore, V(IV) and V(II) may be formed by VO_2^{+} electrolysis at -0.4 and -0.6 V respectively. V(III) is produced most efficiently by reduction of V(IV) at less than -0.6 V, to produce V(II), which reacts chemically to form V(III). The residual V(II) may then be oxidised at -0.25 V. During the initial stage of V(IV) reduction, at < -0.6 V, V^{3+} is the major product, resulting in a current increase, as $k_2 >> k_1$.

CHAPTER 3. EXPERIMENTAL

Unless otherwise mentioned, all aqueous solutions were prepared using water from a Millipore Milli-Q Water Purification System. All pH readings were measured by a Corning pH meter 120 with a glass electrode. The pH meter was calibrated frequently with pH 4.0, 7.0 and 9.2 buffer tablets (BDH) that were dissolved in 100 cm^3 of water. All oxygen concentrations were measured with a KENT EIL 7135 Dissolved Oxygen Meter and electrode. Calibration of the oxygen meter against air saturated water and nitrogenated water was performed as a control every time a set of measurements were made. Air saturated water was produced by stirring water for two hours without allowing the air/solution interface to break. The measured value was used to calibrate the instrument at the measured temperature of the water from tables supplied with the instrument; typically a value of 10.15 ppm oxygen was used at a room temperature of 19 °C. Nitrogenated water was produced by bubbling nitrogen (BOC, oxygen free) through stirred water in a closed vessel for half an hour. Before each experiment, all glassware was rinsed thoroughly with water. If specially clean glassware was required, then it would first be soaked in nitric acid before being rinsed with water. All reagents used were BDH Chemicals Ltd., AnalaR grade purity, unless otherwise mentioned.

3.1. Production of Electrostatically Stabilised Colloids

Electrostatically stabilised colloids were prepared from the reduction of 250 cm^3 of a 5 mol m^{-3} $CuCl_2.H_2O$ solution by the addition of a stoichiometric excess of dimethylaminoborane (DMAB) (as supplied by Lea Ronal), i.e., 12.5 cm^3 of a 0.68 kmol m^{-3} DMAB solution. Filtration of the larger particles from the solution was done using vacuum filtration through 45 μm filter paper (Whatman, 541). Hydrochloric acid was added after reduction by DMAB to change the pH. Another colloid was prepared in which sodium hexametaphosphate was added to 125 cm^3 of 10 mol m^{-3} copper chloride solution prior to reduction as 125 cm^3 of 10 mol m^{-3} $Na_6(PO_3)_6$ solution.

3.2. Measurement of Size and Zeta Potential of Colloids

Electrophoretic mobilities of colloidal dispersions were measured using a Malvern Instruments Ltd., Zetasizer IIc, which uses the technique of laser doppler anemometry. As κa was in the range 10 to 100 for most particles, the zeta potential, ζ, was calculated

from the electrophoretic mobility obtained, u_E, using mobility software supplied by O'Brien and White [53]. This software is based on the complete numerical solution of the set of coupled differential equations that govern the flow field around the colloidal particle, the convective and diffusive motions of ions in the double layer, a complete account of ionic relaxation effects, the electric double layer interactions between the colloidal particle and ions in the diffuse layer and surface conductance effect of ions in the Stern layer.

In-situ particle size analysis was also measurable on the Zetasizer IIc which used the technique of photo-correlation spectroscopy. This measures the equivalent hydrodynamic diameter of the scattering particles. These entities could be primary particles or agglomerates depending on the solution conditions. As measurement of particle size using the Zetasizer was found to be unsatisfactory due to the imposition of an assumed log-normal size distribution on the data, later size analysis was measured using the Malvern 4700 Photo-correlation Spectrophotometer (see **Section 3.24**).

3.3. Viscosity Measurement

All viscosities were measured using a Carrimed Controlled Stress Rheometer, which employs the rotating drum method of viscosity measurement.

3.4. Iso-electric Point (IEP) Determination of Gelatin

The method used to determine the iso-electric points (iep) of gelatins used in the experimental work was based on a method devised by Janus *et al.* [128] and involved deionising a 5 % gelatin solution at 35 ^{0}C by passing it through a mixed resin bed. The resins recommended were Amberlite IR120 and IRA 400. Eastoe and Courts [129] recommended mixing the resins in the proportions of 5 volumes of IRA 400 to 2 volumes of IR120.

100 cm^3 of a mixed resin, Duolite MB 6113 (BDH Chemicals) was placed in a column and was regenerated by first backwashing to separate the less dense anion exchange resin from the cation exchange resin. 4 bed volumes of 5 % NaOH solution was then passed down the column of resin. A tube was inserted down to the cation exchange resin layer and 5 bed volumes of 5 % H_2SO_4 solution were passed through it. The whole bed was then washed thoroughly in water.

Gelatin solutions were made up in water that was heated to 60 °C prior to gelatin addition. 10 g of gelatin was added slowly to 200 cm^3 of water, with vigourous stirring of the solution, to ensure full dispersion. 100 cm^3 of the regenerated resin was added to the solution then solution and resin were stirred magnetically under nitrogen at 35 °C. 10 cm^3 samples were pipetted out from the solution and their pH recorded at five minute intervals. When several consecutive stable readings were achieved, usually after thirty minutes, the value they reached was taken as the iep of the gelatin.

3.5. Fourier Transform Infrared (FTIR) Analysis of Gelatin and Colloid

Fourier Transform Infrared (FTIR) analysis of the 'P87' gelatin, the 2392 gelatin (both mentioned in **Section 4.2**) and a sample of copper colloid concentrate (see **Section 3.6**), was carried out using a Perkin Elmer 1700 FT-IR Spectrometer. The samples were placed in a liquid holder which surrounded a ZnSe prism. The liquid holder was placed in a 25 reflection Attenuated Total Reflectance (ATR) unit to obtain a good signal. The liquid holder uses the principle of the evanescent wave technique, in which a wave reflecting down the length of the prism also penetrates into the solution about 1 nm or so, allowing analysis of the liquid near the prism surface. The FTIR analysis of any protein is very difficult due to the Amide I and Amide II peaks being in the same wavelength range as a water absorption peak. This problem was obviated by using the empty cell for the background spectrum, averaging several scans to yield low noise data, then obtaining the buffer spectra and subtracting the gelatin and buffer spectra from this. As the resultant signal was small, careful cleaning of the cell was required before adequate results could be obtained. The cell parts were immersed in a warm 10 mol m^{-3} sodium dodecyl sulphate solution and rinsed prior to measurement to prevent contamination by organic material. The gelatin solutions were prepared at 2.1 g dm^{-3} gelatin. The as-made colloid was too dark for FTIR analysis and had to be diluted about 200 times with water prior to measurement.

3.6. Manufacture of Copper Colloid Concentrate

Copper colloid concentrate was manufactured in the laboratory according to the Lea Ronal patent [5]. 2 g dm^{-3} of gelatin was dissolved in warm water and added to 20 g dm^{-3} of $CuSO_4.5H_2O$ solution. 20 ppm of palladium ammonium chloride was added and the

pH was adjusted to 2.4 with 25 % H_2SO_4. A solution of 5 g dm^{-3} of dimethylaminoborane (DMAB) was prepared separately and then added to the copper concentrate solution with agitation. After stirring for one hour the colloid was left for 24 hours. 10 $cm^3 dm^{-3}$ hydrazine hydrate was added and after an additional 24 hours, a surfactant was added, to aid colloid deposition. DMAB, gelatin (labelled 'P87') and $Pd(NH_3)_4Cl_2$ were supplied by Lea Ronal as the actual products used in the industrial process for manufacture of copper colloid concentrate. Their purity was unknown, but the same ratios of each were used in the laboratory as in the industrial manufacture of copper colloids.

3.7. Assessment of the Iso-electric Point (IEP) of Colloid

To assess the iso-electric point (iep) of copper colloidal particles, a 1 cm^3 aliquot of prepared concentrate (see **Section 3.6**) was taken and diluted 250 times with water. The colloid was diluted so that it could be measured by the Zetasizer (see **Section 3.2**). Malvern [130] recommend particle concentrations of about 0.01 % v/v or lower for adequate measurement. Dilution by a factor of 250 gave particle concentrations of about 0.009 %. Dilute 10 % sulphuric acid solution was added to the dilute colloid until it reached pH 2. A 10 cm^3 sample was extracted and its zeta potential measured (see **Section 3.2**). A 1 kmol m^{-3} sodium hydroxide solution was then added to the residual colloid in order to increase its pH without changing its ionic strength significantly. 10 cm^3 samples were taken over the range pH 2 - 13 and their zeta potentials measured.

3.8. Analysis of Colloids by UV/Visible Absorption Spectrophotometry

Attempts to measure the absorption spectrum of the copper colloid concentrate (see **Section 3.6**) in a conventional 1 cm path length cell of a Hewlett Packard 8451A Diode Array Spectrophotometer were hindered by the strong absorption of the colloid, which required 250 fold dilution with water to give an adequate absorption spectrum. The resultant spectrum showed very broad flat peaks which indicated that light scattering from the particles was occurring and so an integrating sphere was used which gave a much clearer peak at 100 times dilution. The integrating sphere is a device that fits over the cell and reflects scattered radiation back towards the collector, thus enhancing the signal. An alternative to dilution of the colloid was to use a very thin cell. Only cells down to 1 mm

path length were available and so a 0.01 cm^3 drop of colloid was placed on a microscope slide and a second slide placed on top which spread out the drop. The path length was estimated at 0.01 mm, based on the fact that the drop spread out over the area of the slides.

In order to monitor the reduction of Cu^{2+} by DMAB, the colloid concentrate was prepared at 10 times dilution of its normal concentration (see **Section 3.6**) prior to DMAB addition. On addition of DMAB, also at 10 times dilution of its normal concentration, the spectrum was automatically measured every 3 minutes over 30 minutes in a 1 cm path length cell. This experiment was also repeated at 100 times dilution. Bubbles of hydrogen occurred as the colloid formed, making it necessary to remove and shake the cell prior to measurement.

3.9. Alterations to Copper Colloid Concentrate

Various alterations were made to the basic method of copper colloid concentrate manufacture (see **Section 3.6**) which are listed below.

Nit Norm This colloid was manufactured in a sealed flask under nitrogen (BOC, oxygen free). All solutions were dearaeted prior to gelatin addition, as it proved difficult to blow nitrogen through gelatin solutions due to the formation of surface foam.

Nit x3Gel This colloid was prepared by repeating the *Nit Norm* conditions but increasing the amount of gelatin present by three.

Nit Box This colloid was prepared by repeating the *Nit Norm* conditions but all operations took place in a normal vessel, within a dry box containing a nitrogen atmosphere.

Oxygen This colloid was prepared by bubbling O_2 through the $CuSO_4$ solution prior to gelatin addition. If O_2 was pumped through during DMAB addition, then the colloid agglomerated and sedimented.

pH 8 The pH of this colloid was initially buffered to pH 8 with a 1 kmol m^{-3} borax (Hopkin and Williams Ltd., AnalaR) solution.

Buffered The pH of this colloid was buffered initially to pH 8 with a 1 kmol m^{-3} borax (Hopkin and Williams Ltd. AnalaR) solution but instead of being left, it was monitored closely for changes in pH. If the pH fell below 8 then more of the borax solution was added to buffer it back above this value.

Sonic Sonication by inserting a Sonics and Materials Inc. V1A sonic probe into the reaction vessel during DMAB and hydrazine addition.

All colloids prepared under nitrogen were stored in 500 cm^3 plastic bottles in a nitrogen box. All other colloids were stored in 500 cm^3 plastic bottles under air in a dark cool environment.

3.10. Thermal Stability Test

50 cm^3 of concentrate was pipetted into a 500 cm^3 volumetric flask and diluted to the mark with water to make the stock solution. 150 cm^3 of the stock solution was pipetted into a conical flask and 3 g of potassium persulphate (Aldrich, Analytical grade) were added to this prior to boiling for 5 minutes. After cooling to 20-30 °C, the solution was titrated to a green end point with 0.1 mol dm^{-3} EDTA (disodium salt) using a few drops of 1-(2-pyridylazo)-2-napthol, PAN (BDH, Lab. Reagent) indicator. EDTA is a more powerful 1:1 ligand for Cu^{2+} ions than PAN, which goes green when no more free Cu^{2+} ions are available. From the result of the titration the *Initial Copper* could be calculated:

$$\textit{Initial Copper}\ (g\ dm^{-3}\ Cu) = \text{Titre}\ (cm^3) \times \text{mol}\ dm^{-3}\ \text{EDTA} \times 4.27$$

250 cm^3 of the remaining stock solution was kept at 50 °C for 24 hours before being stood for a further 24 hours at room temperature. 200 cm^3 of the solution was decanted into a beaker without disturbing any sediment and the *Final Copper* was analysed as for *Initial Copper*. The total *Copper Loss* was calculated from

$$\textit{Copper Loss} = \textit{Initial Copper} - \textit{Final Copper}$$

Copper Loss indicates the relative stability of the colloid, i.e., the greater the value, the more unstable the colloid.

3.11. The Effect of Oxygen on DMAB, Hydrazine and Gelatin Solutions

In order to assess the effect of oxygen on the components of the copper colloid concentrate, three solutions containing DMAB, hydrazine hydrate and 'P87' gelatin were made with water and stored in 500 cm^3 plastic bottles under air in a cool dark environment. Another three identical solutions were made up with water that was nitrogenated (BOC, oxygen free) until the O_2 concentration was less than 2 x 10^{-6} kmol m^{-3}, i.e., the lower detection limit of the oxygen meter, and stored in a nitrogen box. All solutions, except

DMAB, were at their initial concentrations as used in the Lea Ronal proprietary process (see **Section 3.6**), i.e., 8.50 $cm^3 dm^{-3}$ hydrazine and 2.10 g dm^{-3} gelatin. The DMAB solution was made at a lower starting concentration (3.00 g dm^{-3} DMAB) than the Lea Ronal solution (6.00 g dm^{-3} DMAB) to account for DMAB that was oxidised immediately on reduction of Cu^{2+} ions. Potential measurements were made with a saturated calomel electrode (S.C.E.) relative to a platinum electrode using the Corning pH meter 120 in potential mode.

3.12. Monitoring of the Concentrations of DMAB and Hydrazine Solutions

Three solutions were made, containing *hydrazine*, *DMAB* and DMAB after reducing Cu^{2+} ions (*DMAB + Cu*). The *hydrazine* solution was made at a similar concentration, 11.78 g dm^{-3} hydrazine hydrate to the starting concentration of the Lea Ronal colloid concentrate, 8.5 $cm^3 dm^{-3}$ hydrazine (see **Section 3.6**). The *DMAB* solution was made at a lower starting concentration, 2.14 g dm^{-3} DMAB, than the Lea Ronal solution, 6.00 g dm^{-3} DMAB, to account for DMAB that was oxidised immediately on reduction of Cu^{2+} ions. The *DMAB + Cu* solution was made by using 20 g dm^{-3} $CuSO_4.5H_2O$ with 0.25 g dm^{-3} $Pd(NH_3)_4Cl_2$ adjusted to pH 2.4 with sulphuric acid, i.e., the same solution used by Lea Ronal but with no gelatin. 6.00 g dm^{-3} DMAB was added to this solution and copper metal precipitated immediately. The concentration of DMAB was measured about an hour after addition to the solution and was found to be almost zero. The titrations for DMAB and hydrazine are described below.

Titration for DMAB:

1. 25 cm^3 of sample was pipetted into a 250 cm^3 conical flask.
2. 25 cm^3 of a 0.4 N KIO_3 solution was pipetted into the flask.
3. 2g KI and 20 cm^3 of a 6N H_2SO_4 solution were added to the flask.
4. 1 cm^3 of 2 g dm^{-3} starch (Hopkin and Williams Ltd., AnalaR) solution was added to the flask as an indicator and the solution was titrated to a clear end point with a 0.1 N sodium thiosulphate solution.

$$\frac{(cm^3 \quad KIO_3 \times (N \quad KIO_3) - cm^3 \quad Na_2S_2O_3 \times (N \quad Na_2S_2O_3)) \times 9.82}{cm^3 \quad \text{Sample Size}} = \text{DMAB} \quad g\,dm^{-3}$$

Titration for hydrazine:

1. 5 cm^3 of the sample was pipetted into 50 cm^3 volumetric flask which was then filled to the mark with water.
2. 25 cm^3 of this solution was pipetted into a 250 cm^3 conical flask.
3. 5 cm^3 of a 10 % HCl solution and 3g of sodium bicarbonate were added to the flask.
4. The solution was titrated to a permanent yellow end point with a 0.1 kmol m^{-3} iodine solution.
6. cm^3 dm^{-3} hydrazine = Titre x kmol m^{-3} iodine x 6.4

The 0.1 N sodium thiosulphate solution was prepared by adding 24.8 g of sodium thiosulphate to 1 dm^3 of freshly boiled and cooled water to which was added 0.1 g of sodium carbonate. The solution was stored in a cool dark place. The solution was standardized with potassium iodate. The potassium iodate standard was prepared by drying potassium iodate at 80 °C overnight and then dissolving 0.8917 g in 250 cm^3 of water. 25 cm^3 of this solution were transferred to a 250 cm^3 conical flask to which was added 1 g of KI and 5 cm^3 of 1 kmol m^{-3} sulphuric acid solution. The solution was titrated with the thiosulphate solution to a faint straw colour to which a few cm^3 of starch solution were added. The titration was continued until the solution went from blue to colourless.

The starch solution was prepared by mixing 1 g of soluble starch (Hopkin and Williams Ltd., AnalaR) and 0.005 g of mercuric iodide (which acted as a preservative) with a little water to make a paste, which was made up to 500 cm^3 with boiling water.

The 0.1 kmol m^{-3} iodine solution was prepared by dissolving 12.7 g of iodine in 1 dm^3 of water to which 40 g of KI was added. The solution was tightly stoppered and kept in a cool dark place.

3.13. Scanning Electron Microscopic (SEM) Analysis of Colloid Size

The sizes of copper colloid particles determined by scanning electron microscopy (SEM) were compared with size distributions obtained *in-situ* by photo-correlation spectroscopy on a Malvern Instruments Ltd., Zetasizer IIc. The procedure was as follows: three aluminium SEM stubs were polished with 0.3 μm then 0.075 μm elementary particle size, highly pure aluminium oxide (BDH Chemicals), then rinsed with water. One was coated with carbon by heating a carbon filament in a vacuum chamber, the other two were left blank. A small drop of the *Nit Norm* (see **Section 3.9**) colloid sample was then put on the stub, smeared over the surface with a microscope slide and left to dry. One sample

was diluted by a factor of ten before being put on the stub. The stubs were then coated with either gold or carbon by using the appropriate filament in a vacuum chamber. An analysis of the results revealed that the stub that was primarily coated with carbon before colloid deposition and then re-coated with carbon, denoted C/C, gave the best image and therefore the three stubs were cleaned, repolished and the freshly made *Nit Box* (see **Section 3.9**) colloid sample was analysed with C/C coating on the stubs.

3.14. Analysis of Colloid Dispersion Media

Successful separation of the dispersed phase from continuous phase was effected by vacuum filtration of the *Nit Box* and *pH8* colloids (see **Section 3.9** for details) through 0.1 μm Whatman cellulose filter paper, after it was found that centrifuging was inadequate. The UV/Visible absorption spectra of the colourless dispersion media was obtained using a Hewlett Packard 8451A Diode Array Spectrophotometer. The spectra of the dispersion media of the colloids were compared to that of a similarly filtered 0.1 kmol m^{-3} $CuSO_4.5H_2O$ solution which had been reduced to a copper precipitate by the addition of a 0.5 cm^3 m^{-3} hydrazine hydrate solution, i.e., the same proportions as for the colloid concentrate (see **Section 3.6**). On reduction with hydrazine, the copper sulphate solution turned dark blue and a precipitate formed immediately. On filtration it was found that the filtrate became cloudy indicating that a slow reduction was still occurring. After 48 hours the reduction was complete as no further cloudiness occurred in the filtrate after filtration. Several solutions were also prepared for spectral comparison; $CuSO_4.5H_2O$ solutions at 0.1 and 0.2 kmol m^{-3} and a 0.1 kmol m^{-3} $CuSO_4.5H_2O$ solution to which 2.1 g m^{-3} "P87" gelatin and 0.25 g dm^{-3} $Pd(NH_3)_4Cl_2$ had been added, then adjusted to pH 2.4 with sulphuric acid, i.e., the copper colloid concentrate solution (see **Section 3.6**)

3.15. Analysis of the Effectiveness of Rinsing by X-ray Photoelectron Spectroscopy (XPS)

A copper colloid concentrate was prepared (see **Section 3.6**) and plated onto two 1 cm^2 glass slides using the Lea Ronal plating procedure, i.e., 30 cm^3 of the concentrate was added to 70 cm^3 water and warmed to 28-32 °C, the glass slides were then immersed in the colloid for 15 minutes with slow stirring of the colloid. One slide was rinsed using the Lea Ronal rinsing procedure; i.e., the slide was rinsed twice for 1.5 minutes in water and

once for 1.5 minutes in 50 cm^3 dm^{-3} hydrazine hydrate adjusted to pH 6 with orthophosphoric acid. The other slide was left unrinsed. The surfaces of both slides were then analysed using X-ray Photoelectron Spectroscopy (XPS) on a VG Escalab II.

3.16. Steric Stabilisation of Copper Colloids

In order to study the mechanisms of stability for copper colloids, several natural and synthetic polymers were substituted for gelatin in the copper colloid concentrate solution (see **Section 3.6**). The copper colloid concentrate solution was prepared with the following polymers substituted for gelatin:

1) 0.01 to 2.4 g dm^{-3} of poly(ethylene glycol) of MM 200 and 20 000 (BDH Chemicals Ltd.) and poly(ethylene oxide) of chain lengths MM 300 000 and 5 000 000+ (BDH Chemicals Ltd.).

2) A solution of butyl ethyl ether (Aldrich, Laboratory Reagent) was prepared by dissolving 0.3 g in 20 cm^3 acetone then diluting to 140 cm^3 with water. This solution was substituted for gelatin in volumes from 20 cm^3 to 60 cm^3 which were added to 350 cm^3 samples of the colloid concentrate solution prior to reduction with DMAB.

3) A solution of hexaethyleneglycol dodecyl ether (Aldrich, Laboratory Reagent) was prepared by dissolving 0.04 g in 10 cm^3 of acetone before addition to the 350 cm^3 of the colloid concentrate solution. The solution turned cloudy and cleared only after addition of sulphuric acid to decrease the pH to 2.4.

4) 0.02 to 0.2 g dm^{-3} 3-Mercaptopropionic acid, MPA (Aldrich Chemicals), which was chosen for its mercapto group, known to have an affinity for forming strong bonds with copper, and its carboxyl group, known to hydrogen bond to glass.

5) 0.428 g dm^{-3} β-cyclodextrin (BCD) (supplied by J. Pagington of Cyclodextrin News).

6) 0.07 to 7 g starch (soluble, Hopkin + Williams Ltd., AnalaR) and 0.07 to 7 g dextrin (yellow, BDH Technical).

7) 0.5 g of polyethylene(propylene oxide), MM 12 000 (ICI, Pluronic) was added to 140 cm^3 of copper colloid concentrate solution.

3.17. Stabilisation of Copper Colloids in Organic Dispersion Media

100 cm^3 of copper colloid concentrate was prepared (see **Section 3.6**) and was added to 100 cm^3 of iso-octane to which 1 cm^3 of Versatic acid (C10) (Fluka, purum) or 1 cm^3 of erucic acid (Fluka, puriss.) had been added. The solutions were sonicated with a Sonics and Materials Inc. V1A sonic probe which was inserted into the reaction vessel until an emulsion formed (approximately five minutes). The solutions were then allowed to separate.

In a further attempt to stabilise copper particles in a non-aqueous medium, 0.205 g of $CuSO_4.5H_2O$ was dissolved in 250 cm^3 methanol but it was found that $Pd(NH_3)_4Cl_2$ was only sparingly soluble. 5 cm^3 erucic acid (C22) (Fluka, puriss.) was added to the methanol as a stabiliser. 15 cm^3 of a 115 g DMAB dm^{-3} methanol solution was used as the reductant.

3.18. Monodisperse Colloids of Copper Hydrous Oxide

In an attempt to form a monodisperse colloid of copper hydrous oxide by forced hydrolysis as suggested by Matijevic [131], a solution was prepared which contained 40 mol $Cu(NO_3)_2$ + 0.2 kmol EDTA (disodium salt) + 1.2 kmol m^{-3} NaOH. 100 cm^3 of solution was aged at 100 °C for 70 minutes in a salted water bath. A similar solution, except for the addition of 0.24 g of 'P87' gelatin when the solution was at 60 °C, was also aged in this way.

3.19. Copper Ion Reduction by Regenerative Aqueous Reductants

Copper colloid production was attempted using Cr(II) as a reductant. The Cr^{2+} ion solution (about 0.5 kmol m^{-3}) was produced by reduction of a chromium(III) sulphate solution, in a packed bed electrode of vitreous carbon chips. 25 cm^3 of copper colloid concentrate solution was prepared (see **Section 3.6**), to which 200 cm^3 of Cr(II) solution was added. The solution turned dark immediately and was left stirring for 72 hours, after which time, large, visible particles were present in a dark green solution. Addition of hydrazine to the solution precipitated the pale violet compound $CrCl_2.(N_2H_4)$. A similar solution was prepared to which no hydrazine was added. A third colloid was prepared in which palladium was omitted from the copper solution.

Copper reduction was also attempted with V(II). Solutions of V(II) were difficult to produce. V_2O_5 was only sparingly soluble in a 49 % sulphuric acid solution, and only a 14 mol m^{-3} V(V) solution was formed. 12 g of zinc powder was added to 100 cm^3 of solution and it was left overnight under nitrogen (BOC, oxygen free). After this time, there was only a blue V(IV) solution present with unreacted zinc present. The solution was vacuum filtered with 1.6 μm glass microfibre filter paper (Whatman, GF/A) and a further 1.75 g of zinc was added to the filtrate causing the solution to turn violet, indicating the presence of V(II), almost immediately. 100 cm^3 of the V(II) solution was added to 350 cm^3 of the copper colloid concentrate solution under nitrogen to prevent V(II) oxidation. The solution turned black immediately and was left overnight. Hydrazine was added after 18 hours and a light blue precipitate formed immediately. This was filtered off using filter paper (Whatman, 541) without disturbing the black colloid. Addition of hydrazine to V(IV) solution formed the same light blue precipitate which seemed to be a solid VO^{2+}/N_2H_4 compound. Addition of a small amount of ammonia to this solution gave a brown solution which was evidence of V(IV). Therefore, it seems that the addition of hydrazine to colloids prepared using V(II) is unnecessary.

3.20. Other Alternative Reductants to Dimethylaminoborane (DMAB)

Methanal and hydrazine were investigated as alternative reductants to DMAB.

The reduction of copper ions directly onto silica using methanal was attempted. 50 cm^3 of a 37 % methanal solution was added to 50 cm^3 of a 0.14 kmol m^{-3} $CuSO_4.5H_2O$ solution. A cleaned 1 cm x 3 cm microscope slide was suspended in 100 cm^3 of Fehling's solution to which 50 cm^3 of methanal had been added and the solution was heated at 50 °C overnight. Fehling's solution was prepared according to the CRC Handbook [106]. 34.66 g of $CuSO_4.5H_2O$ was dissolved in 500 cm^3 of water. 173 g of potassium sodium tartrate and 50 g of NaOH were dissolved in 500 cm^3 of water. Before use, the two solutions were added together in equal volumes to form $Na_2[(OOC.CHO)_2Cu]$.

1 cm^3 of hydrazine hydrate was added to 80 cm^3 of water and this solution was added to 400 cm^3 of prepared copper colloid concentrate solution (see **Section 3.6**) instead of DMAB.

3.21. Potentials of Copper Colloidal Particles

Potentials of copper particles of the colloids *Nit Norm, Nit Box* and *Nit x3Gel* (see **Section 3.9**) were inferred from measurement of the potential of a copper (99.99 %, Matthey, Specpure) macro electrode against a saturated calomel electrode (S.C.E.) in the colloid. Potentials were measured using a Corning pH meter 120 in potential mode. Stable values were more difficult to achieve with colloids stored in air, probably due to the reduction of dissolved oxygen.

3.22. Analysis of the Oxidation of Dimethylaminoborane (DMAB) using Cyclic Voltammetry

Cyclic voltammetry experiments were performed with microcomputer controlled equipment comprising of a laboratory-built bipotentiostat, driven by a Hi-Tek Instruments wave-form generator. Current/potential data were recorded by an IBM PC compatible microcomputer with a Metrabyte DASH A/D card using Lotus Measure software.

Several electrodes were used:

The copper electrode consisted of a poly-crystalline 2.55 mm radius copper rod with a purity of 99.99 % (Matthey, Specpure). It was fixed within an Araldite epoxy resin tube and could be mounted on an electrode holder that comprised a copper wire inside a glass tube, ending in a copper stud. Contact between the stud and the rod was achieved via silver loaded epoxy adhesive (RSC Components Ltd.). Before each experiment the electrode was polished with 0.075 μm elementary particle size, highly pure aluminium oxide, rinsed with water and immediately transferred into the electrolyte.

The platinum electrode consisted of a platinum flag attached to a platinum wire sealed in a glass tube. The electrode was lacquered with Lacomit (W. Cannings Ltd.) except on the active surface area (0.865 cm^2) facing and parallel to the counter electrode. The relative roughness of the surface are was measured using the electrochemical technique of Sawyer [132]. To ensure that the surface of the electrode was non-oxidised, the electrode was cycled between O_2 and H_2 evolution and then into the double layer region prior to any experiment.

The palladium coated platinum electrode was manufactured according to the method reported by Bucur and Stoicovici [133]. The platinum flag electrode was immersed in 50 cm^3 of a 2 % $Pd(NH_3)_4Cl_2$ in 1 kmol HCl solution and connected to a Weir 400 T power source which was used to pass a cathodic deposition current of 3 mA until the surface of

the electrode was no longer shiny (about 30 minutes). The electrode was then rinsed with water, dried in air and lacquered with Lacomit except on the active surface area (0.865 cm^2) facing and parallel to the counter electrode.

The palladium electrode consisted of a palladium flag attached to a palladium wire, sealed in a glass tube. The electrode was lacquered with Lacomit except on the active surface area (1.44 cm^2) facing and parallel to the counter electrode.

The potential of the electrode was measured via a Luggin capillary with respect to a saturated calomel electrode (+241 mV vs. the standard hydrogen electrode, S.H.E.). The tip of the Luggin probe was placed close to the working electrode surface to minimise any uncompensated ohmic drop due to solution resistance between the reference electrode and the working electrode. Potentials were calculated by the computer to refer to S.H.E. A platinum flag electrode was used as a counter electrode.

The background electrolyte consisted of 100 cm^3 of 50 mol m^{-3} potassium hydrogen pthalate solution to which a few drops of sulphuric acid were added, whilst stirring, until pH 2.4 was reached. DMAB was added to this solution as required.

The cell was deareated by bubbling high purity nitrogen (BOC, oxygen free) through the solution.

3.23. Electrode Impedance Spectroscopy of a Copper Surface

The electrode impedance spectroscopy experiments were performed with a microcomputer controlled apparatus comprising a Solartron 1250 Frequency Response Analyser connected to the electrochemical cell via a 1286 Electrochemical Interface. For experiments at low frequencies, the cell was placed in a Faraday Cage to decrease adventitious electromagnetic noise. Conventional electrochemical measurements could also be performed with this equipment. The arrangement of the electrochemical cell is shown below.

Figure 3.23.1. Electrode impedance spectroscopy (EIS) electrochemical cell.

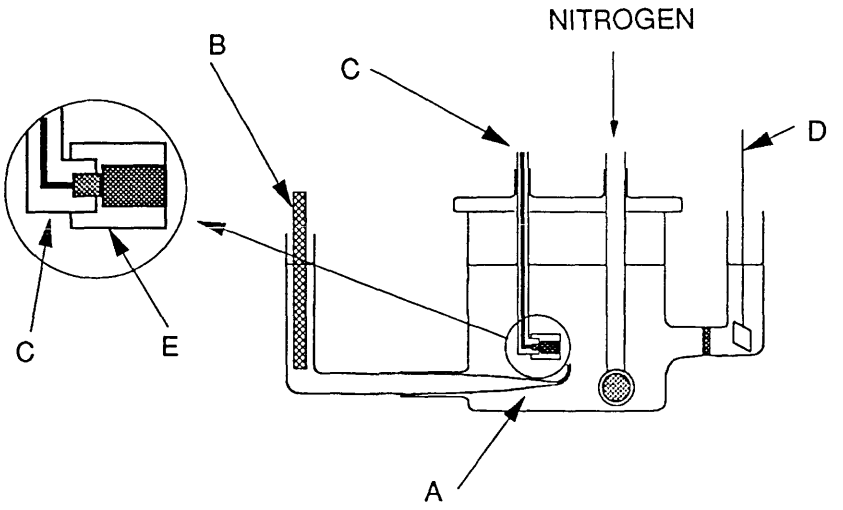

The electrode (E) was a poly-crystalline 2.55 mm radius copper rod with a purity of 99.99 % (Matthey, Specpure). It was fixed within an Araldite epoxy resin tube and could be mounted on an electrode holder (C) that comprised a copper wire inside a glass tube, ending in a copper stud. Contact between the stud and the rod was achieved via silver loaded epoxy adhesive (RSC Components Ltd.). Before each experiment the electrode was polished with 0.075 μm elementary particle size, highly pure aluminium oxide (BDH Chemicals), rinsed with water and immediately transferred into the electrolyte. The potential of the electrode was measured via a Luggin capillary (A) with respect to a saturated calomel electrode (B) (+241 mV vs. the standard hydrogen electrode, S.H.E.). Potentials were calculated by the computer to refer to S.H.E. A platinum flag electrode (D) was used as a counter electrode.

Depending on the pH required, the background electrolyte consisted of:

pH 2.9 electrolyte - few drops of sulphuric acid to 100 cm^3 of 50 mol m^{-3} potassium hydrogen pthalate solution whilst stirring until pH 2.4 was reached.

pH 9 electrolyte - few drops of sulphuric acid to 100 cm^3 of 13 mol m^{-3} borax (Hopkin and Williams Ltd., AnalaR) solution whilst stirring until pH 9 was reached.

The cell was deareated by bubbling high purity nitrogen (BOC, oxygen free) through the solution.

3.24. Size Analysis of Colloid Particles using Photo-correlation Spectroscopy

Due to the high light absorption of copper colloid concentrates (see **Section 3.6**) it was necessary to dilute samples before analysis. It was found that dilution by at least 200 times was necessary before particle size measurement using *in-situ* photo-correlation spectroscopy was possible. The solutions used for dilution were a) water, b) water that was nitrogenated (BOC, oxygen free) until the O_2 concentration was less than 2×10^{-6} kmol m^{-3}, i.e., the lower detection limit of the dissolved oxygen meter and c) a 0.1 kmol borax (Hopkin and Williams Ltd., AnalaR) m^3 solution, i.e., designed to be at a similar concentration to the colloid concentrate prior to dilution.

In-situ size analysis using photo-correlation spectroscopy was initially carried out on the Malvern Zetasizer IIc (see **Section 3.2**) as it was convenient to measure both electrophoretic mobility and particle size simultaneously. However, the Zetasizer was not capable of model-independent particle size measurements as the data processing software fits a log-normal distribution to all size analyses. Therefore, a Malvern 4700 Photo-Correlation Spectrophotometer was also used to measure particle size. Results from the two instruments were compared by using samples of colloid catalyst which had been diluted by 250 times in a 1 mol m^{-3} KCl solution to achieve good scattering. Identical samples were loaded into each machine, immediately after dilution, and the analyses run simultaneously. A measurement time of two minutes was chosen, which allowed the instrument to make 10 readings then calculate the average which was used. Processing of the results by the computer took about another minute which meant that there was a total interval of three minutes between results. In order to compare measured sizes with the size of known particles, a latex dispersion was prepared adding a few drops of 370 nm diameter, monodisperse latex (Polysciences Inc.) to a 1 mol m^{-3} KCl solution until an adequate light scattering dispersion was obtained, and then measuring its particle size on both instruments.

In order to compare the effect of electrolyte and concentration of colloid on particle size, two electrolytes were used for dilution, 1 mol m^{-3} KCl and 1 mol m^{-3} H_2SO_4, i.e., a monovalent and divalent electrolyte, at three dilution concentrations i.e., 250, 500 and 1000 times dilution of the colloid. At dilutions of less than 250 times, measurement was possible, but much "haloing" due to secondary scattering was observed which gave spurious results. To remove coarse solids, another colloid sample was vacuum filtered through 1.6 μm glass microfibre filter paper (Whatman, GF/A) and the experiment repeated.

The effect of electrolyte concentration on colloid size was investigated by diluting one sample of colloid 250 times with a 1 mol m^{-3} KCl solution and a second sample 250 times with a 10 mol m^{-3} KCl solution, prior to size analysis.

3.25. Measurement of Colloid Particle Size during its Process Stages

During the production of a copper colloid concentrate (see **Section 3.6**), the particle size was measured using the Malvern 4700 PCS at three stages; a) prior to, and b) post hydrazine hydrate addition and c) the final size after addition of the surfactant. The final product was also vacuum filtered through 1.6 μm glass microfibre filter paper (Whatman, GF/A) to remove any coarse solids and measured. The particle size was measured after diluting the colloid by a factor of 250 with 1 mol m^{-3} KCl solution.

3.26. Effect of Initial pH on Colloid Particle Size

A colloid concentrate was prepared without addition of H_2SO_4 prior to DMAB addition and its particle size was measured with the Malvern 4700 PCS after diluting the colloid by a factor of 250 with 1 mol m^{-3} KCl solution.

3.27. Effect of Seeding Copper Solution post Reductant Addition

A copper colloid concentrate was prepared but the Pd(II) solution was added after the addition of the DMAB solution to see what effect this had on the relative nucleation and growth kinetics. The particle size was measured with the Malvern 4700 PCS after diluting the colloid by a factor of 250 with 1 mol m^{-3} KCl solution.

3.28. Effect of Micromixing on Colloid Particle Size

In order to achieve the highest mixing rate possible, a laboratory-built micromixing head which could be sonicated by a Sonics and Materials Inc. V1A sonic probe was used to mix equal volumes of DMAB solution and copper solution (containing Cu(II), Pd(II) and gelatin, adjusted to pH 2.4 with H_2SO_4). The layout of the apparatus is shown in **Figure 3.28.1**.

Figure 3.28.1. *Layout of micromixing apparatus.*

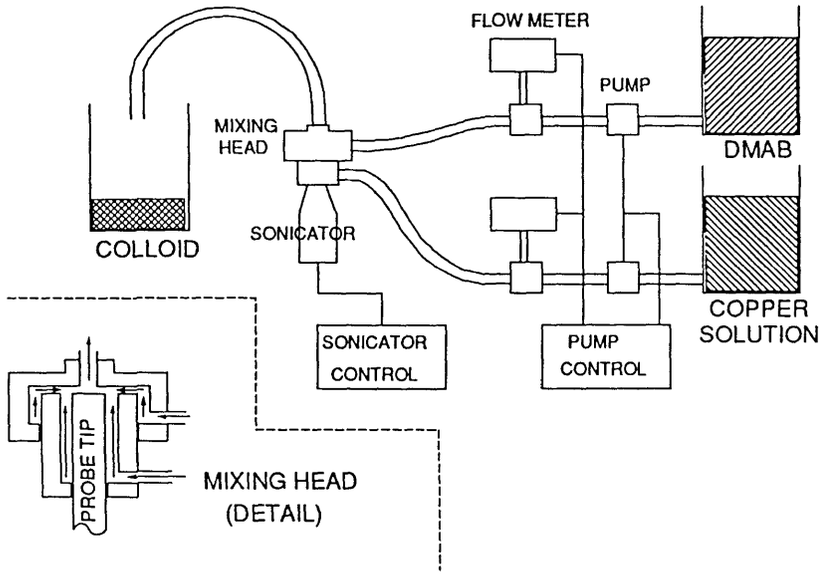

The concentrations of DMAB and the copper in the two solutions used were altered from the basic method (see **Section 3.6**) so that there were equal volumes of each at the required concentration, i.e. the DMAB solution was at a concentration of 12 g m^{-3} DMAB and the copper solution was at a concentration of 40 g m^{-3} Cu. The two solutions were pumped at 25 $dm^3 min^{-1}$ through the mixing head and the resulting colloid collected. The samples collected for analysis were taken mid-stream to allow for fluctuations on start-up. Halfway through the run, the sonicator was turned on and another mid-stream sample taken. The subsequent additions of hydrazine hydrate and surfactant were done using a magnetic stirrer.

3.29. Palladium Colloid Formation

A palladium colloid was formed by the addition of 8 cm^3 of a 9.6 g dm^{-3} DMAB solution to 140 cm^3 of a 0.25 g dm^{-3} $Pd(NH_3)_4Cl_2$ solution to which was added 0.3 g of "P87" gelatin, i.e. the palladium concentration was that used in the Lea Ronal industrial process (see **Section 3.6**). It was not possible to measure the size of the palladium colloid particles as they were too small to scatter light (the PCS has a detection limit of about 3 nm).

A second palladium colloid was prepared using DMAB under similar conditions, but without the addition of gelatin.

Another palladium colloid was formed using hydrazine as a reductant instead of DMAB. A similar solution of Pd was prepared and 30 cm^3 of 8.5 cm^3 dm^{-3} hydrazine hydrate was added instead of the DMAB solution. The colloid took seven minutes before it turned black indicating colloid formation. The colloid was left overnight and the particle size measured using PCS, for which no dilution of the colloid was necessary.

3.30. Effect of Gelatin Concentration on Particle Stability

A 2.108 g dm^{-3} "P87" gelatin in 1 mol m^{-3} KCl solution was prepared. This solution was diluted with 1 mM KCl solution to form gelatin solutions at various concentrations. A copper colloid concentrate was diluted by a factor of 250 with these various solutions and a series of particle size measurements were carried out on the diluted colloid using the PCS.

In order to assess the effect of gelatin viscosity, a Carrimed Controlled Stress Rheometer was used to measure the change in gelatin viscosity with concentration. This instrument employs the concentric cylinders form of viscosity measurement. A 2.1 g dm^{-3} "P87" gelatin solution was diluted with water to various concentrations so that all samples had the same thermal history. Viscosity measurements were carried out at each concentration.

The experiment was repeated using the same concentration of gelatin, but this time the gelatin was prepared in a 1 mol m^{-3} KCl solution and the dilution was done with 1 mol m^{-3} KCl.

Perchloric acid (60 %) was added to a solution of 2.1 g dm^{-3} gelatin until it had a low pH. A sample was removed and increasing aliquots of NaOH were added to neutralise the acid with subsequent removal of samples at selected pHs, thus ensuring a constant ionic strength. The viscosity of these samples was measured as above.

3.31. Rotating Ring-Disc Electrode (RRDE) Analysis of Gelatin Oxidation

The rotating ring-disc electrode was controlled by a laboratory-built bipotentiostat, driven by a Hi-Tek Instruments wave-form generator and a Weir 4000T voltage supply. Current/potential data were recorded by an IBM PC compatible microcomputer with a

Metrabyte DASH A/D card using Lotus Measure software. Conventional electrochemical measurements could also be performed with this equipment. The arrangement of the electrochemical cell is shown below.

Figure 3.31.1. *Rotating Ring-Disc Electrode (RRDE) cell.*

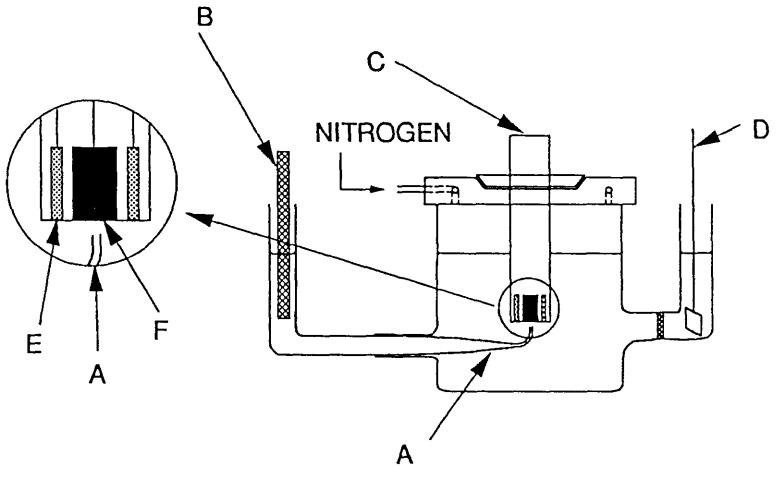

Experiments were conducted in a two compartment cell, with a RRDE (C) in one compartment and a platinum flag electrode (D) in the other. The potential of the RRDE was measured via a Luggin capillary (A) with respect to a saturated calomel reference electrode, S.C.E. (B), but potentials were calculated by the computer to refer to S.H.E.. The disc electrode (F) was a poly-crystalline copper rod with a purity of 99.99 % (Matthey, Specpure) and a surface area of 1.2×10^{-4} m^2. It was fixed within an Araldite epoxy resin tube and could be mounted in the rotating platinum ring electrode (E). The ring-disc electrode could then be mounted in the ring-disc assembly (range of rotation rate 0 - 3000 rpm). Before each experiment the electrode was polished with 0.075 μm elementary particle size, highly pure aluminium oxide (BDH Chemicals) and then immediately transferred into the electrolyte.

The background electrolyte was prepared by the addition of 461 cm^3 of a 0.1 mol m^{-3} sodium hydroxide solution to 500 cm^3 of a 0.1 mol m^{-3} potassium dihydrogen orthophosphate solution, made up to 1000 cm^3 to give a pH of 8.

The cell was deareated by bubbling high purity nitrogen (BOC, oxygen free) through the solution.

CHAPTER 4. RESULTS AND DISCUSSION

4.1. Production of Electrostatically Stabilised Colloids

In principle, electrostatic stabilisation is one alternative to steric stabilisation with gelatin, but as shown in **Figure 2.3.2.2**, in **Section 2.3.2**, electrostatically stabilised colloids are stable only at low ionic concentrations. Attempts to produce copper colloids from a copper chloride solution (chosen because of the monovalent counter ion) by reduction with a suitably powerful reducing agent, dimethylaminoborane (DMAB), resulted in slow copper formation followed by precipitation of a light brown precipitate from solution. On reduction, the solution went from turquoise to light brown, but became clear on filtration. Filtration of the larger particles from the solution gave a solution containing particles in the range 350 to 800 nm with a mean diameter of 620 nm and a zeta potential of -23 mV, which meant that the colloid was in the unstable region of a potential energy diagram (see **Figure 4.1.1** - "Unstable colloid"). This colloid agglomerated when left overnight. Addition of acid to increase the zeta potential, and hence the electrostatic-distance repulsion (e.g., in **Figure 2.1.1**), led to almost immediate precipitation. This was most likely due to the increase in the concentration of counter (Cl^-) ions that decreased the diffuse double layer thickness and hence led to decreased stability.

In an attempt to avoid the problem of the benefit of the increased magnitude of the zeta potential being counteracted by the increase in ionic strength, hexametaphosphate (HMP), $(PO_3)_6^{6-}$, was added to the solution to act as a highly charged, adsorbed counter ion. This gave a dark yellow colloid that formed after about 30 minutes. The particles had equivalent hydrodynamic diameters in the range 25 to 250 nm with an average of 80 nm and a zeta potential of 83 mV; under such conditions, a potential energy-distance diagram (see **Figure 4.1.1** - "Colloid stabilised with HMP") predicts that the colloid should be electrostatically stabilised. However, a gradual increase in particle size occurred over one week, the colloid became a cloudy brown colour and eventually the particles precipitated. This was thought to be partially due to the phenomenon of Ostwald ripening that led to agglomeration. In any dispersion there will be a dynamic equilibrium between the dissolution and deposition of the dispersed phase. In a polydispersed sol, the smaller particles will have a greater solubility than the larger particles and hence the larger particles will tend to grow at their expense. Once larger particles predominate then the colloid becomes electrostatically unstable and agglomeration occurs.

Figure 4.1.1. *Potential energy vs. distance diagram for electrostatically stabilised colloids at 10 mol m^{-3} Cu, based on measured particle size and zeta potentials.*

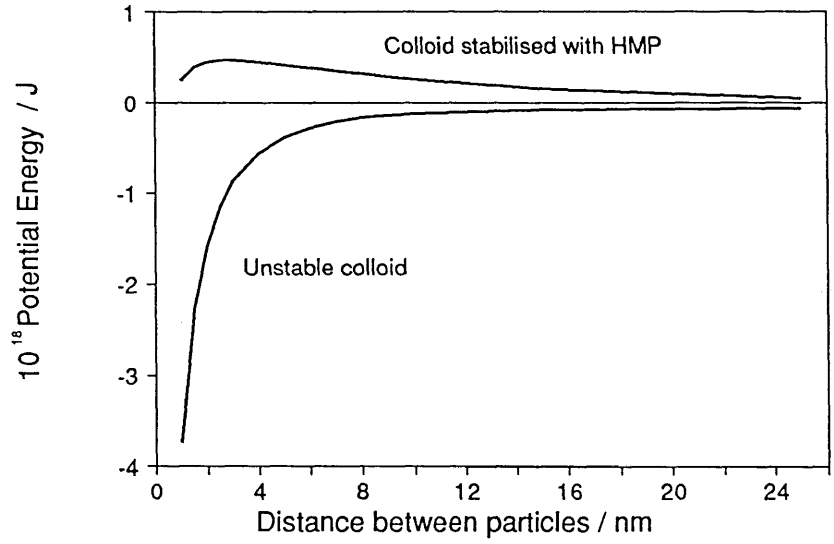

4.2. Analysis of Gelatin

The iso-electric points (ieps) of two gelatins were determined; "P87", the gelatin used in the Lea Ronal colloid manufacturing process (see **Section 3.6**) and another sample, "2392", which did not stabilise copper colloid dispersions. The ieps were 8.8 for P87 and 5.3 for 2392. Based on the discussion in **Section 2.3.5**, the difference in iep indicates that P87 was an acid-processed gelatin and 2392 was a lime-processed gelatin. Amino acid analysis by gel electrophoresis indicated that both gelatins were similar in composition, with the main difference being the decrease in amide nitrogen in the 2392 sample. No information was obtainable about the chain-lengths of the gelatins, but at the same concentration (about 4 %) the 2392 sample was visibly more viscous at room temperature indicating longer chain lengths.

FTIR analysis of the two gelatins gave similar absorption peaks at the same dilution. The P87 gelatin had a peak at 1641 nm (absorption = 0.1976 % of transmission) and 1559 nm (absorption = 0.1142 % of transmission) whereas the 2392 gelatin had a peak at 1650 nm (absorption = 0.1435 % of transmission) and 1554 nm (absorption = 0.1118 % of transmission). These peaks correspond to the Amide I bond and Amide II bond. The

Amide III peaks were too low to be distinguishable from noise. Although the peaks were similar, the P87 gelatin contained 40 % more amide groups, which indicates why it appeared to be a better stabiliser.

4.3. Assessment of the Iso-electric Point (IEP) of Colloids and its Effect on Particle Size

The pH dependence of the zeta potential of the copper colloid was determined, shown in **Figure 4.3.1**, which indicates an iso-electric point (iep) of about pH 8-9.

Figure 4.3.1. *Zeta potential vs. pH for a copper colloid concentrate diluted by 250 times with water.*

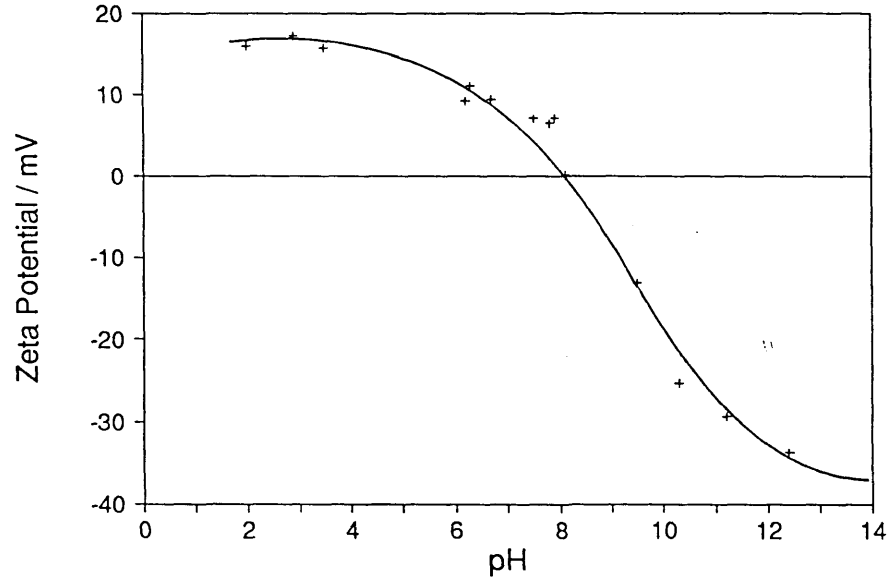

The graph shows the classic S-curve of zeta potential dependence on pH. The iep of the colloid lies in the same region as the iep of the P87 gelatin (see **Section 4.2**) and it was assumed that the gelatin had completely enveloped the particle, so that the particle responded electrostatically as gelatin. It was unlikely that *particle* concentration affected the zeta potential. Electro-osmosis and electrophoresis are simply opposite expressions for the same relative motion of particle and fluid, and electro-osmotic flow through a porous bed is not affected appreciably until the double layers on either side of the pore begin to overlap. The effect of the volume fraction of solids, V_s, was analysed by Levine

and Neale [135] and was found to be only important at very high particle concentrations and low values of κa, neither of which apply to the colloid systems under investigation with $V_s = 8 \times 10^{-4}$ and κa in the range 10 to 100.

Further evidence of a gelatin enclosed particle came from measurement of the colloid particle size with pH, shown in **Figure 4.3.2**, which was done at the same time as zeta potential measurement.

Figure 4.3.2. *Colloid particle size vs. pH for a copper colloid concentrate diluted by 250 times with water.*

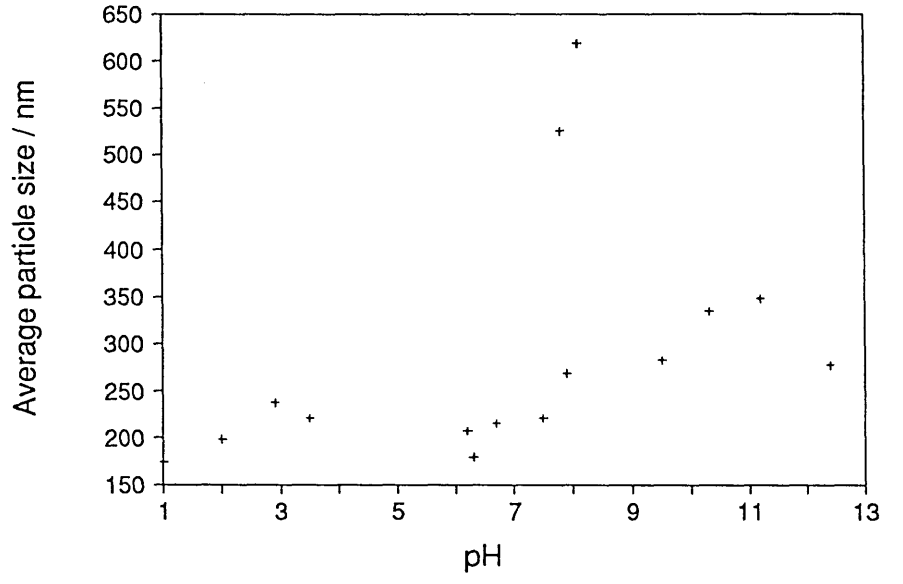

The graph shows that there was a large increase in the average particle size measured at around the iep of the colloid indicated in **Figure 4.3.1**. This would be expected at the iep of gelatin as this is the point where minimum swelling of the gelatin strands takes place, allowing closest approach of particles and hence agglomeration. This graph indicates that the copper/gelatin particle behaves as a gelatin particle at the iep.

4.4. Effect of Oxygen on Colloids

Colloids manufactured by Lea Ronal are stored in plastic drums that are permeable to air. To assess the effect of oxygen on copper colloids, a colloid was prepared in a vessel under nitrogen (*Nit Norm*). The colour of this concentrate was black/green. Repeating the experiment, but increasing the amount of gelatin present by three, gave a dark red concentrate (*Nit x3Gel*). A sample was also prepared by bubbling oxygen through it, prior

to DMAB addition, this sample was black (*Oxygen*). If O_2 was pumped through during DMAB addition, then the colloid agglomerated and sedimented from solution. These three samples are compared in **Table 4.4.1**.

Table 4.4.1. *Effect of oxygen on particle size and electrophoretic mobility of colloids.*

Colloid	Particle Size			Electrophoretic Mobility / $m^2 V^{-1} s^{-1}$	pH
	Average / nm	Polydispersity	90 % in range / nm		
Nit Norm	180	0.69	50-700	+0.90	8.11
Nit x3Gel	360	0.62	100-1300	+0.07	8.74
Oxygen	260	0.65	70-1000	+0.45	8.40

The pH of these samples was near the iep of the P87 gelatin (pH 8.8) (see **Section 4.2**) where a minimum swelling of gelatin in water occurs; it is feasible that as the pH of a colloid approaches the iep of the gelatin then the adsorbed layer decreases in volume and the particles are able to approach closer and agglomerate to form larger particles. This hypothesis was supported by the degree of polydispersity which decreased slightly as the pH approached the iep. The Zetasizer IIc software analyses the average correlation function to calculate the mean size and distribution width, which is called the polydispersity. The mean size and polydispersity are related to the peak amplitude and variance of a log-normal distribution, which is used as the model for the distribution and is a good assumption for many physical systems. Away from the iep, the charged, solvated strands of gelatin project into solution and give more protection, both conformationally and electrostatically, to the particle. Assuming that the gelatin packs in an orderly way around the particles then the increase in the average size of the particles in the *Nit x3Gel* sample cannot be accounted for merely by an increase in the concentration of gelatin present. The red colour of the *Nit x3Gel* might be due to the change in optical property of the gelatin near its iep, or due to a change from Rayleigh to Mie scattering with size (see **Section 2.1**). On dilution with water the *Nit x3Gel* sample went green whether the water had been nitrogenated or not. The samples were stored and their particle size and mobility determined after about six months. The results are shown below.

Table 4.4.2. *Effect of oxygen on particle size and electrophoretic mobility of colloids after six months.*

Colloid	Particle Size			Electrophoretic Mobility	Time
	Average / nm	Polydispersity	90 % in range / nm	/ m^2 V^{-1} s^{-1}	/day
Nit Norm	360	0.54	110-1260	+0.27	170
Nit x3Gel	1540	3.12	90-29230	+0.18	190
Oxygen	500	0.24	230-1170	+0.24	180

In all cases, the particle size had increased, suggesting that particle agglomeration had occurred with time. Unlike the other two samples, the *Nit x3Gel* sample stayed at a pH near the iep of gelatin (pH 8.8), and this could have enhanced particle agglomeration.

4.5. Comparison of Absolute Stability and Thermal Stability of Colloids

All colloids made were kept in 500 cm^3 plastic bottles in a dark cool environment until the solids sedimented from solution. Samples under nitrogen were kept in plastic bottles in a nitrogen box. The experiment conditions, the average life times of the colloids and the results of the thermal stability tests are listed in **Table 4.5.1.**

Table 4.5.1. *Experimental conditions for the manufacture of colloids and their stabilities.*

Experiment	Conditions	Time Stability / day	Thermal Stability / g dm^{-3} Cu
Norm	Colloid made following Lea Ronal recipe.	118	0.41
pH 8	As above but colloid initially buffered to pH 8 with borax.	127	0.21
Sonic	Colloid made following Lea Ronal recipe but sonication used during DMAB and hydrazine addition.	79	0.34
Nit Norm	Colloid made following Lea Ronal recipe in nitrogenated vessel.	410	0.20
Nit x3Gel	As above, but three times more gelatin added than normal	420	<0.01
Nit Box	Colloid made following Lea Ronal recipe in a nitrogen box.	365	0.18
Oxygen	Colloid made following Lea Ronal recipe, oxygenated prior to DMAB addition.	184	0.82

There was a low correlation between absolute (time dependent) stability and thermal stability for laboratory-made colloids. As all samples stored under nitrogen were stable for longer than samples stored under air, the mechanism of destabilisation would appear to be enhanced by oxygen, although oxygenation of the solution prior to colloid formation does not appear to affect stability. The pH of a normal colloid stored under air and the pH of colloids stored under nitrogen were plotted over the time stored, shown in **Figure 4.5.1.**

Figure 4.5.1. *Time dependence of pH for colloids stored under nitrogen and colloids stored under air.*

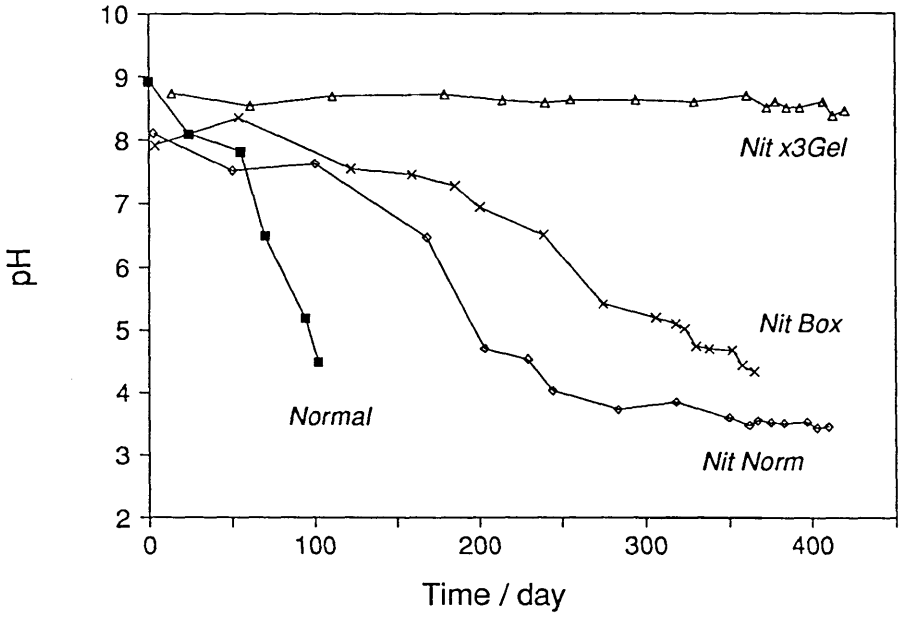

All samples stored under nitrogen lasted for about one year, i.e., three to four times longer than samples stored under air. It was probable that the pH decrease was due to the oxidation of excess hydrazine, which releases H^+ ions. This hypothesis is examined in **Section 4.7** and **Section 4.8.** By whatever means H^+ ions were produced with time, the extra gelatin present in the *Nit x3Gel* colloid appeared to buffer the pH decrease. However, increasing the gelatin concentration is impractical in the commercial process as this decreases the adherence of the copper colloid to PCBs.

4.6. Stability of Colloid at Constant pH

To assess whether the decrease in pH with time was a cause or an effect of colloid instability, a copper colloid was monitored closely for changes in pH. If the pH of the colloid fell below 8, a few drops of borax solution were added to buffer it back above this value. The graph of the pH of this colloid is shown in **Figure 4.6.1.**

Figure 4.6.1. *Time dependence of pH for buffered colloid.*

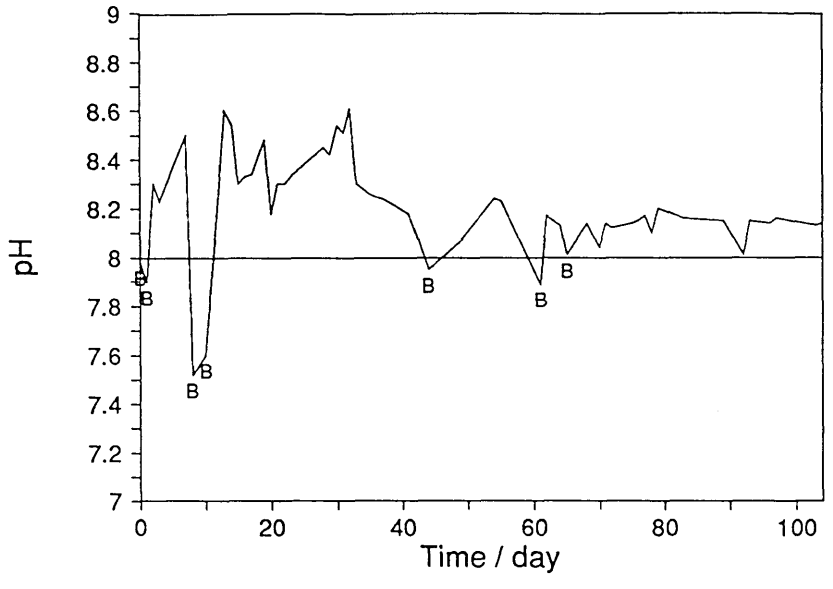

B - Borax added at 4 g dm^{-3}

After 125 days, there was 20 % supernatant visible; this was usually taken as the failure of a colloid to stay dispersed. On agitation, the colloid was easily redispersed and remained so for several hours, indicating a possible secondary minimum effect. After 145 days, there was 40 % supernatant and the viscosity of the colloid had decreased notably. Buffering against the pH decrease did not seem to increase colloid stability beyond the life time observed with other 'normal' colloids (see **Table 4.5.1**). These results indicate that the pH decrease was not the cause of colloid instability but a symptom of it.

4.7. Analysis of Colloids by UV/Visible Absorption Spectrophotometry

Measurement of the UV/Visible absorption spectrum of a copper colloid concentrate at 250 times dilution with water, without an integrating sphere, gave a very broad flat peak at 650 to 750 nm; however, when the integrating sphere was used, there was a much clearer peak at 624 nm for a colloid at 100 times dilution with water. Measurement of the colloid spectrum directly using a very small path length gave a peak at 594 nm. Mie theory predicts a λ_{MAX} of 586 nm for a 50 nm copper particle [27]. Clearly, the presence of a peak indicates an unoxidised colloid. These results are similar to the results of Hirai *et al.* [20], who found clear spectrophotometric absorbance peaks at 570 nm for copper colloid solutions, which

they attributed to excitation of surface plasmons of copper particles. Papavassiliou and Kokkinakis [28] found a clear adsorption peak at 580 nm (2.1 eV) for the optical adsorption spectra of copper particles.

On addition of dilute DMAB solution to a dilute copper colloid concentrate solution (see **Section 3.6**), the solution immediately turned dark green. The absorption gradually increased across the whole spectrum until a sharp peak emerged at 593 nm after 18 minutes. After 26 minutes, this peak was swamped by the continued increase in absorption across the whole spectrum. When the experiment was repeated at 100 times dilution, there was no change in absorption, even after 30 minutes.

4.8. Monitoring of pH and Oxygen Concentration of DMAB, Hydrazine and Gelatin Solutions

As mentioned in **Section 4.6**, storing the colloid under nitrogen increased the stability of the colloid. To assess the effect of oxygen on the components of the Lea Ronal colloid, three solutions containing DMAB, hydrazine and gelatin were made and stored under air in a cool dark environment and another three identical solutions were made up with nitrogenated water and stored in a nitrogen box. All solutions were at their initial concentrations as used in the Lea Ronal proprietary process, except the DMAB solution that was made at a lower starting concentration to account for DMAB that is oxidised immediately on reduction of Cu^{2+} ions. The time dependence of oxygen concentration and pH are shown in **Figures 4.8.1** to **4.8.4**, the dotted lines show linear regressions through the measured points for samples stored under nitrogen.

Figure 4.8.1. *Time dependence of O_2 concentration for 3 g dm^{-3} DMAB solution, a) under air (■) and b) under nitrogen (+).*

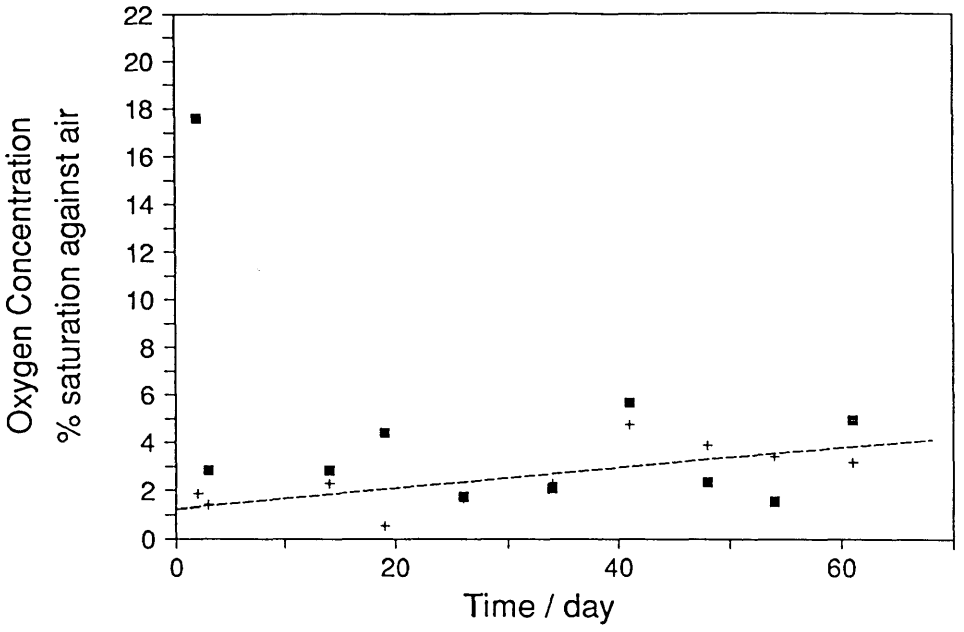

Figure 4.8.2. *Time dependence of O_2 concentration for 8.5 cm^3 dm^{-3} hydrazine solution, a) under air (■) and b) under nitrogen (+).*

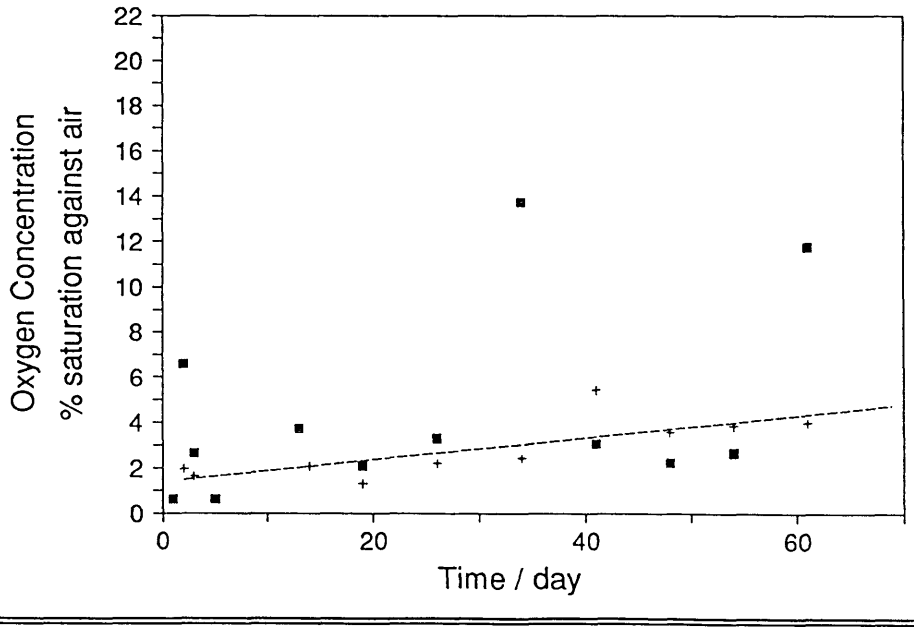

Figure 4.8.3. *Time dependence of O_2 concentration for 2.1 g dm^{-3} gelatin solution, a) under air (■) and b) under nitrogen (+).*

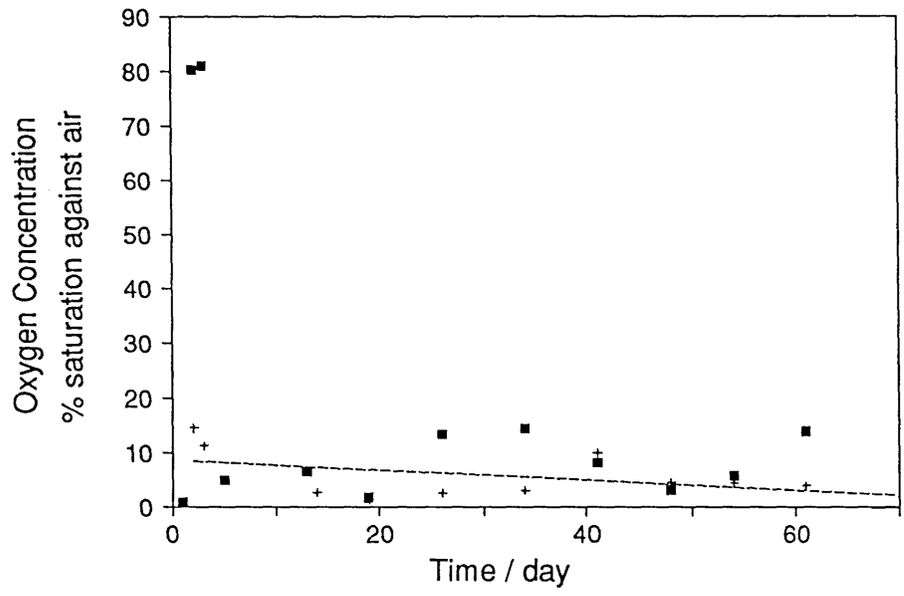

The regression lines show a general, but slight, increase in the concentration of O_2 in DMAB and hydrazine; if their concentrations were decreasing, then their ability to consume O_2 was also declining. The regression line for the gelatin solution appeared to decrease slightly, but this may be due to the downward trend over the first 20 days. The O_2 concentration was low and similar in all cases, except for an initial rise in O_2 in the gelatin under air sample. The pH of the solutions was also monitored and the results are shown in **Figure 4.8.4.**

Figure 4.8.4. *Time dependence of pH for 3 g dm^{-3} DMAB solution, 8.5 cm^3 dm^{-3} hydrazine solution and 2.1 g dm^{-3} gelatin solution.*

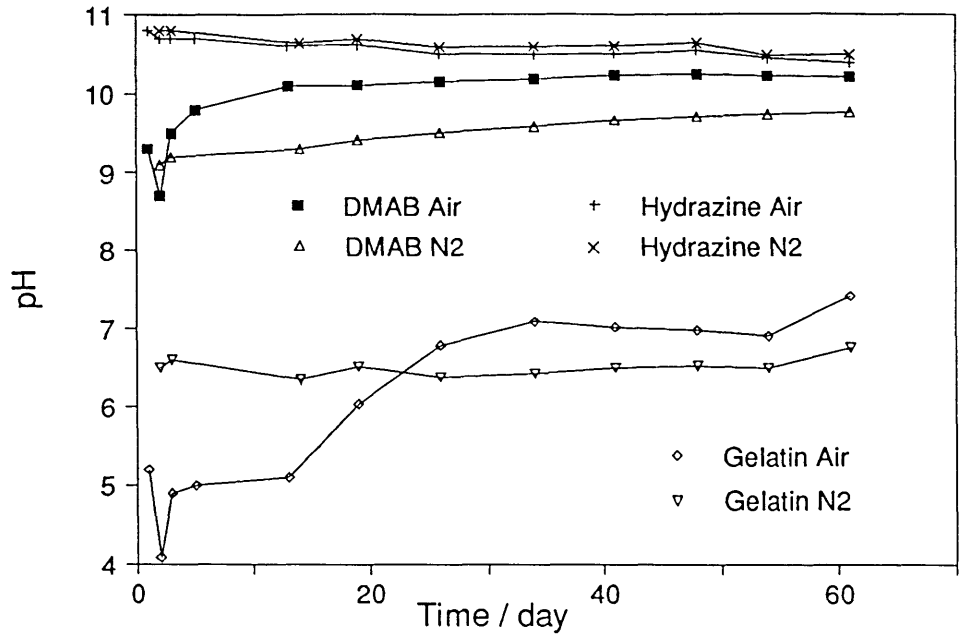

The pH of the hydrazine solutions both under air and nitrogen decreased gradually with time indicating that hydrazine was being oxidised gradually.

A potential-pH diagram of nitrogen, giving the region of stability of hydrazine, shows that the potential of a platinum indicator electrode in both solutions adopted potentials just above those required to reduce water, as shown in **Figure 4.8.5.**

Figure 4.8.5. *Potential-pH diagram for the nitrogen/water system at 25 °C,* $a_{N_2H_4} = 0.4$.

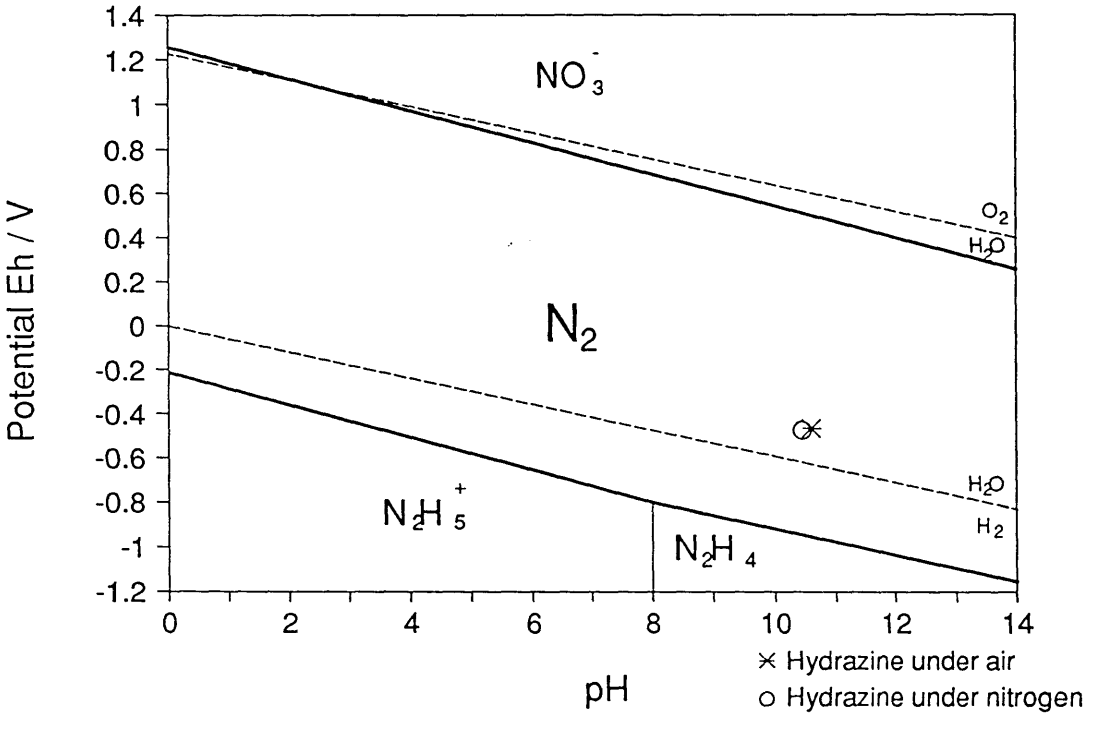

The pH of DMAB under air was higher than that of the DMAB under nitrogen; both gradually increased, possibly due to oxidation of the DMAB consuming protons:

$$Me_2NHBH_3 + 1.5O_2 + H^+ \Leftrightarrow H_3BO_3 + Me_2NH_2^+$$

The O_2 concentration in the DMAB under air solution decreased rapidly after the first few days and remained low, indicating that O_2 was consumed according to the above reaction. A similar reaction presumably happened to the DMAB under nitrogen sample as well, due to the low concentrations of O_2 still present in solution, although at a slower rate. This was indicated by the observed redox potential adopted by a platinum indicator electrode in the DMAB under nitrogen solution, on a boron/water potential-pH diagram, shown in **Figure 4.8.6.** No data is available for DMAB and therefore it was assumed that as BH_4^- is one of the first oxidation products of DMAB then a boron/water potential-pH diagram would be a good model of DMAB ions in solution.

Figure 4.8.6. *Potential-pH diagram for the boron/water system at 25°C, a_B = 0.05.*

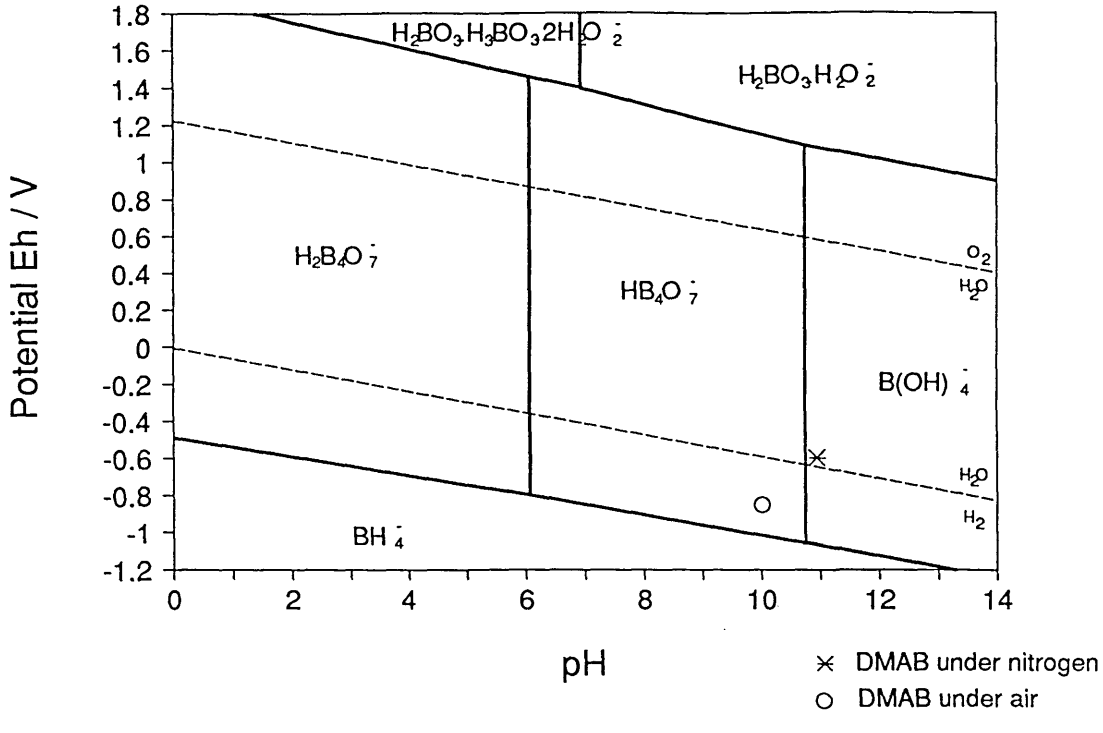

The DMAB under air sample appeared below the hydrogen line and when a Pt electrode was inserted in the solution to measure its potential, bubbles of H_2 were visible, indicating a mixed potential was adopted.

The gelatin solution appeared to be stable in air for at least two weeks before the pH increased to near neutral, with subsequent flocculation and precipitation of gelatin on day 19. The increase in pH was possibly due to the buffering action of gelatin.

The gelatin under nitrogen solution flocculated after 41 days, taking almost twice as long as the solution under air and thus it is obvious that oxygen had some effect on the stability of gelatin.

4.9. Monitoring of the Concentrations of DMAB and Hydrazine Solutions

As DMAB and hydrazine solutions appeared to be gradually oxidised with time, three solutions were made containing, *hydrazine*, *DMAB* and DMAB after reducing Cu^{2+} ions (*DMAB + Cu*). The *hydrazine* solution was made at a similar concentration to the starting concentration of the Lea Ronal colloid. The *DMAB* solution was made at a lower

starting concentration than the Lea Ronal solution to account for DMAB that is oxidised immediately on reduction of Cu^{2+} ions. The *DMAB + Cu* solution was made by using the same solution used by Lea Ronal, but with no gelatin. DMAB was added to this solution and copper metal precipitated immediately. The concentration of DMAB was measured about an hour after addition to the solution and was found to be almost zero. A plot of the concentrations with time for the three solutions is shown in **Figure 4.9.1.**

Figure 4.9.1. *Time dependence of concentration for a 11.78 g dm^{-3} hydrazine solution, a 2.14 g dm^{-3} DMAB solution, and a 20 g dm^{-3} Cu with 6 g dm^{-3} DMAB (DMAB + Cu) solution.*

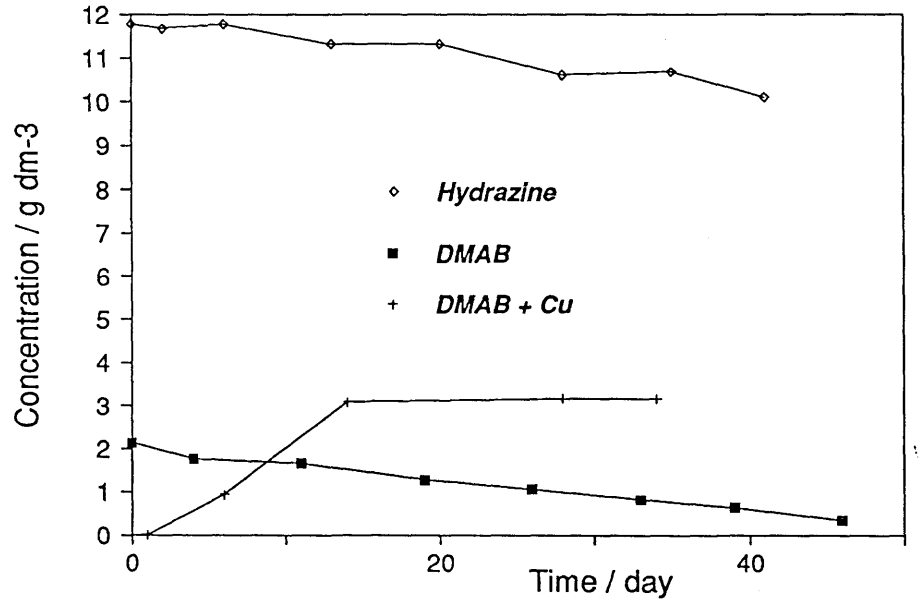

The concentrations of *DMAB* and *hydrazine* both decreased slowly with time which was also indicated by the change in pH in **Figure 4.8.4.** The concentration of DMAB in the *DMAB + Cu* sample appeared to increase from zero and then plateau. This was probably because the iodide used in the titration was oxidised either by Cu^{2+} ions that were in solution at such a low pH (1.31), or by aerial oxidation which was catalysed by the presence of copper. This means that it would be impossible to measure DMAB concentrations in a colloid solution using this method as it was found that unreduced cupric ions are present in copper colloid dispersions (**Section 4.11**).

4.10. Scanning Electron Microscopic (SEM) Analysis of Colloid Particle Size

The sizes of copper colloid particles determined by scanning electron microscopy (SEM) were compared with size distributions obtained in-situ by photo-correlation spectroscopy on a Zetasizer IIc.

An analysis of the images of the *Nit Norm* colloid (see **Section 4.4** for details) revealed roughly spherical, 700 to 4500 nm particles, most of which were agglomerates. The back scattered electron image showed that there was free gelatin between all particles and agglomerates. The analysis was performed 51 days after the preparation of the *Nit Norm* sample and the particle sizes observed can be compared with those obtained by the Zetasizer in **Tables 4.4.1** and **4.4.2.** The particles appeared to be in the order x10 larger when viewed by SEM than when measured in-situ which suggests that agglomeration occurred when the samples were dried.

Analysis of the *Nit Box* sample showed smaller particles which were in the range 40 to 530 nm; agglomeration in some instances gave irregular particles of up to 2000 nm. The analysis was performed 9 days after the preparation of the *Nit Box* sample and the particle sizes observed can be compared with the sizes 90% in the range 170 to 1720 nm obtained by the Zetasizer 135 days after sample preparation. In this case, allowing for particle agglomeration which occurred with time, there appears to be a good correlation between the particle size observed using the SEM and measured by the Zetasizer.

4.11. Analysis of Colloid Dispersion Media

Successful separation of the dispersed phase from the continuous phase was effected by filtering the colloid with cellulose filter paper. The UV/Visible spectra of the colourless dispersion media were measured and the results of the analyses for the *Nit Box* and *pH8* samples (see **Table 4.5.1** for experiment details) are compared to a) the dispersion medium filtered from the precipitate obtained from the reduction of $CuSO_4$ by N_2H_4, b) two solutions containing $CuSO_4$ and c) the solution used for colloid concentrate manufacture prior to reduction by DMAB in **Table 4.11.1.**

Table 4.11.1. *UV/Visible spectroscopic characterisation of dispersion media of two colloid concentrates compared to aqueous solutions containing copper.*

Dispersion medium /Aqueous solution	Characteristic Peaks λ / nm	Absorption
Nit Box	292	0.32
pH 8	317	2.96
$CuSO_4$(0.1 kmol m^{-3})/ N_2H_4	292	0.32
$CuSO_4$ (0.1 kmol m^{-3})	292/800	0.59/1.11
$CuSO_4$ (0.2 kmol m^{-3})	292/794	0.93/2.56
$CuSO_4$ (0.1 kmol m^{-3})/ gelatin/ $PdCl_2$/ H_2SO_4	292/808	0.67/1.07

Only one characteristic peak, at 292 nm, emerged for the *Nit Box* dispersion medium. The reason for the slight shift and large increase in absorption of the *pH 8* peak could have been due to the addition of borax leading to the formation of a Cu(II)/borate complex. The 0.1 kmol m^{-3} $CuSO_4/N_2H_4$ dispersion medium (chosen to be at a similar concentration to a Lea Ronal colloid) exhibited a very similar peak to the *Nit Box* sample, except that it was slightly broader. The 292 nm peak of the 0.1 kmol m^{-3} $CuSO_4$ solution is characteristic of Cu(II) in solution and corresponds to a charge-transfer band, whereas the peak at 800 nm is an absorption band which corresponds to $Cu(H_2O)_6^{2+}$. The absorption peaks of the Lea Ronal solution prior to the addition of DMAB were due primarily to Cu(II), and only when a reductant was added and copper metal formed did the 800 nm peak disappear. These results indicate that there was unreduced Cu(II) in colloid concentrates, but it was not complexed by water.

4.12. Analysis of the Effectiveness of Rinsing by X-ray Photoelectron Spectroscopy (XPS)

The surfaces of two glass slides were analysed using X-ray Photoelectron Spectroscopy (XPS), both of which had been plated with colloid concentrate, but only one of which had been rinsed before analysis. The results of the analyses are shown below.

Table 4.12.1. *XPS analysis of copper colloid coated microscope slides.*

Element	Rinsed Slide / normalised count	Unrinsed Slide / normalised count	Ratio
Si	4145	1122	3.7:1 (as SiO_2)
O	9706	9518	
O_2 assigned to SiO_2	8290	2244	
O_2 Remaining	1416	7274	1:5.1 (as gelatin)
N	1180	3005	1:2.6 (as gelatin)
Cu	73	887	1:12.2

Of the total oxygen measured, a stoichiometric proportion was assigned to Si as SiO_2, the remainder was assigned to gelatin. The nitrogen measured was all assigned to gelatin. The discrepancy between the ratio of gelatin according to N and O values might be accounted for by aerial oxidation of the dried surface film. The rinsed sample was analysed several hours before the unrinsed one; hence it is probably more accurate to judge the amount of gelatin present by the N value than the O. These results show that although the amount of gelatin was decreased by a factor of about three by rinsing and the copper concentration on the surface was decreased by a factor of twelve. Visual inspection of the surface showed a very uneven coating of copper on the surface of the slide.

4.13. Steric Stabilisation of Colloids

To study the mechanisms of stability and possibly replace gelatin as a stabilising agent for copper colloids, several natural and synthetic polymers were substituted for gelatin in the copper colloid concentrate solution prior to reduction by DMAB. The results of these substitutions are shown below.

Table 4.13.1. *Results of substitution of gelatin in copper colloid concentrate solution by natural and synthetic polymers.*

Polymer	Addition Concentration / g dm^{-3}	Result
Poly(ethylene glycol), Chain length 200	2.4	Tendency to agglomerate the particles, causing them to precipitate out quickly.
Poly(ethylene glycol), Chain length 20,000	2.4	Tendency to agglomerate the particles, causing them to precipitate out quickly.
Poly(ethylene oxide), Chain length 300,000	2.4	Tendency to agglomerate the particles, causing them to precipitate out quickly.
Poly(ethylene oxide), Chain length 5,000,000+	2.4	Tendency to agglomerate the particles, causing them to precipitate out quickly.
Poly(ethylene oxide), Chain length 5,000,000+	0.01 to 1.2	Fine dispersion, but larger, visible particles which precipitated
Butyl Ethyl Ether	0.12 to 0.37	Agglomeration occurred after about 30 minutes of stirring.
Hexaethyleneglycol dodecyl ether (HDE) in acetone	0.11	Black colloid with froth. After 30 minutes the colloid turned red and precipitated.
3-Mercaptopropionic acid	0.02 to 0.2	Elemental sulphur precipitation prior to reduction
β-cyclodextrin	0.43	Black agglomerated precipitate formed immediately
Starch	0.7 to 7	Colloid stable for about 3 weeks but large amount of precipitate.
Starch	0.07	Colloid agglomerates and precipitates
Dextrin	0.07 to 7	"
Polyethylene (propylene oxide), MM 12,000	3.57	"

Poly(ethylene glycol) (PEG) of chain lengths 200 and 20,000 and poly(ethylene oxide) (PEO) of chain lengths 300,000 and 5,000,000+ (5M+) were substituted for gelatin at addition concentrations of 2.4 g dm^{-3}. As the particles appeared to agglomerate quickly, it was thought that bridging flocculation was occurring. Poly(ethylene oxide), chain length 5,000,000+, appeared to give the best dispersion of these polymers, and so an attempt was made to find the concentration at which bridging flocculation gave way to steric stabilisation. Several concentrations were tried but none of these gave a satisfactory result.
To utilise the propensity of the carbonyl bond to form hydrogen bonds and to test shorter chain lengths, a non-ionic surfactant, butyl ethyl ether was tested as a steric stabiliser. At no concentration was a stable colloid formed and this was probably due to the very short chain length being insufficient to stabilise the colloid sterically.
A longer chain length alkyl ethyl oxide with more carbonyl groups, hexaethyleneglycol dodecyl ether (HDE) was also tried. On addition of DMAB, the solution turned black and a stable foam appeared, similar to when gelatin was present, indicating a significant decrease in surface tension, and stabilisation of the foam by the hydrophilic molecules. However, shortly after this, the colloid agglomerated and precipitated.
In an attempt to utilise the strong sulphur-copper bond, a steric stabiliser with a sulphur head group was used [136]. 3-Mercaptopropionic acid (MPA) was chosen for its mercapto group, and its carboxyl group which was known to form a bond with glass. However, on addition of the MPA to colloid concentrate solution, elemental sulphur precipitated, implying there was a chemical interaction leading to the oxidation of sulphide.
β-cyclodextrin (BCD) is a molecule consisting of a ring of seven dextrin molecules, which form a torus shape with both a hydrophilic and a hydrophobic end. It was thought that this property could be used in the steric stabilisation of copper colloids. Alternatively, the 1 nm hydrophobic hole in the centre of the molecule could be used as a site to grow copper nuclei, which could then be used to seed a saturated solution of copper salt, enabling monodisperse copper colloids to be produced. However, replacing gelatin with the BCD produced an unstable colloid and a black agglomerated precipitate formed almost immediately.
Starch and dextrin were used instead of gelatin to assess their stabilising ability. 0.7 to 7g dm^{-3} starch solutions were found to stabilise the colloid for about 3 weeks but the amount of precipitate on the base of the flask was higher than that of an equivalent colloid stabilised with gelatin. 0.07 g dm^{-3} starch solutions and dextrin solutions at any concentration were found to agglomerate the colloid and cause precipitation.

Polyethylene(propylene oxide) of MM 12,000 used instead of gelatin agglomerated and precipitated the colloid immediately.

4.14. Stabilisation of Colloids in Organic Dispersion Media

In an attempt to stabilise copper particles in a non-aqueous medium, a sample of copper colloid concentrate was sonicated with iso-octane which contained Versatic acid as a stabilising agent. Versatic acid was used as it was thought that the carboxyl group would bond to the particle leaving the non-polar tail to stabilise the colloid sterically. The hydrophobic copper particles concentrated and agglomerated at the oil/water interface, and the former black aqueous colloid became a clear solution. It appeared that there was a possibility of stabilising copper particles in a non-aqueous medium, but as the Versatic acid had a chain length of 10, it may not have been large enough to prevent agglomeration. The experiment was repeated, replacing Versatic acid with erucic acid (C22) but the same result occurred.

In an attempt to make a colloid by reduction of Cu^{2+} ions in a non-aqueous medium, $CuSO_4$ and $Pd(NH_3)_4Cl_2$ were dissolved in methanol. However, both were only sparingly soluble compared to their solubility in water, the latter especially so. Erucic acid was added to the solution as a stabiliser. On addition of DMAB, the solution turned black but after 35 minutes, visible, $\approx$ 100 μm (by inspection), particles formed which settled out slowly. On sonication, the particles redispersed, but settled out after 5 minutes. On redispersion the colloid turned brown. Here again, it appeared that erucic acid was not large enough to protect the close approach of particles from causing agglomeration.

4.15. Monodisperse Colloids of Copper Hydrous Oxide

LaMer's qualitative explanation of the mechanism of the formation of monodispersed sulphur sols by the decomposition of sodium thiosulphate in acidic solution is illustrated in **Figure 4.15.1** [137][138].

Figure 4.15.1. *Schematic presentation of the concentration change with time of a solute species generated in-situ, before and after self-nucleation. C_s = solubility, C^* = critical supersaturation.*

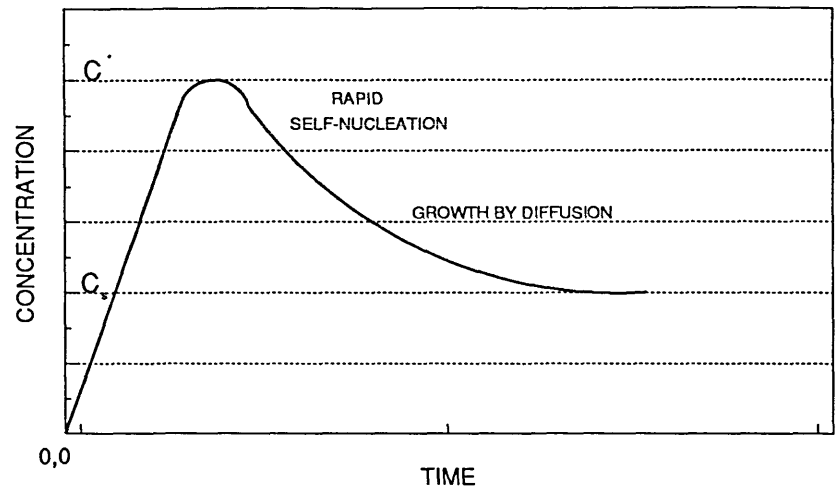

The concentration of the molecularly dispersed sulphur slowly released from $Na_2S_2O_3$ increased until critical supersaturation was reached, at which time the nucleation of the solid sulphur took place. The nuclei then grew by diffusion only, i.e., no secondary nucleation took place. Matijevic [131] applied similar ideas to the generation of metal (hydrous) oxide particles. Assuming only hydroxylation of a metal species in solution, the mechanism of precipitation is similar to:

$$n[M(H_2O)_p]^{z+} - \xrightarrow{OH^-} \rightarrow [M_n(H_2O)_{np-m}(OH)_m]^{(nz-m)+} - \xrightarrow{OH^-} \rightarrow nM(OH)_z$$

These complexes act as precursors to nucleation and their rate of generation will affect subsequent particle growth. As the compositions of metal salt solutions are sensitive to various parameters, reproducible precipitation is difficult to assure by simple addition of a base to an electrolyte solution. Hydroxylation of metal ions is greatly accelerated by increasing solution temperature. Such forced hydrolysis facilitates the formation of the complex precursors to nucleation of metal (hydrous) oxide sols. The process involves deprotonation of hydrated metal ions according to

$$n[M(H_2O)_p]^{z+} \rightarrow [M_n(H_2O)_{np-m}(OH)_m]^{(nz-m)+} + mH^+$$

The complexes responsible for nucleation can be generated by judicious choice of pH, aging temperature and time. McFayden and Matijevic [139] devised a method for the formation of monodispersed copper (hydrous) oxide sols and this method was followed. After the experiment, large, visible particles precipitated, with no evidence of

monodispersity. These particles dissolved after one day. The experiment was repeated with gelatin in the solution to see if this affected the nucleation precursor, or if it would stabilise the resultant particles. Similar results to the first experiment were obtained. It was not possible to measure the size or electrophoretic mobility of these particles using the Zetasizer as the particles were > 3000 nm, i.e., too large for light scattering, and the electrolyte too strong, i.e., high ionic strengths produce high currents which cause severe ohmic heating effects. Brown, copper hydrous oxide particles in the order of 1200 nm (measured by SEM) were obtained by McFayden and Matijevic. Such particles would be too large and unstable for plating purposes.

4.16. Copper Ion Reduction by Regenerative Aqueous Reductants

As mentioned in **Section 2.7**, the use of regenerative aqueous reductants provides a possibly more economic method of copper reduction to form colloids than using unregenerated chemical systems. This being the case, two regenerative aqueous couples were used to reduce Cu^{2+} ions, Cr(II)/Cr(III) and V(II)/V(IV).

On addition of a Cr(II) solution to the copper colloid concentrate solution, the solution went dark immediately and after some time, large visible particles were present in a dark green solution. The zeta potential of these particles at 30 times dilution was about 15 mV; however, the particle size was too large to be measured by photo-correlation spectroscopy. A second test, omitting palladium as a catalyst for the reduction step, still indicated a very fast reaction, giving larger particles and a copper mirror finish to the bottom of the conical flask in which the reaction took place.

Copper reduction was also attempted with V(II) ions. The solution turned black immediately, indicating a fast reaction time. **Table 4.16.1** indicates zeta potentials and particle sizes measured for different dilutions of the colloid.

Table 4.16.1. *Dilution dependence of zeta potential and particle size of a copper colloid produced by the oxidation of V(II) in the presence of gelatin.*

Dilution factor	30	15	10
Zeta Potential / mV	15	14	15
Particle Size / nm	260	240	*

* - Solution to dark for light scattering.

Table 4.16.1 indicates that in this small dilution range, no major changes occurred in particle size and zeta potential. The zeta potential was similar, but the particle size slightly larger than those of colloids prepared using DMAB. This indicates that the relative potential or overpotential of the system could affect the size of particle produced. This solution was stable for about three months when kept under nitrogen and indicates that V(II) is a promising reductant. The larger particle sizes compared to those of particles formed by reduction of Cu(II) ions with DMAB may be due to coloumbic repulsion between the V(II) ion and the Cu(II) ion which could cause slower electron transfer, hence a slower nucleation rate and larger particles.

4.17. Other Alternative Reductants

Two powerful reductants, methanal and hydrazine, were investigated as possible alternatives to using DMAB. The reduction of copper ions directly onto silica using methanal was attempted as copper mirroring of beakers had been observed by Robey [140]. The result of adding methanal to a cold solution of copper sulphate was patchy, crystalline growth occurring on the floor of the beaker after two hours, not a mirror finish. A cleaned microscope slide was suspended in a solution of hot Fehling's solution overnight, as suggested by Robey, and a copper precipitate formed which, again, did not adhere to the glass very well. Mirroring occurred only in tiny scratches in the beaker, where presumably conditions were more favourable for nucleation and growth to occur.

Using hydrazine as a substitute for DMAB produced a pea green colloid from which a precipitate settled out after about 30 minutes. On filtration, the precipitate was white and could be dissolved in acid to form a blue solution. As the pH increased from 2.4 to about 5 on addition of hydrazine to the copper solution and with reference to the potential-pH diagram of the copper/water system (see **Figure 2.7.1.1**), it was assumed that this increase had caused the precipitation of $CuO/Cu(OH)_2$ prior to Cu^{2+} reduction. If during the manufacture of copper colloid concentrates (see **Section 3.6**), the copper sulphate/gelatin/palladium solution was left for more than 30 minutes prior to the addition of H_2SO_4, the pH also rose to about 5 and a similar white precipitate was observed.

4.18. Potentials of Copper Colloidal Particles

Potentials obtained from colloids stored under nitrogen were plotted on a potential-pH diagram of the copper/water system, **Figure 4.18.1.** The potential of a 'normal' colloid was measured as about +40 mV after 66 days (pH 8.06). Comparison of these potentials shows that the colloid particles are just in the metal region of the diagram.

Figure 4.18.1. *Potential-pH diagram of the copper/water system at 25 °C, $a_{Cu} = 0.1$, showing the relative positions of colloidal particles stored under nitrogen.*

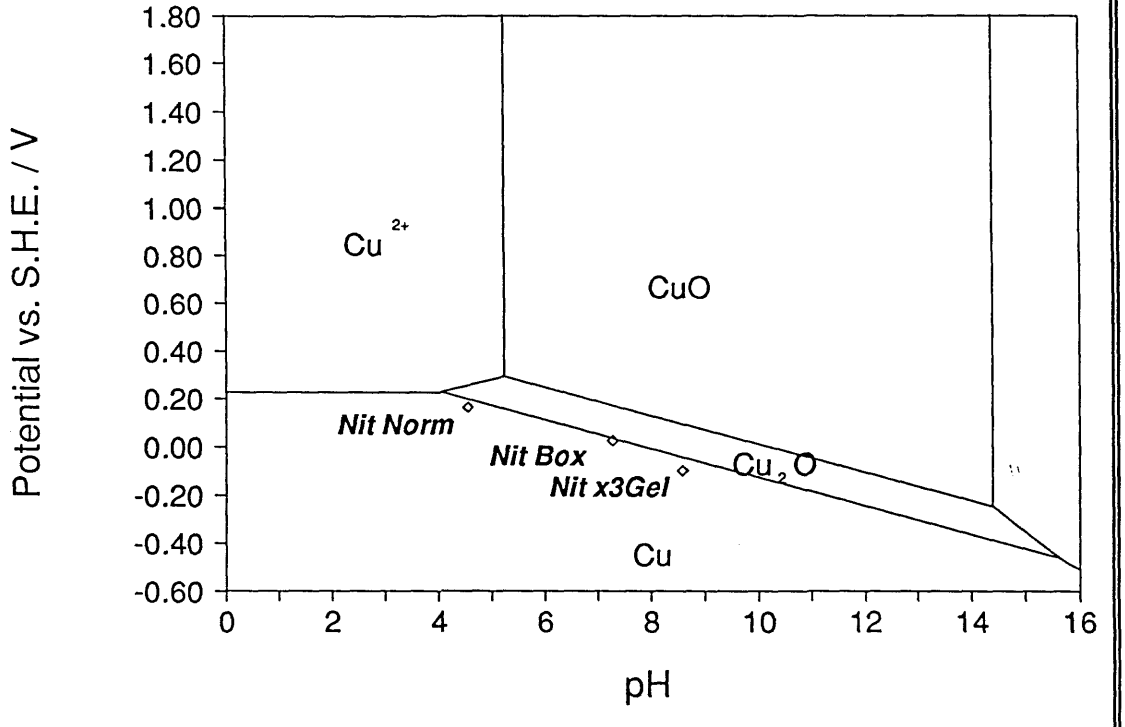

Nit x3Gel, *Nit Box* and *Nit Norm* experimental conditions are detailed in **Table 4.5.1.**

4.19. Analysis of the Oxidation of Dimethylaminoborane (DMAB) using Cyclic Voltammetry

To understand more about the formation of copper colloids, the oxidation of DMAB was studied using cyclic voltammetry in acidic conditions; copper and platinum electrodes were used to enable oxidation at high potentials to be investigated. Oxidation at a mercury electrode did not give good results due to the formation of mercury chloride on the mercury surface. The results of these experiments are shown in **Figures 4.19.1** to **4.19.4.**

Figure 4.19.1. *Cyclic voltammogram of copper electrode in a) background electrolyte only, pH 2.4 (+) and b) 1 mol m^{-3} DMAB in background electrolyte, pH 2.4 (-). Sweep rate = 100 mV s^{-1}.*

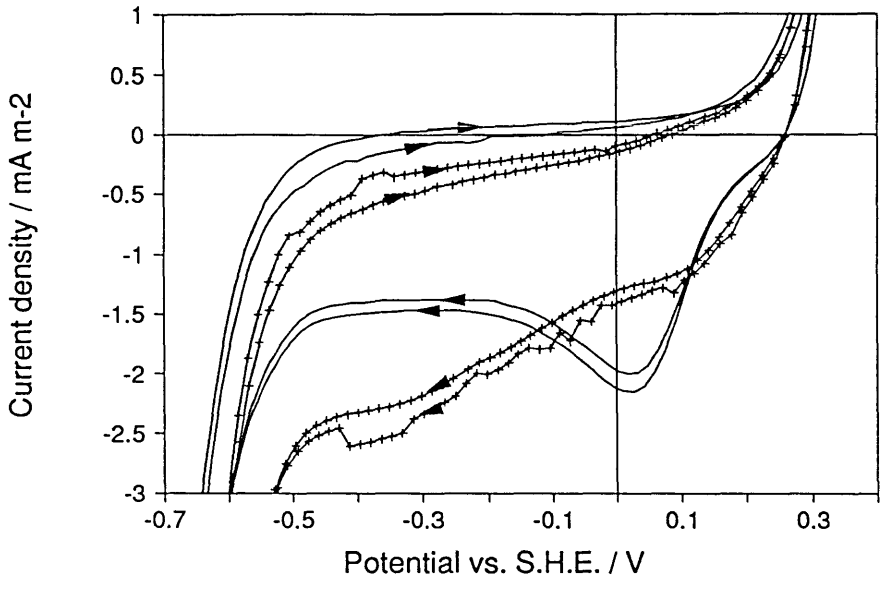

When DMAB was present, a small copper reduction peak appeared that did not occur with background electrolyte only which could indicate that DMAB has the ability to complex Cu(II) in solution, or that DMAB oxidation at these potentials affects the net current density

Figure 4.19.2. *Cyclic voltammogram of copper electrode in a) background electrolyte only, pH 2.4 (+) and b) 1 mol m^{-3} DMAB in background electrolyte, pH 2.4 (-). Sweep rate = 10 mV s^{-1}.*

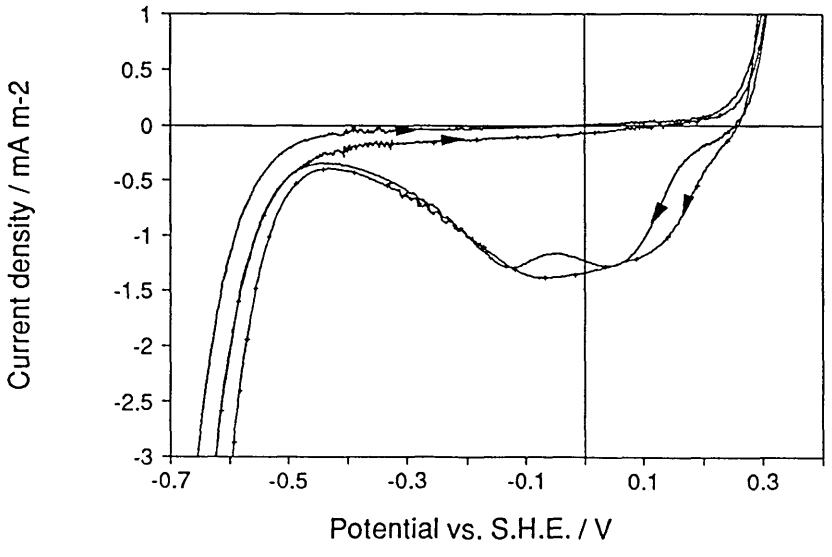

At a slower potential sweep rate there appeared to be more time for copper reduction to proceed. With background electrolyte only, there was a broad reduction peak, but with DMAB present there were two copper reduction peaks which indicates further evidence for a Cu-DMAB complex which first adsorbed, and was then reduced. The possibility of a Cu-DMAB complex was suggested indirectly from the observations of Ohno *et al.* [141] who reported that a copper electrode dissolved at pH 7.0 and 25 °C in 2 g dm^{-3} DMAB.

Figure 4.19.3. *Cyclic voltammogram of platinum electrode in background electrolyte only, pH 2.4. Sweep rate = 100 mV s^{-1}.*

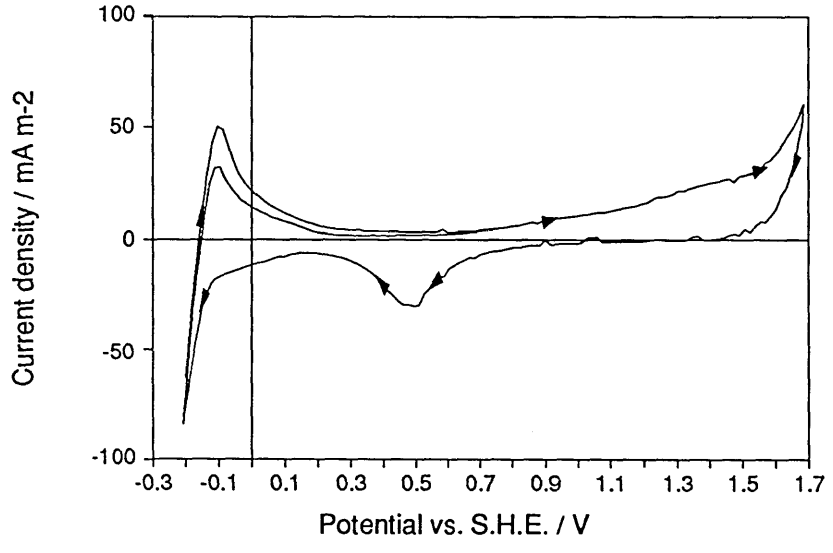

Figure 4.19.4. *Cyclic voltammogram of platinum electrode in 1 mol m^{-3} DMAB in background electrolyte, pH 2.4. Sweep Rate = 100 mV s^{-1}.*

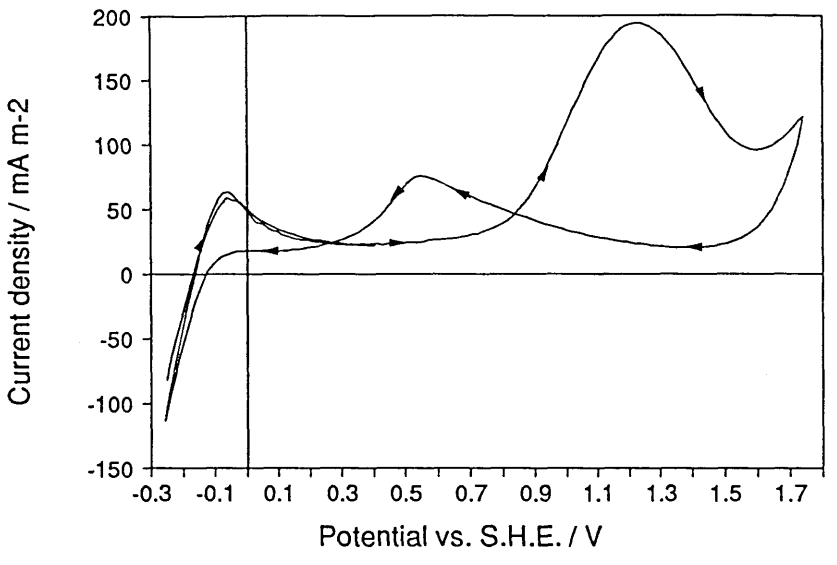

When a platinum electrode was used, a large peak occurred at +1.1 V to +1.2 V. This would appear to correspond to the oxidation of DMAB to boric acid. A similar peak was observed by Sazonova and Gorbunova [38] in alkaline solution. At higher temperatures, up to 70 °C, other peaks at lower potentials were observed which were thought to correspond to the oxidation of borane at the electrode surface. The unusual net current peak on the negative-going potential sweep was probably due to the reduction of platinum oxide on the surface of the electrode producing a fresh surface for further oxidation of DMAB.

When preparing colloid solutions, it was noted that reduction of copper by DMAB was very fast when palladium was present (<1 s), but very slow for copper sulphate alone (≈ 18 hours). It was thought that as Pd was the catalyst for copper reduction and DMAB oxidation in the copper colloid system, a palladium metal surface would catalyse the oxidation of DMAB in this system. As no noticeable oxidation occurred using a palladium coated platinum electrode, a palladium metal electrode was manufactured, but unfortunately, addition of DMAB to the background electrolyte did not change the shape of the voltammogram, even when the sweep rate was lowered from 100 to 10 mV s^{-1}. As the reaction appeared too slow to follow by voltammetry, the reaction was investigated using the Hewlett Packard 8451A Diode Array Spectrophotometer. It was seen that clear solutions of DMAB absorb only below about λ = 195 nm, which made it difficult to judge

when changes occurred due to oxidation. The effect of putting powerful oxidising agents into the solution such as H_2O_2 to oxidise DMAB had the effect of swamping the DMAB signal.

4.20. Electrode Impedance Spectroscopy (EIS) of a Copper Surface

Electrode impedance spectroscopy was used to measure the capacitance of the double layer obtained at a copper surface. Information about the charge at a copper surface would be useful in understanding the bonding mechanisms of steric stabilisers. Gelatin was added to the electrolyte to assess the change in capacitance and hence charge at the surface. Before EIS work was commenced the solutions were analysed using cyclic voltammetry to define a perfectly polarised double layer region. The results are shown in **Figures 4.20.1** and **4.20.2.**

Figure 4.20.1. *Cyclic voltammogram of copper electrode in a) pH 2.9 background electrolyte (+) and b) 2 g dm^{-3} gelatin in background electrolyte (-). Sweep rate = 100 mV s^{-1}.*

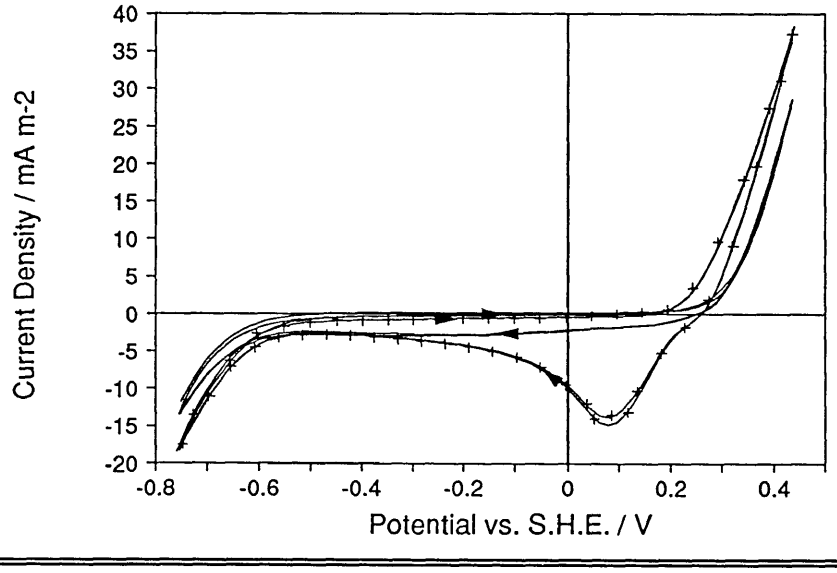

Figure 4.20.2. *Cyclic voltammogram of copper electrode in a) pH 9 background electrolyte (+) and b) 2 g dm^{-3} gelatin in background electrolyte (-). Sweep rate = 100 mV s^{-1}.*

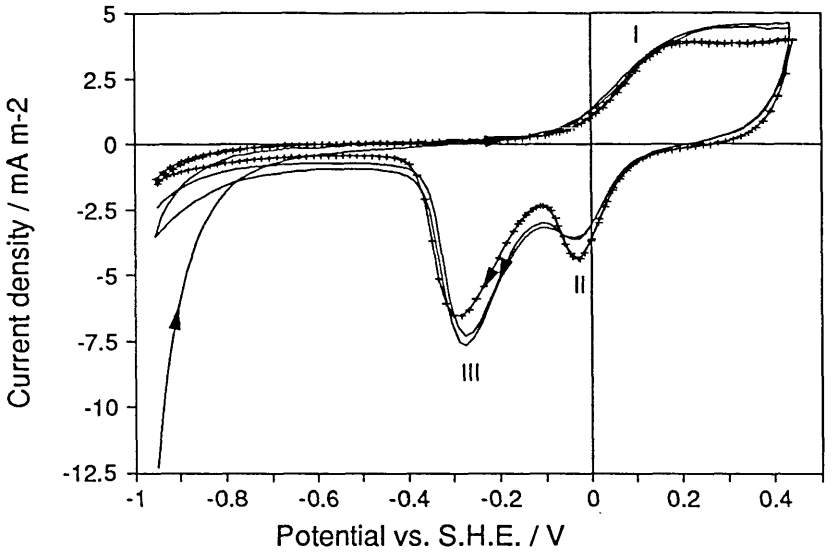

The potential range extended from the onset of hydrogen evolution to the beginning of cuprous hydroxide formation. When gelatin was added to the pH 2.9 electrolyte, the copper reduction peak disappeared which indicated that gelatin prevented the reduction of copper ions at the surface. Gelatin affected the diffusion of Cu^{2+} ions both away from and back to the electrode, but the net effect was to decrease the reduction current. This may be due to the effect of gelatin on the viscosity and the Cu^{2+} ion concentration, which in turn affect the limiting current density. The limiting current density, i_L is related to the diffusion coefficient, D, by

$$i_L = -\frac{zFD}{\delta} C_{Cu^{2+}}$$

where z = number of electrons,

F = Faraday constant,

δ = double layer width and

$C_{Cu^{2+}}$ = concentration of Cu^{2+} ions.

The diffusion coefficient is related to the viscosity, η, by the Stokes-Einstein relation:

$$D = \frac{kT}{6\pi\eta a}$$

where k = Boltzman constant,

T = temperature and

a = effective ionic radius.

Therefore, as the viscosity increased, the limiting current density decreased. Peak I was the formation of cupric oxide:

$$Cu + H_2O \rightarrow CuO + 2H^+2e^-$$

The first reduction peak, peak II, was the reduction of cupric oxide to cuprous oxide:

$$2CuO + 2H^+2e^- \rightarrow Cu_2O + H_2O$$

The second reduction peak, peak III, was the reduction of cuprous oxide to copper:

$$2Cu_2O + 2H^+2e^- \rightarrow 2Cu + H_2O$$

The fact that the reduction potential did not return to its initial value of about -0.25 V in gelatin indicated that there was an accumulation of CuO at this sweep rate. Further evidence for this hypothesis was the decrease of the CuO reduction peak in the presence of gelatin. The impedance spectra for the copper electrode in pH 2.9 and 9 electrolyte solutions, with and without gelatin are shown in **Figures 4.20.3** and **4.20.4.**

Figure 4.20.3. *Impedance spectra of copper electrode in a) pH 2.9 background electrolyte and b) 2 g dm^{-3} gelatin in background electrolyte. Potential = -0.2 V vs. S.H.E., frequency range = 1 to 65000 Hz.*

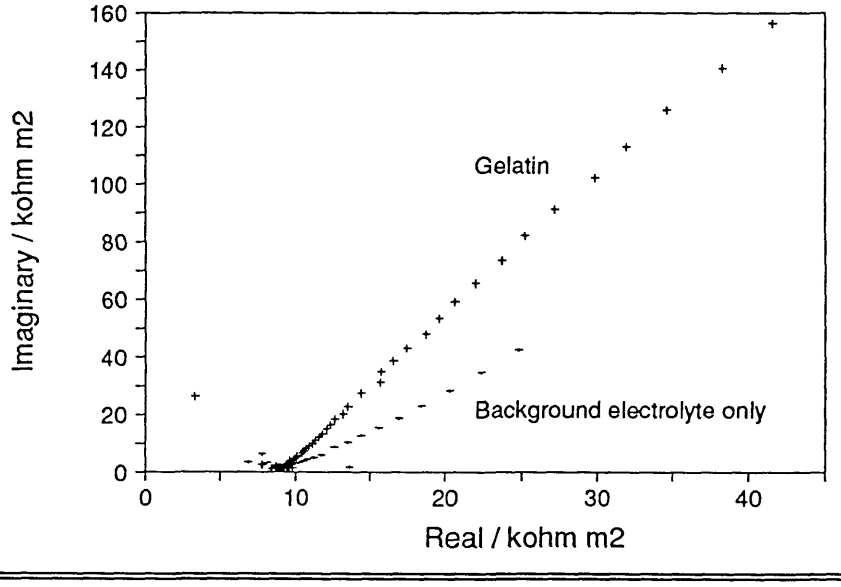

Figure 4.20.4. *Impedance spectra of copper electrode in a) pH 9 background electrolyte and b) 2 g dm^{-3} gelatin in background electrolyte. Potential = -0.2 V vs. S.H.E., frequency range = 1 to 65000 Hz.*

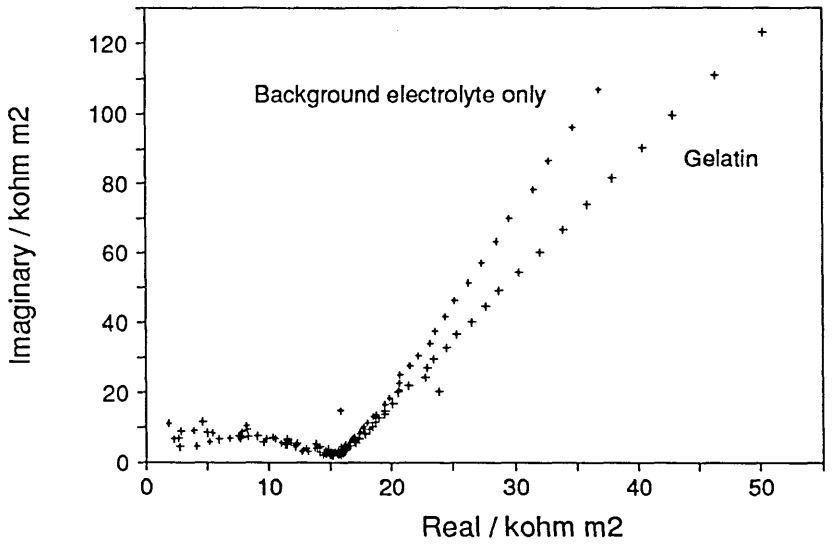

In the frequency range over which these readings were taken, there was an unusual response from all conditions which took the form of a straight line. If this were at 45°, then it could be assigned to the Warburg diffusional impedance. As the angle was steeper than this, it appears that there were capacitative effects taking place which may have been due to Cu(II) ion diffusion from the electrode. To examine the response more closely, frequencies >6000 Hz were used to obtain **Figures 4.20.5** to **4.20.8**.

Figure 4.20.5. *Impedance spectra of copper electrode in pH 2.9 background electrolyte only. Potential = -0.2 V vs. S.H.E.*

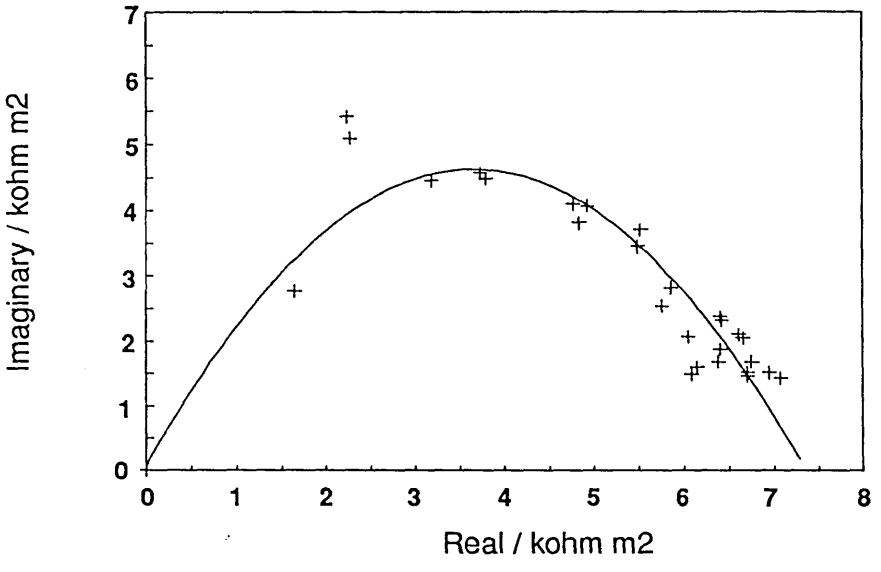

Figure 4.20.6. *Impedance spectra of copper electrode in pH 2.9 background electrolyte and 2 g dm^{-3} gelatin. Potential = -0.2 V vs. S.H.E.*

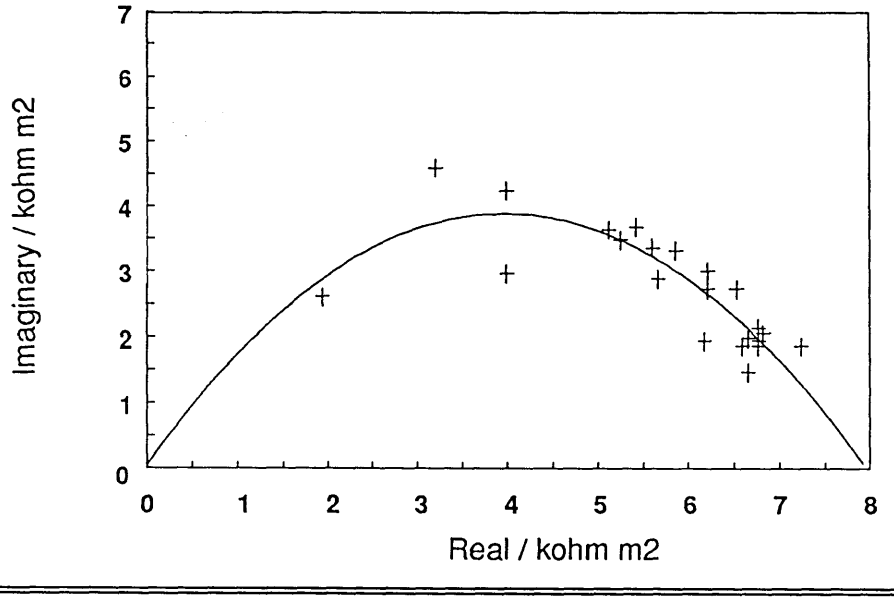

Figure 4.20.7. *Impedance spectra of copper electrode in pH 9 background electrolyte only. Potential = -0.2 V vs. S.H.E.*

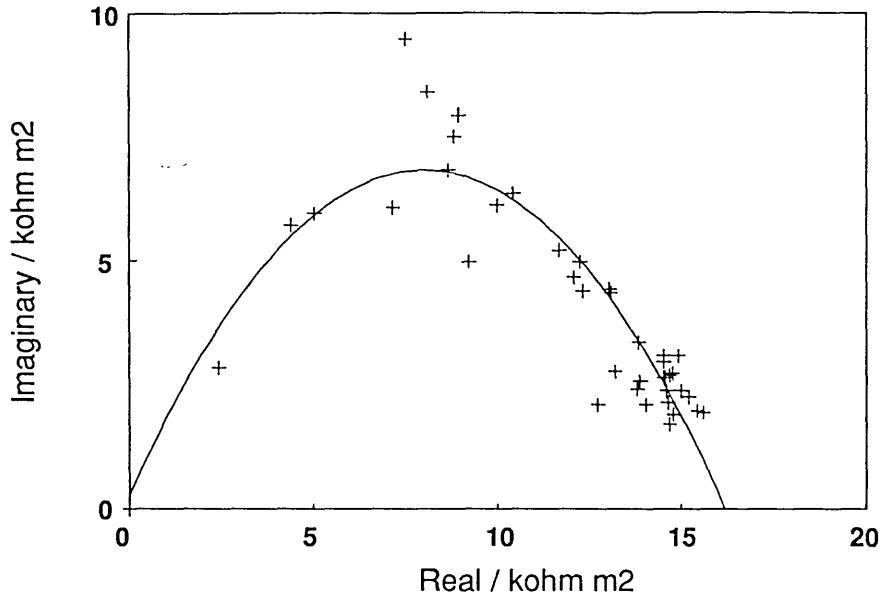

Figure 4.20.8. *Impedance spectra of copper electrode in pH 2.9 background electrolyte and 2 g dm^{-3} gelatin. Potential = -0.2 V vs. S.H.E.*

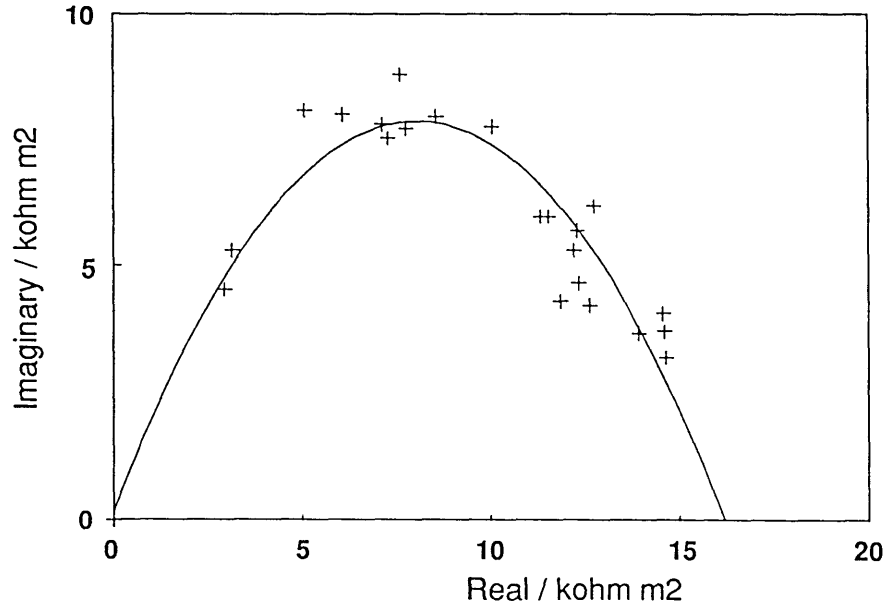

These plots exhibited much "noise" at high frequencies which may have been due to stray capacitance between connecting leads to earth and the leads themselves or self inductance of leads. Values of the capacitance of the double layer and its resistance are listed in the **Table 4.20.1.**

Table 4.20.1. *Values of the capacitance and resistance of the double layer at a copper electrode in the presence or absence of gelatin.*

Conditions	pH	Potential vs. S.H.E. / V	Capacitance / F m^{-2}	Resistance / kohm m^{-2}
No gelatin	2.9	-0.1	1.3	4.5
Gelatin	2.9	-0.25	1.7	4.0
No gelatin	9	-0.3	1.1	6.8
Gelatin	9	-0.2	0.9	7.8

Although there are many studies of copper electrodes in alkaline solution in the literature, most of these investigations are concentrated on the study of oxide formation on copper surfaces. Wanner *et al.* [142] found capacitance peaks in the order of 0.8 F m^{-2} in the polarizable region (-1.2/-0.4 V at pH 11.8) in sodium sulphate and sodium fluoride electrolytes which they ascribed to the specific adsorption of OH^- ions. The hysteresis of the curves indicated that the adsorption was not a simple reversible reaction.

The capacitances obtained seemed low and therefore the cell geometry was changed and a potential sweep was carried out at fixed frequencies to obtain more accurate data.

Cycling the potential over a range of frequencies from 1000 to 100 000 Hz gave impedance spectra in the presence and absence of gelatin, as shown in **Figure 4.20.9.**

Figure 4.20.9. *Impedance spectra of copper electrode in a) pH 2.4 background electrolyte (+) and b) 1 g dm^{-3} gelatin in background electrolyte (■). Potential = -0.2 V vs. S.H.E.*

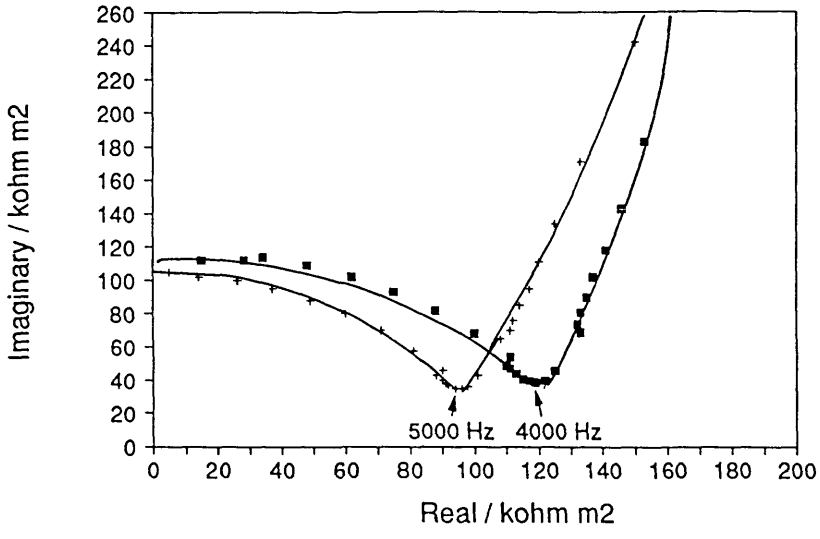

Attempts to measure the capacitance were made by sweeping the potential at fixed frequencies, **Figures 4.20.10** to **4.20.13.**

Figure 4.20.10. *Capacitance vs. potential curve of copper electrode in a) pH 2.4 background electrolyte (+) and b) 1 g dm^{-3} gelatin in background electrolyte (■). Potential = -0.2 V vs. S.H.E.*

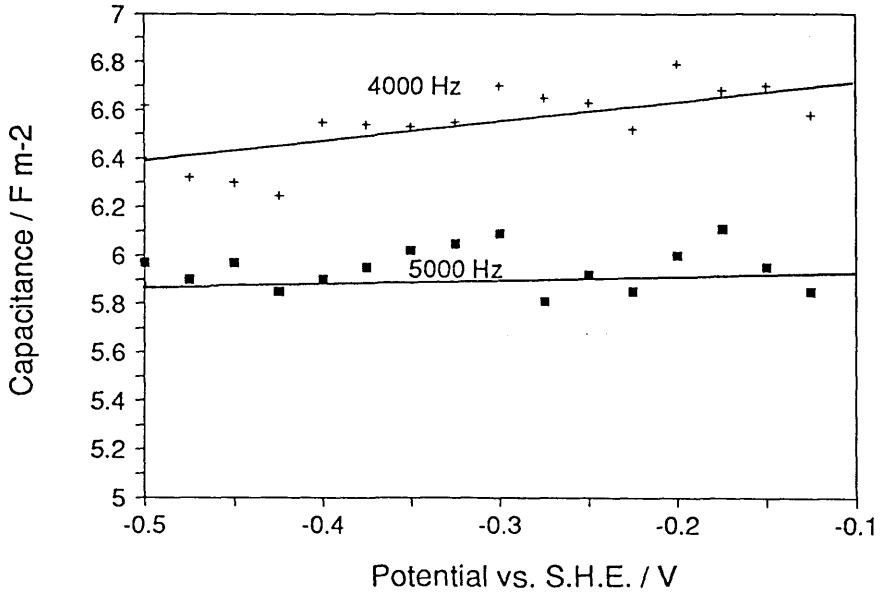

Figure 4.20.11. *Capacitance vs. potential curve of copper electrode in a) pH 2.4 background electrolyte (+) and b) 1 g dm^{-3} gelatin in background electrolyte (■). Potential = -0.2 V vs. S.H.E., frequency = 100 Hz.*

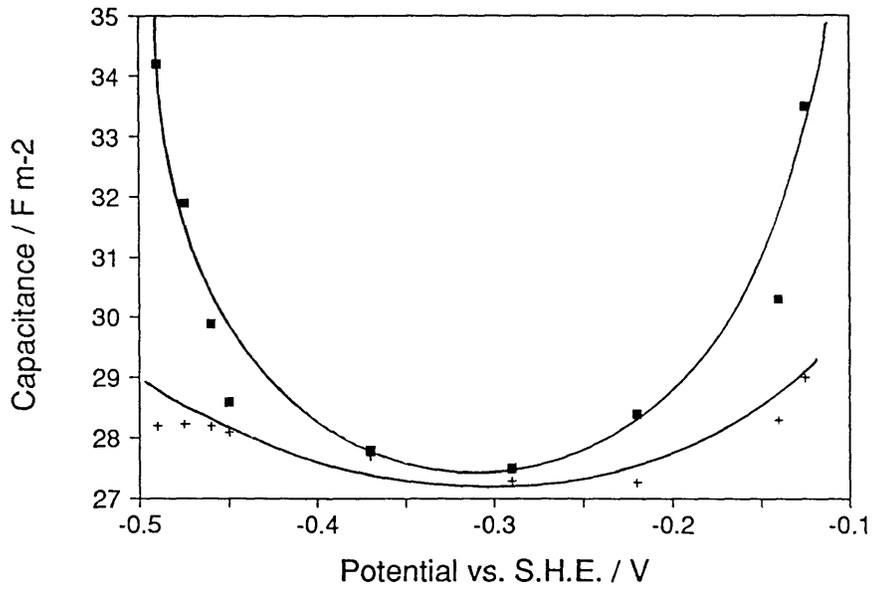

Figure 4.20.12. *Capacitance vs. potential curve of copper electrode in a) pH 2.4 background electrolyte (+) and b) 1 g dm^{-3} gelatin in background electrolyte (■). Potential = -0.2 V vs. S.H.E., frequency = 1000 Hz.*

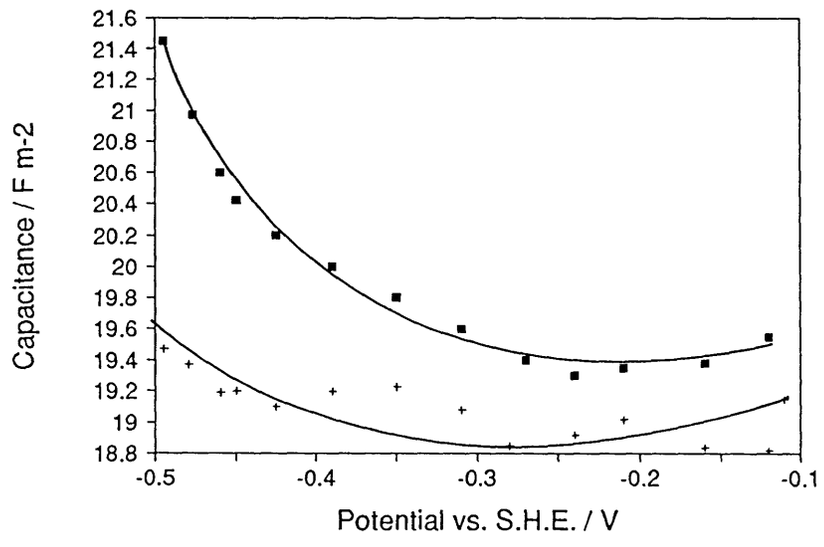

Figure 4.20.13. *Capacitance vs. potential curve of copper electrode in a) pH 2.4 background electrolyte (+) and b) 1 g dm^{-3} gelatin in background electrolyte (■). Potential = -0.2 V vs. S.H.E., frequency = 10000 Hz.*

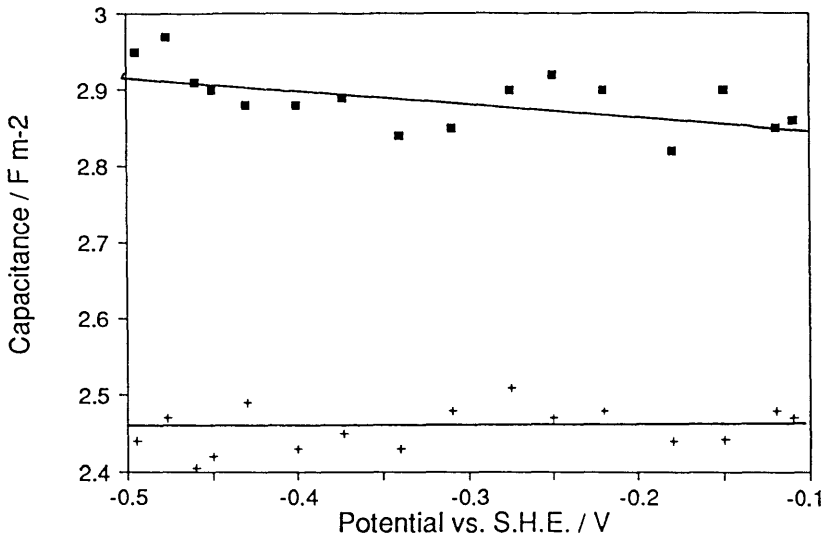

At the same frequency, the capacitance of the double layer appeared to decrease when gelatin was present; however, **Figure 4.20.11** shows that at similar points on the impedance spectra shown in **Figure 4.20.10**, the capacitance of the double layer when gelatin was present was higher. It is apparent from **Figure 4.20.10** that the change in the impedance spectra due to gelatin has two components. Firstly, there was an increase in the diffusion coefficient leading to an increase in diffusion resistance, and secondly there was an increase in the capacitance of the double layer which may have been due to gelatin decreasing the concentration of Cu^{2+} ions in the diffusion layer.

4.21. Size analysis of Colloid Particles

Analysis of the size and dispersity of copper colloid particles presented several problems which were tackled in various ways. Particle sizes were typically in the order of 100 to 300 nm. Size analysis using the scanning electron microscope was found to give problems associated with drying of the samples (mentioned in **Section 4.10**). *In-situ* size analysis was carried out using photo-correlation spectroscopy which measures the equivalent hydrodynamic diameter of the scattering particles. These entities could be primary particles or agglomerates depending on the solution conditions.

4.21.1. *Analysis of the Method of Dilution used to obtain Adequate Light Scattering*

Due to the high light absorption of copper colloid concentrates, it was necessary to dilute samples before analysis. Dilution should be to the point where the particles are non-interacting and do not give multiple scattering of light, i.e., for photo-correlation spectroscopy, the scattering of light from individual particles is required. Different methods were used in diluting the colloid and the results obtained from measuring these samples on the Zetasizer are shown in **Table 4.21.1.1.**

Table 4.21.1.1. *Comparison of methods of dilution of colloid to obtain particle size and electrophoretic mobility data.*

Method of dilution	Particle Size			Electrophoretic Mobility / $m^2 V^{-1} s^{-1}$	pH
	Average / nm	Polydispersity	90 % in range / nm		
Water	590	0.55	170-2000	+0.28	7.21
Oxygen free water	780	6.1	14-3000	+0.10	7.21
0.1 kmol m^{-3} borax	920	6.6	45-3000	+0.21	7.94

The results indicate that the particle size and electrophoretic mobility measured was dependent on the method used to dilute the solution, possibly due to the effect ion concentration on the conformation of gelatin leading to agglomeration.

4.21.2. *Comparison of Size Distributions obtained with a Zetasizer IIc and PCS7 Photo-correlation Spectrophotometer (PCS)*

In-situ size analysis using photo-correlation spectroscopy was initially carried out on the Zetasizer as it was convenient to measure both electrophoretic mobility and particle size simultaneously. However, the Zetasizer is not capable of model-independent particle size measurements as the data processing software fits a log-normal distribution to all size

analyses. Therefore, a Malvern 4700 Photo-Correlation Spectrophotometer was also used to measure particle size. The results of measuring the particle sizes of five samples of copper colloid concentrate are shown in **Figures 4.21.2.1** to **4.21.2.5.**

Figure 4.21.2.1. *Time dependence of average mean particle size for copper colloid catalyst after dilution by a factor of 250.*

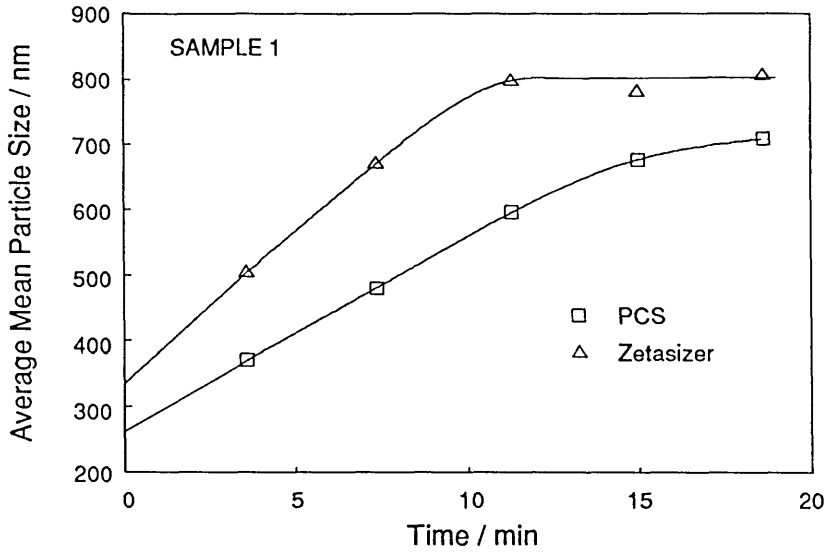

Figure 4.21.2.2. *Time dependence of average mean particle size for copper colloid catalyst after dilution by a factor of 250.*

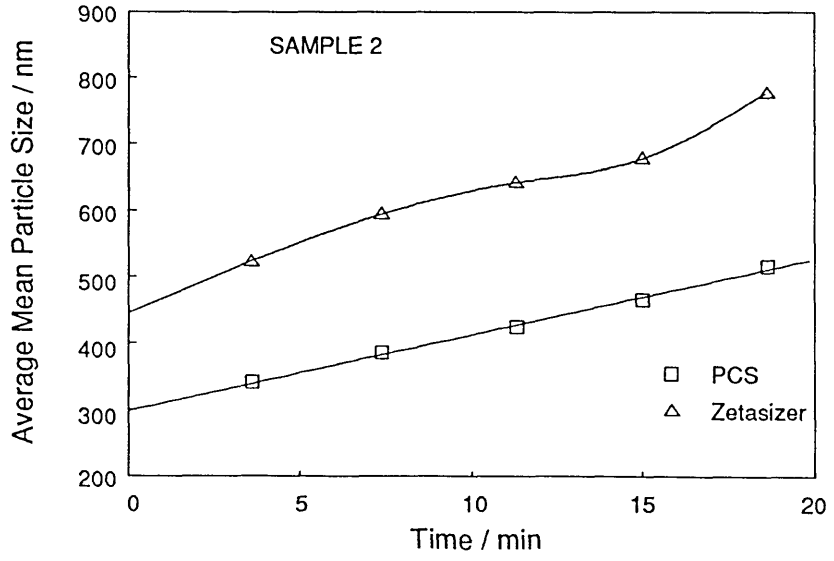

Figure 4.21.2.3. *Time dependence of average mean particle size for copper colloid catalyst after dilution by a factor of 250.*

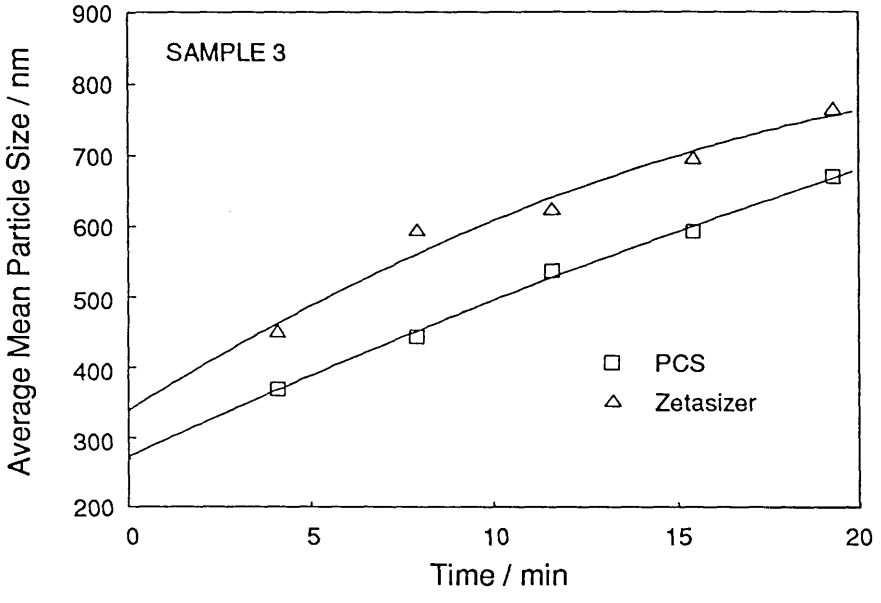

Figure 4.21.2.4. *Time dependence of average mean particle size for copper colloid catalyst after dilution by a factor of 250.*

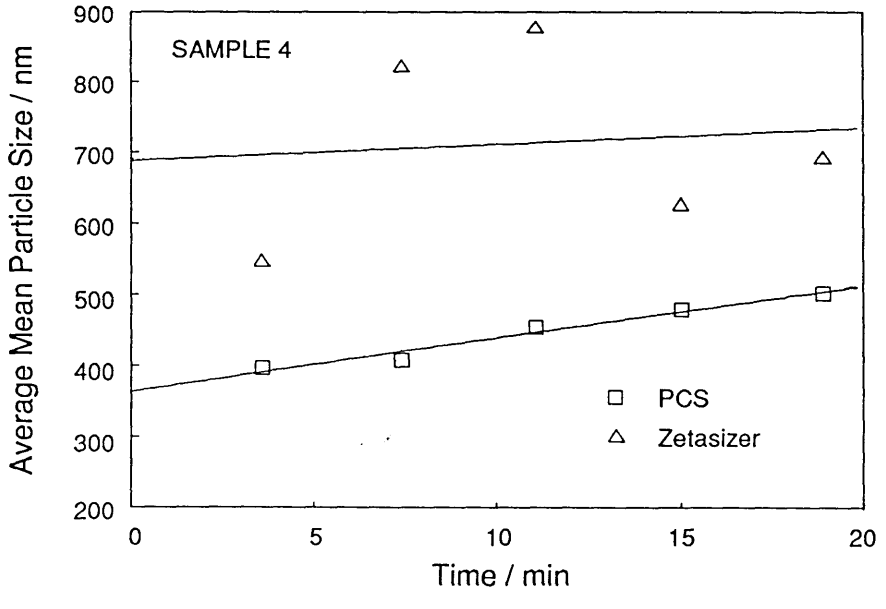

Figure 4.21.2.5. *Time dependence of average mean particle size for copper colloid catalyst after dilution by a factor of 250.*

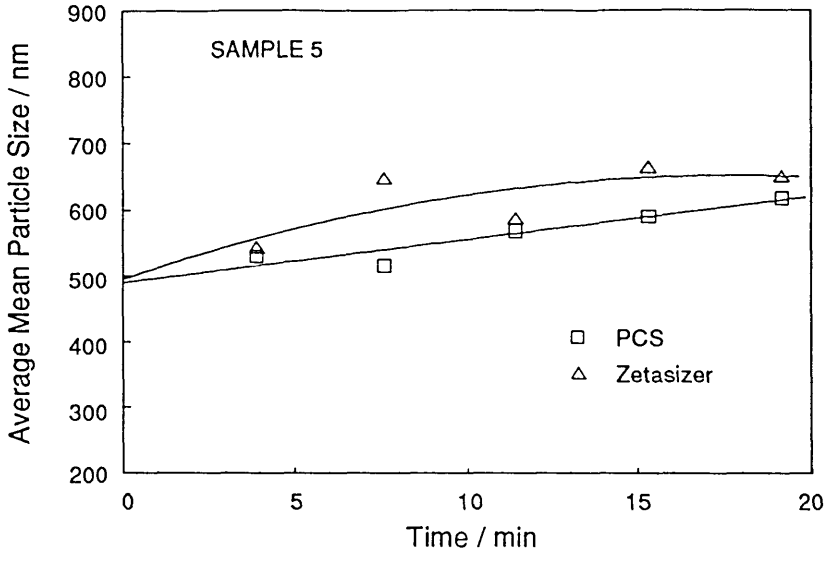

The Zetasizer gave an average mean particle size that was always greater than that given by the PCS, (on average 150 nm larger) although values varied widely. The distribution was always much wider on the Zetasizer as well (e.g., for the latex dispersion in **Figure 4.21.2.6** the Zetasizer gave a value of 90 % of particles in the size range 110 to 1550 nm whereas the PCS gave 90 % in the range 318 to 680 nm). To get a more accurate assessment of the difference between the two instruments, the results of the particle size measurement of a monodisperse latex by both instruments are shown in **Figure 4.21.2.6.**

Figure 4.21.2.6. *Time dependence of average mean particle size for a latex dispersion in 1 mol m^{-3} KCl.*

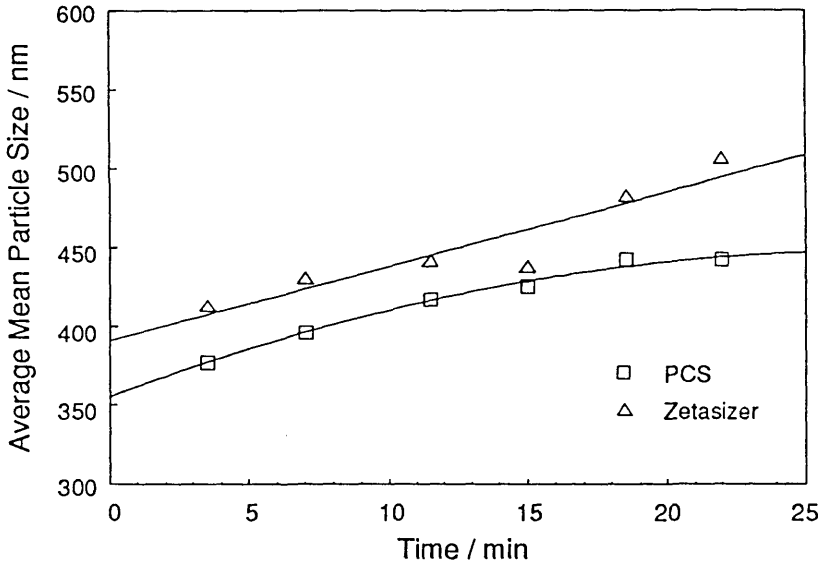

The curve obtained from the PCS was smoother than that obtained from the Zetasizer, and similar to curves obtained in **Figures 4.21.2.1** to **4.21.2.5**. The size was smaller by 40 nm on average, and the first reading (378 nm) was closer to the manufacturers specified size (370 nm) than that given by the Zetasizer (413 nm).

In all cases, particle size increased over the time of measurement. This was most likely due to coagulation as the curves obtained from the PCS measurements of the copper colloid concentrates are similar to the curve for the latex dispersion which was known to be caused by coagulation. The latex dispersion was electrostatically stable in water, but in a dilute electrolyte, it agglomerated due to the effects of increased electrolyte concentration described in **Section 2.3.2** and illustrated in **Figure 2.3.2.2**. It was likely that when the copper colloid concentrate was diluted, then electrostatic stabilisation became as important as steric stabilisation in maintaining a dispersed colloid.

4.21.3. Effect of Electrolyte and Dilution on Measured Particle Size

Section *4.21.1* showed that the measurement of particle size using photon-correlation spectroscopy was dependent on the method of dilution used. As the electrolyte concentration was decreased when diluting with water, the colloid was diluted with an electrolyte. The strength of the electrolyte is important in that it can affect both the charge on the particles, through the concentration of potential determining ions, and the

conformation of the gelatin that surrounds the copper core of the particle. Either of these effects can lead to changes in size or cause agglomeration. Two electrolytes were used for dilution; KCl and H_2SO_4, i.e., a monovalent and divalent electrolyte, at three concentrations. The results are shown below.

Figure 4.21.3.1. *Effect of valency of electrolyte and dilution on the time dependence of average mean particle size of a copper colloid concentrate prior to addition of hydrazine.*

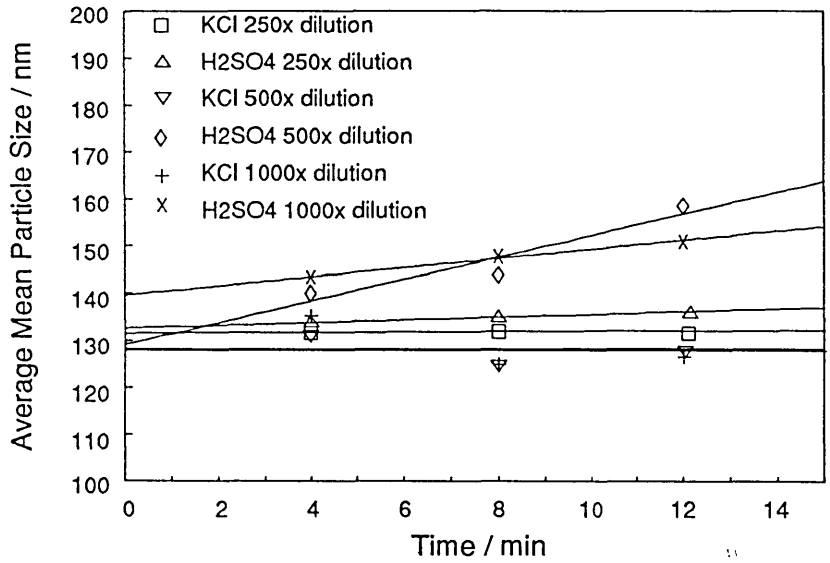

At all concentrations of H_2SO_4 there was an increase in average particle size with time that was not evident with KCl. This indicates that the particles were electrostatically stabilised when diluted, as the monovalent ion appears to give a more stable dispersion than the divalent ion. As shown in **Section 2.3.2**, $\kappa \propto z$, and as κ increases, the double layer decreases leading to decreased stability. **Figure 4.21.3.2** shows the difference in potential energies between particles in monovalent and divalent systems for similar particles. Both systems are unstable, but the monovalent system can be seen to be more stable than the divalent system.

Figure 4.21.3.2. *Total energy of interaction between two spherical copper particles in a) a 1 mM monovalent electrolyte and b) a 1 mM divalent electrolyte at a zeta potential of 40 mV.*

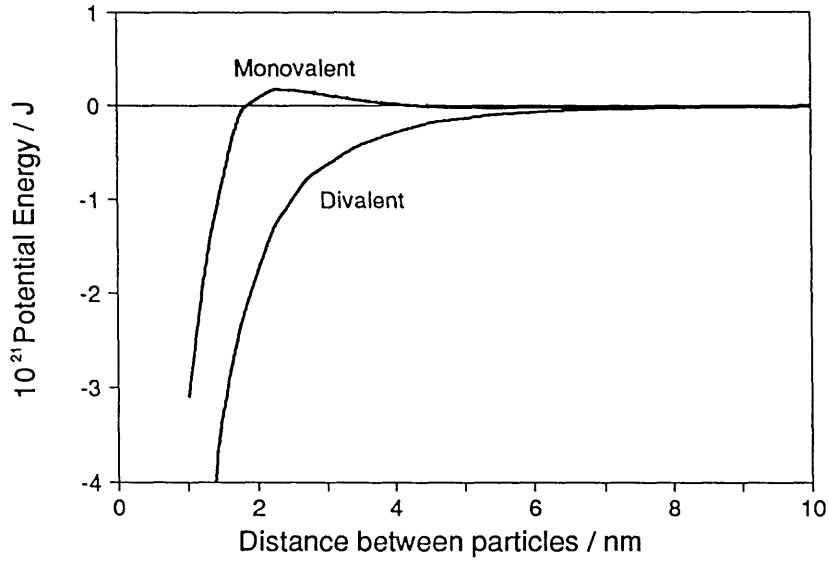

Dilutions greater than a factor of 250 had the effect of increasing average particle size when the electrolyte was H_2SO_4 and giving unreproducible results when the electrolyte was KCl. At dilutions less than 250 times, measurement was possible, but much "haloing" due to secondary scattering was observed which gave spurious results. A different colloid sample was filtered with glass microfibre filter paper to remove any coarse solids and the experiment repeated (see **Figure 4.21.3.3**). The results obtained confirm the effect seen in **Figure 4.21.3.1.**

Figure 4.21.3.3. *Time dependence of average mean particle size for a filtered copper colloid concentrate prior to addition of hydrazine, at 250 times dilution in 1 mol m^{-3} solutions of a monovalent and divalent electrolyte.*

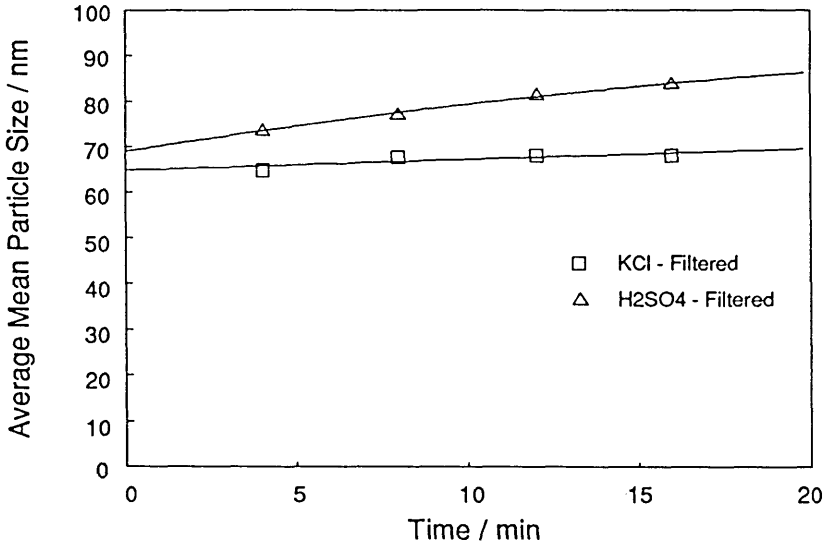

4.21.4. Effect of Concentration of Electrolyte used for Dilution

Having found that a dilution of 250 times using KCl gave the best results, the concentration of KCl was then varied to observe the effect on size. The results are shown in **Figure 4.21.4.1.**

Figure 4.21.4.1. *Effect of concentration on the time dependence of average mean particle size for a copper colloid concentrate prior to addition of hydrazine at 250 times dilution in 1 mol m^{-3} KCl.*

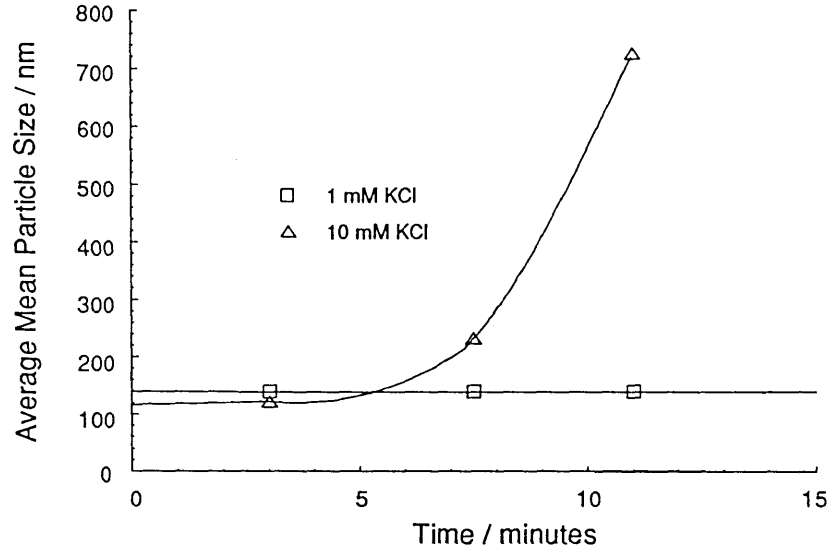

The graph indicates that the measured particle size started at roughly the same value for both concentrations, but was followed by a rapid increase in agglomeration for the 10 mM KCl solution. This gives more evidence that the colloid was stabilised electrostatically when diluted because, as shown in **Section 2.3.2**, $\kappa \propto c^{1/2}$, therefore at higher concentrations of electrolyte the particle double layer thickness decreased which led to a net attraction between particles and hence agglomeration. The effect can be seen in **Figure 4.21.4.2.**

Figure 4.21.4.2. *Graph of the total energy of interaction between two 5 nm spherical copper particles in various concentrations of monovalent electrolyte at a zeta potential of 25 mV.*

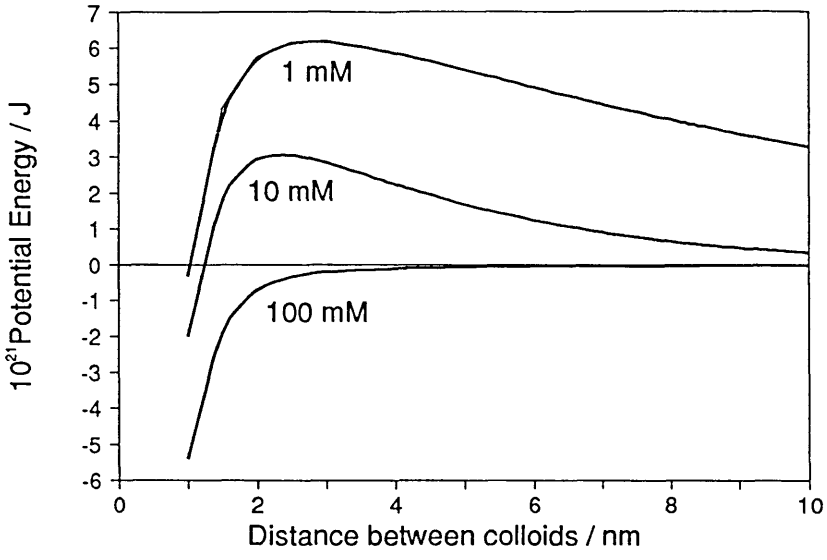

Having found that optimum conditions for colloid particle size were 250 times dilution with 1 mM KCl, this was used as the standard method in subsequent testwork.

4.22. Measurement of Colloid Particle Size during its Process Stages

During the production of a copper colloid concentrate, the particle size was measured at three stages; a) prior to, and b) post hydrazine addition and c) the final size after addition of the surfactant. The final product was also filtered to remove any coarse solids and measured. The results of these measurements are shown in **Figure 4.22.1.**

Figure 4.22.1. *Time dependence of average mean particle size for a normal copper colloid concentrate diluted 250 times in 1 mol m^{-3} KCl.*

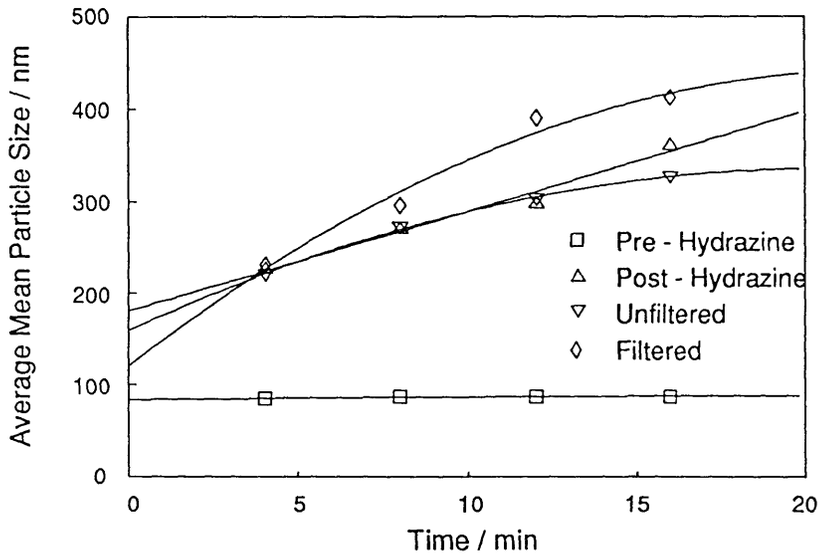

As there were only four measurements made with time, the "best fit" lines that have been drawn through the points lend clarity to the graph rather than suggest some functional relationship. A single measurement on the PCS took about 3.5 minutes and so the points were placed over the average of that time. The point at which the extrapolated lines reach zero time does not necessarily imply that the particles were this size at the moment of dilution. The best indicator of colloid size, or at least the one that can be used for fairest comparison, is the first measurement, with the proviso that this is probably larger by 10 to 20 nm than the real particle size.

The size of the particles increased after hydrazine addition, indicating that it was responsible for further particle growth by the reduction of free Cu(II) known to be present. All measurements post hydrazine addition showed a marked increase in particle size with time, indicating that agglomeration occurred, possibly due to the increased ionic strength. This may indicate the absolute stability of the concentrate, suggesting it was more stable prior to the addition of hydrazine. The addition of surfactant appeared to have little effect on particle size or stability. Filtering in this case seemed to have little effect on the average size of particles measured, but agglomeration seemed more rapid, suggesting that some free gelatin may be removed from the system.

4.23. Effect of Initial pH on Colloid Particle Size

The pH of the copper solution used in the production of a copper colloid is lowered from about 4 to 2.4 by the addition of H_2SO_4 (see **Section 3.6**). pH can have a critical effect on particle size due to its effect on the extent of formation of polynuclear hydroxy species of Cu(II) [22], its effect on double layer thickness and effect on the conformation of gelatin. A colloid sample was made without addition of H_2SO_4 which resulted in a pH of 4.5 prior to addition of DMAB. The average particle size measured is shown below in **Figure 4.23.1**.

Figure 4.23.1. *The effect of not adding acid prior to DMAB addition on the time dependence of average mean particle for a copper colloid concentrate diluted 250 times with 1 mol m^{-3} KCl solution.*

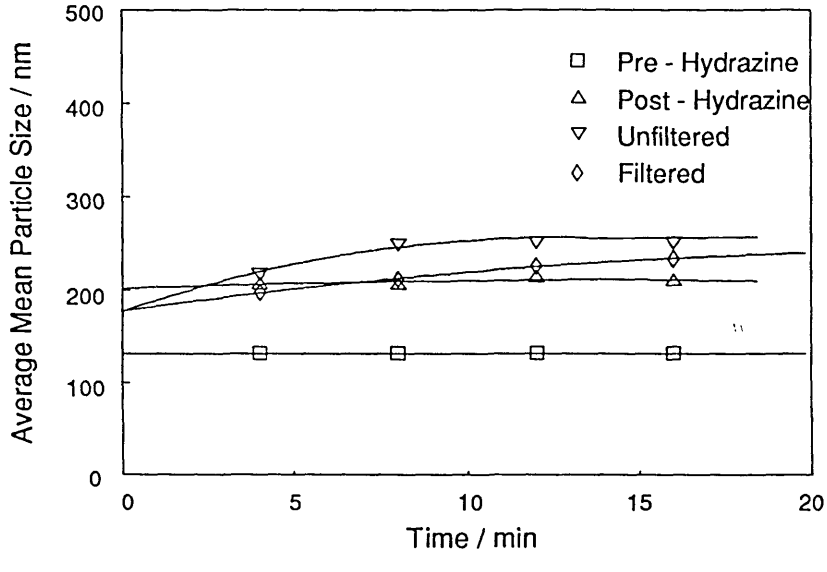

By comparing this graph with **Figure 4.22.1**, it can be seen that in both cases the unfiltered final size was around 220 nm, though there are several interesting differences between the graphs. Firstly, the initial particle size, prior to hydrazine addition, was significantly larger (130 vs. 85 nm), although the final sizes were very similar (218 vs. 221 nm). This indicates that as the pH was higher in this sample, the copper ions could have hydrolysed to a greater extent and thus formed larger particles. A second possibility is that the difference in pH caused by lack of acid addition alters the conformation of gelatin and thus changes particle size. The first possibility is the most likely as the pHs differ greatly from the iep of the gelatin (pH 8.8). If the first possibility were true then the polydispersity of the sample would be expected to be greater, but on average, it was the same. The second point of

interest is that the slopes were not as steep as the normal sample, indicating that the sample was more stable to agglomeration. Filtering, or the addition of the surfactant appeared to have little effect.

4.24. Effect of Seeding Copper Concentrate Solution post DMAB Addition

The reaction kinetics of the reduction of Cu(II) by DMAB are exceedingly slow, unless a catalyst is added, such as Pd(II). DMAB can be added to a copper solution and no reaction will appear to take place until Pd(II) is added. In the normal production of a colloid, Pd(II) is added before DMAB, and this acts as a homogeneously dispersed catalyst for subsequent nucleation of copper particles. An experiment was carried out in which a small volume of Pd(II) was added to the bulk copper solution, after the addition of DMAB, to see what effect this had on the relative nucleation and growth kinetics. The results are shown in **Figure 4.24.1.**

Figure 4.24.1. *Effect of adding Pd(II) solution after the addition of DMAB on the time dependence of average mean particle size for a copper colloid concentrate diluted 250 times with 1 mol m^{-3} KCl solution.*

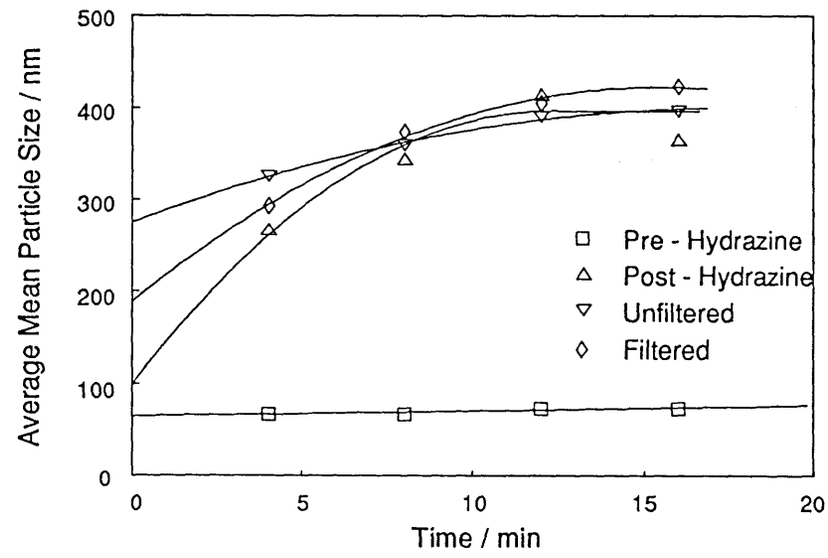

By comparison with **Figure 4.22.1**, which shows the behaviour of a normal sample, it can be seen that although the product after DMAB addition was slightly smaller (70 nm vs. 85 nm) the final product was considerably larger (330 nm vs. 220 nm). This suggests that when a small volume of catalyst was added to the reaction mixture, the nucleation rate

exceeded the particle growth rate. The DMAB already present in the solution immediately reduced Pd(II) to Pd, which formed as clusters. When copper nucleation started on these clusters, the result was smaller particles. When further reductant was added, because there was more Cu(II) in solution than normal, it could reduce to form larger particles. Thus the result of adding the seeding catalyst last was to form larger particles. A slight increase in the polydispersity was also noted (0.32 vs. 0.30) which might indicate the presence of larger particles.

4.25. Effect of Micromixing on Colloid Size

It can be seen from **Figure 4.24.1** that the order of mixing was important, but the effect of mixing rate on particle size and dispersity was unknown. The maximum mixing rate in was dependent on mixing the copper solution at high speed with a magnetic stirrer and adding the DMAB slowly. To achieve the highest mixing rate possible, a micromixing head which could be sonicated was used to mix equal volumes of DMAB and copper colloid concentrate solution. The results of the size analyses are shown in **Figures 4.25.1** and **4.25.2**.

Figure 4.25.1. *Effect of micromixing on the time dependence of average mean particle size for a copper colloid concentrate diluted 250 times with 1 mol KCl solution.*

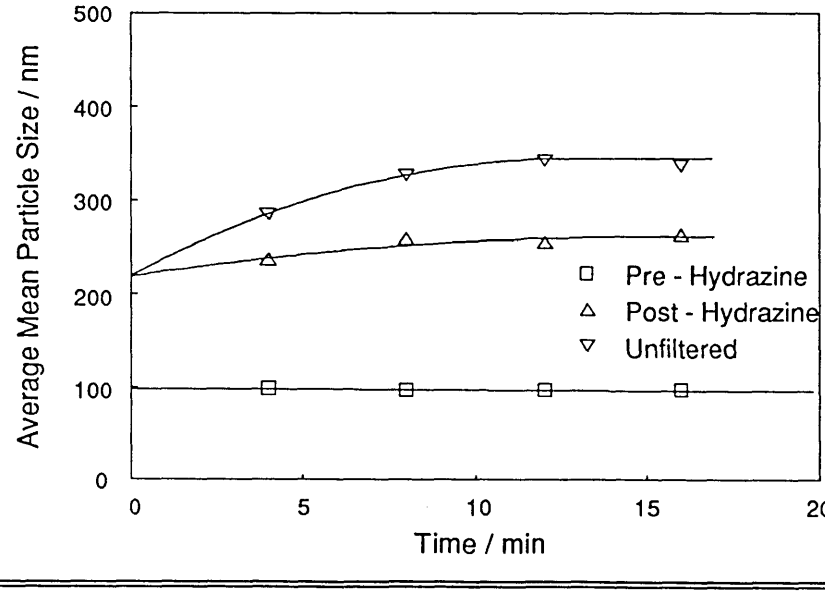

Figure 4.25.2. *Effect of micromixing and sonication on the time dependence of average mean particle size for a copper colloid concentrate diluted 250 times with 1 mol KCl solution.*

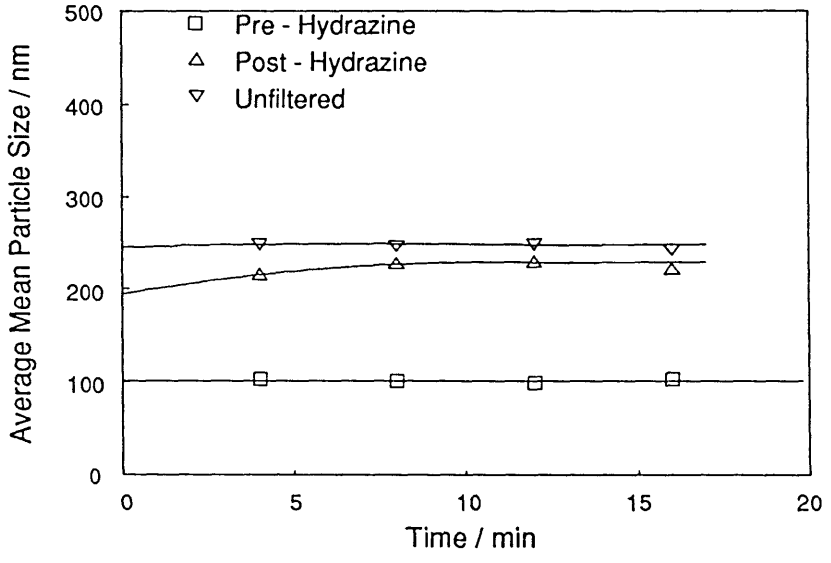

The initial particle sizes were slightly larger than the normal sample (100 nm vs. 85 nm) and gave larger final particle sizes (275 nm vs. 230 nm), although these values may not be significant. The main difference between the normal and micromixed samples was that the micromixed colloids, on dilution, appeared to be more stable with time. This may be connected with the polydispersity which was lower for the micromixed samples (0.23 for the sonicated sample, < 0.26 for the unsonicated micromixed sample, < 0.30 for the normal sample). To check whether these effects were significant, the size and polydispersity of these samples was measured again after one month, the polydispersity results have reversed themselves in order of degree (0.28 for the normal sample, < 0.29 for the unsonicated micromixed sample, < 0.39 for the sonicated sample), and the size of the sonicated particles were much larger (530 nm) than the micromixed (400 nm) and normal sample (370 nm). All the colloid particle sizes had increased with time, suggesting gradual agglomeration, but the sonicated sample increased most in size and dispersity. This suggests that sonication increased the rate of agglomeration of particles due to the increased particle/particle collision rate. The rate of colloid growth was low and incomplete until hydrazine was added. Micromixing and/or sonication did not appear to increase nucleation or growth rates.

4.26. Palladium Colloid Formation

Copper colloid growth is known to be slow and yet when DMAB was added to a Cu(II) salt solution containing a small amount of Pd(II), it turned black immediately. In order to find out how palladium affected the growth rate of copper particles, a solution of Pd(II) in gelatin was made up at the same concentration used in the Lea Ronal industrial process, i.e., 1 mol m^{-3} Pd. DMAB was added and the same immediate change to black was noted. It was not possible to measure the size of the palladium colloid particles as they were too small to scatter light (the PCS has a detection limit of about 3 nm). Palladium colloids formed by the reduction of $PdCl_2$ with $SnCl_2$ having particle sizes of about 1 nm were reported by Matijevic *et al.* [143]; ultracentrifugation revealed the presence of solids in the colloid that were otherwise undetectable.

In order to assess the stabilising forces acting on the palladium colloid, a second colloid was prepared using DMAB under similar conditions but without the addition of gelatin. The colloid formed immediately but precipitated when left overnight. This indicates that the ionic concentration was too high for the colloids to be electrostatically stable and that the gelatin acted as an effective steric stabiliser for palladium as well as copper.

Another palladium colloid was formed using hydrazine as a reductant instead of DMAB. The colloid took seven minutes before it turned black indicating colloid formation. The colloid was left overnight and the particle size measured using PCS. The results of the measurement are shown below.

Figure 4.26.1. *Time dependence of average mean particle size for a palladium colloid prepared using hydrazine.*

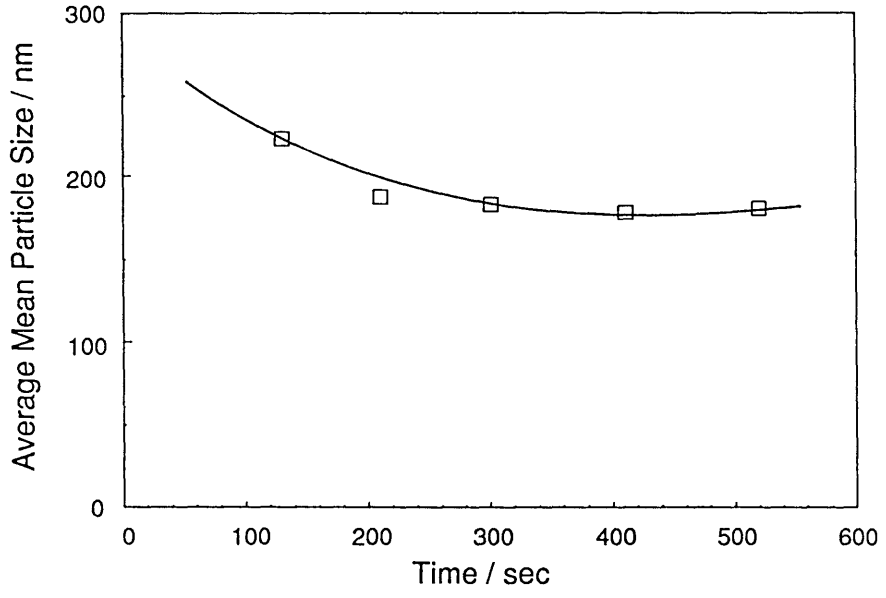

The colloid showed stability and it is thought the slight decrease in size over the first few minutes was due to equilibration of the sample from room temperature (about 19 °C) to the cell bath temperature (25 °C). A similar effect was observed for other measurements using the PCS.

4.27. Effect of Gelatin Concentration on Particle Stability

Dilution of a sample of normal copper colloid, in order to measure its size using photo-correlation spectroscopy (PCS), caused aggregation of the particles (**Section 4.21**). This suggests that the gelatin tended to desorb from the particles, weakening the steric stabilisation and leaving a weaker electrostatic stabilisation. Further evidence of gelatin desorbtion was observed from the rapid agglomeration of particles that occurred when the electrolyte concentration of the dilute solution was increased. An alternative possibility to gelatin desorbtion was the formation of bridging flocculation on dilution.

A series of particle size measurements were carried out on a diluted colloid at constant ionic concentration, with various concentrations of gelatin. The results are presented in **Figure 4.27.1.**

Figure 4.27.1. *Effect of gelatin concentration on the time dependence of average mean particle size for a copper colloid concentrate diluted 250 times with 1 mol m^{-3} KCl.*

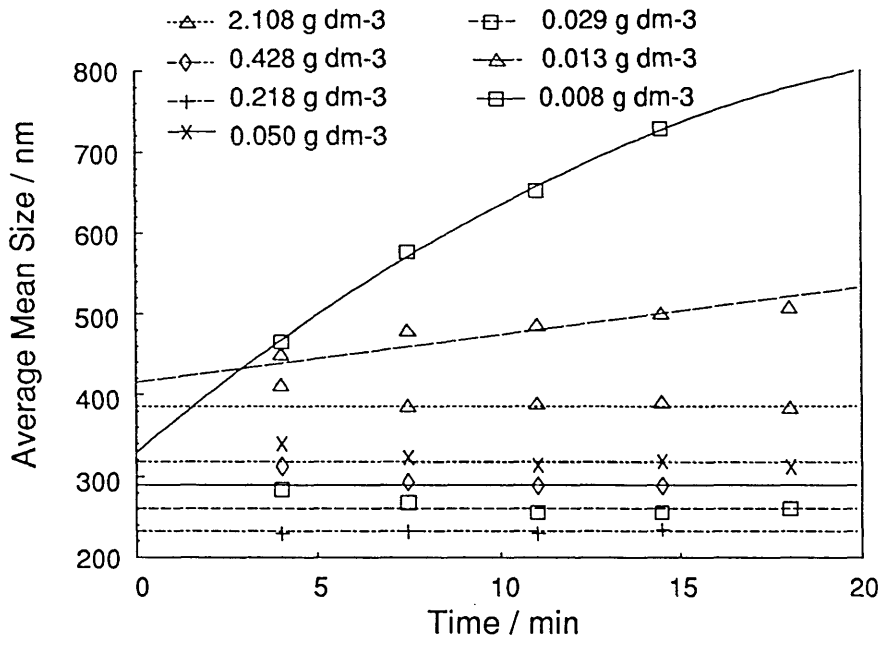

It can be seen that at all concentrations greater than 0.029 g dm^{-3} gelatin, the colloid was stable for the duration of the test, whereas at concentrations below this, agglomeration occurred. This was possibly the boundary between steric and electrostatic stabilisation. **Figure 4.27.2** shows a plot of particle size against gelatin concentration and indicates that a minimum occurred at about 0.1 g dm^{-3} gelatin. This might be a concentration at which there was minimum adsorption of gelatin, marking the transition between particle stabilisation and bridging flocculation. Hence it is possible to say that at this concentration of colloid, from 2.10 to 0.10 g dm^{-3} gelatin, steric stabilisation occurred, from 0.10 to 0.03 g dm^{-3} gelatin, electrosteric forces were acting and below 0.03 g dm^{-3} gelatin, electrostatic forces dominated.

Figure 4.27.2. *Gelatin concentration dependence of average mean particle size for a copper colloid concentrate diluted 250 times with 1 mM KCl.*

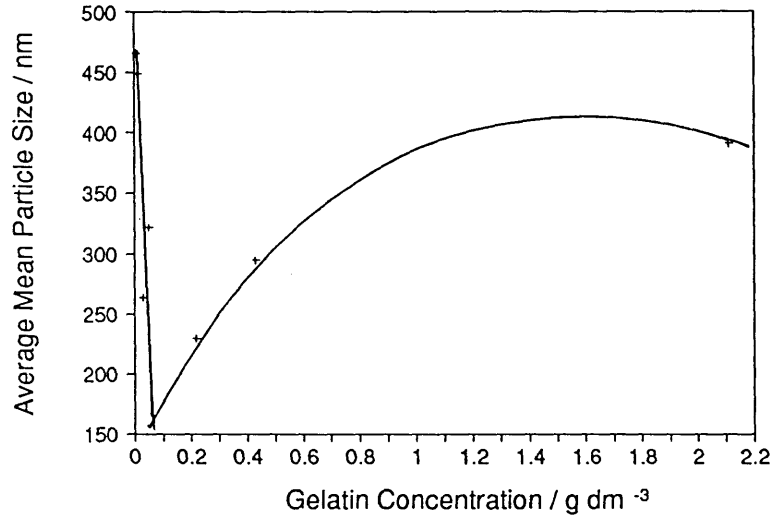

In order to assess the effect of gelatin viscosity, a concentrated solution of gelatin was diluted with water and its viscosity measured at various concentrations. The graph below was obtained.

Figure 4.27.3. *Gelatin concentration dependence of gelatin viscosity at 25 ^{0}C for gelatin in water.*

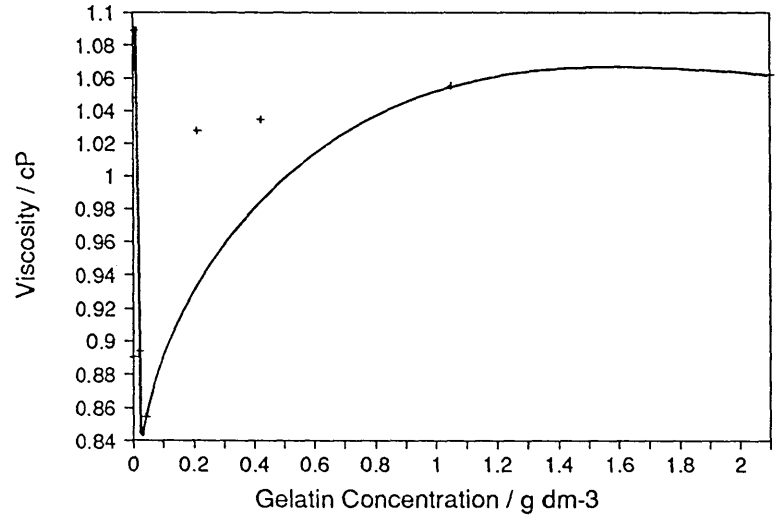

There is a remarkable correlation between **Figures 4.27.2** and **4.27.3** which indicates that the particle size is dependent upon the gelatin viscosity; both exhibit a minimum at about 0.1 g dm^{-3} gelatin, with an increase in viscosity at concentrations lower than this. This

minimum was possibly due to the effect of complete solvation of gelatin molecules, although the interactions of cross-linking polymers are complex [144]. It was also possible that ionic strength or pH had an effect and so the viscosity of gelatin was measured in a constant ionic strength solution. The results are shown in **Figure 4.27.4.**

Figure 4.27.4. *Gelatin concentration dependence of gelatin viscosity at 25 ^{0}C for gelatin in 1 mM KCl.*

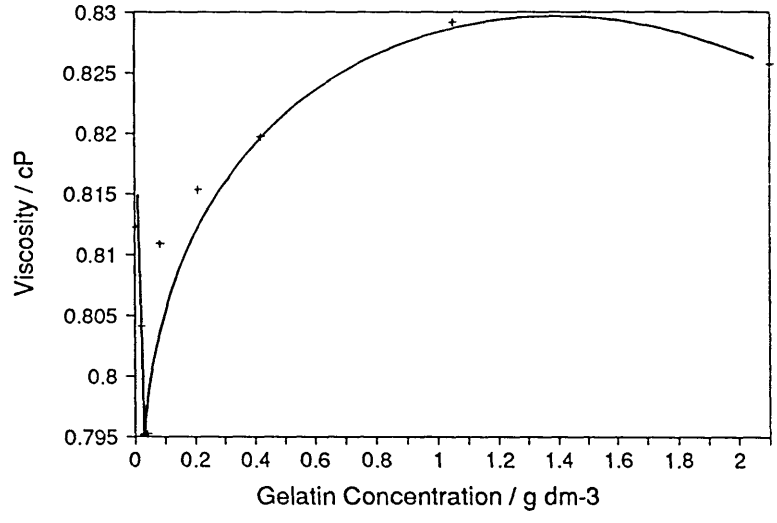

The same effect was observed again indicating that the change in viscosity was more likely to have been due to an intrinsic property of the gelatin rather than the effect of the change in ionic concentration of solution. One ionic effect was possibly the change in pH with gelatin concentration. Ions associated with acid-produced gelatin are present on rehydration and render the gelatin solution slightly acidic. The viscosity of samples of gelatin buffered to various pHs at constant ionic strength was measured and a graph plotted of viscosity vs. pH as shown in **Figure 4.27.5.**

Figure 4.27.5. *pH dependence of gelatin viscosity at a concentration of 2.1 g dm^{-3} gelatin and 25 °C.*

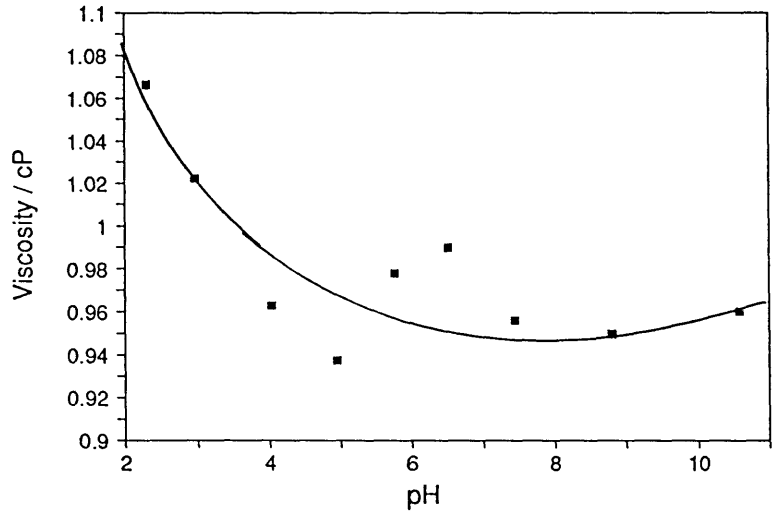

This graph indicates that the viscosity increased markedly only below pH 4; the pH change of the samples whose viscosities are shown in **Figures 4.27.3** and **4.27.4** are shown in **Figure 4.27.6.**

Figure 4.27.6. *Gelatin concentration dependence of pH at 25 °C for gelatin diluted in a) water (◆) and b) 1 mM KCl (+).*

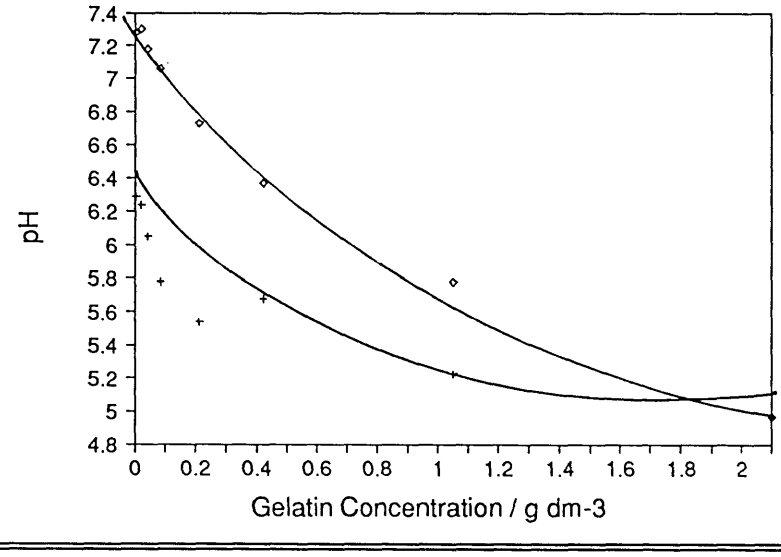

As the pH of these two samples, on dilution, lies in the range 5 to neutral, it was thought that the pH would have only a minor effect on the changes in viscosity seen in **Figures 4.27.3** and **4.27.4.**

4.28. The Oxidation of Gelatin

Balakrishnan and Venkatesan [145] investigated the reduction of oxygen on copper in Cl^-, SO_4^{2-}, NO_3^- and NH_4^+ media, using the rotating ring-disc electrode technique. From their work it is clear that the kinetics of oxygen reduction are strongly influenced by the presence of oxide on the electrode surface. Voltammograms obtained in NaCl, Na_2SO_4 and NH_4Cl were similar in nature and showed two peaks on the anodic sweep. These peaks were not observed in $(NH_4)_2SO_4$. Overall, the rate of oxygen reduction increased in the order $(NH_4)_2SO_4 > H_2SO_4 > NaCl > HCl > Na_2SO_4 > NH_4Cl$. Tafel slopes for oxygen reduction varied from 65 to 240 mV depending on the medium. The two peaks were identified as due to the reactions:

$$O_2 + 2H^+ + 2e \Leftrightarrow H_2O_2 \qquad (1)$$

$$H_2O_2 + 2H^+ + 2e \Leftrightarrow 2H_2O \qquad (2)$$

or

$$H_2O_2 + 2e \Leftrightarrow 2OH^- \qquad (3)$$

depending on the pH.

In acid chloride and sulphate media, no H_2O_2 was detected, suggesting that direct reduction to H_2O occurred. A plot of I_d/I_r vs. $\omega^{\frac{1}{2}}$ indicated that in Na_2SO_4, oxygen is reduced to peroxide only and is stabilised as O_2H^- ion in alkaline media; in $(NH_4)_2SO_4$ the direct reduction of oxygen to water runs in parallel with its reduction to water via the peroxide intermediate.

The fact that the peaks due to reactions (1) and (2)/(3) occur in the positive-going direction, as well as the increase in the oxygen reduction current, indicate that reduction of the surface oxide must occur prior to oxygen reduction, which is faster on an oxide-free surface.

It has been suggested that the anodic formation of passive films on copper in alkaline solutions occurs by a dissolution-precipitation mechanism, involving the reactions [146]:

$$Cu + OH^- \rightarrow Cu(OH) + e$$

followed by:

$$2Cu(OH) \Leftrightarrow Cu_2O + H_2O$$

If copper ions are present, it has been shown by Skinner *et al.* [147] that they can catalyse the reduction of peroxide in the following way:

$$Cu^+ + H_2O_2 \rightarrow Cu^{2+} + OH^- + OH^{\cdot} \qquad k_1 = 260\ dm^3\ mol^{-1}\ s^{-1}$$

$$Cu^+ + OH^{\cdot} \rightarrow Cu^{2+} + OH^-$$

As gelatin appeared to act as a buffer to oxidation (see **Section 4.5**), the reduction of O_2 was studied in the presence and absence of gelatin using a rotating Pt ring Cu disc electrode (RRDE).

Cyclic voltammograms of the background electrolyte and the background electrolyte with gelatin under air and nitrogen are shown in **Figures 4.28.1** and **4.28.2**. The difference in reduction current between the two figures due to the reduction of oxygen is shown clearly. Both figures reveal that the reduction currents with and without gelatin were similar, although hydrogen evolution appeared to occur at less negative potentials on the reduction sweep when gelatin was not present, indicating that gelatin inhibits hydrogen evolution.

Figure 4.28.1. *Cyclic Voltammogram of background electrolyte with and without 2.1 g dm^{-3} gelatin at a copper electrode under nitrogen. Sweep rate = 100 mV s^{-1}.*

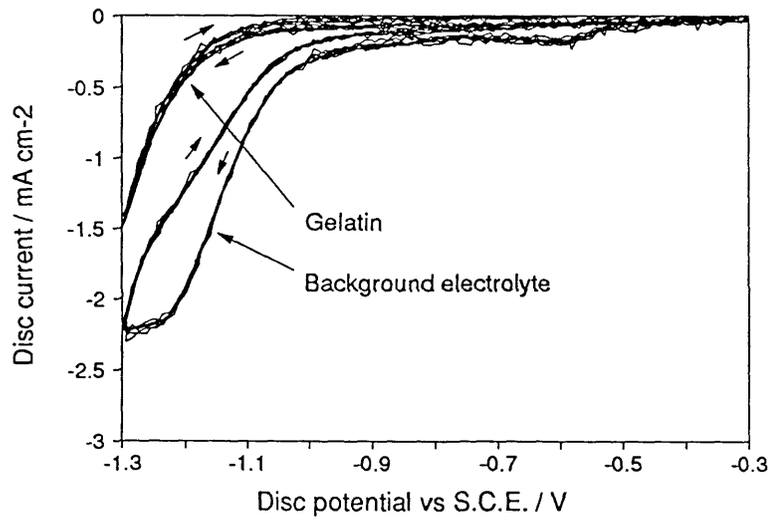

Figure 4.28.2. *Cyclic Voltammogram of background electrolyte with and without 2.1 g dm^{-3} gelatin at a copper electrode under air. Sweep rate = 100 mV s^{-1}.*

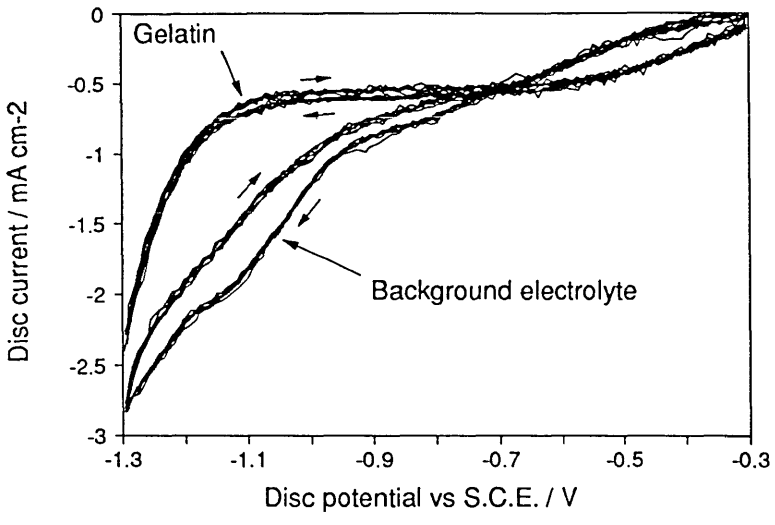

From these diagrams, -0.8 V was chosen as the disc potential at which to study oxygen reduction, with minimal hydrogen evolution, in order to elucidate the oxygen reduction mechanism on copper in the presence of gelatin.

The diffusion limiting current, i_L is given by the Levich equation [148]:

$$i_L = 1.55(D_{O_2})^{2/3}\nu^{-1/6}nFAc_{O_2}\omega^{1/2}$$

where D_{O_2} is the diffusion coefficient of oxygen, 1.92×10^{-5} $cm^2 s^{-1}$ in background electrolyte [106] and 1.80×10^{-5} $cm^2 s^{-1}$ with gelatin, ν is the kinematic viscosity of the solution, 8.34×10^{-3} $cm^2 s^{-1}$ in background electrolyte and 8.92×10^{-3} $cm^2 s^{-1}$ in gelatin, n is the number of electrons per O_2 molecule, F is the Faraday constant, 96485 A s (mol e^-)$^{-1}$, A is the electrode area, 0.204 cm^2, c_{O_2} is the concentration of oxygen, 2.5×10^{-7} mol cm^{-3}, and ω is the rotation rate of the electrode, s^{-1}.

In order to obtain Levich plots of the currents detected, it was necessary to measure the viscosity of the background electrolyte solution, with and without gelatin. The viscosities were found to be 0.828 cP and 0.892 cP respectively. The concentration of oxygen was measured by a dissolved oxygen meter and electrode.

Figures 4.28.3 and **4.28.4** show the experimental data and the lines predicted by the Levich equation with n = 2 and n = 4, both with and without gelatin present. The reduction process

appeared to involve 4 electrons at low rotation rates, but as the velocity increased, there was a marked deviation from this line, indicating that intermediates were being produced and dispersed away from the disc. This occurred with and without gelatin.

Figure 4.28.3. *Oxygen reduction current density vs.* $\omega^{1/2}$ *compared to the current given by the Levich equation for 4 and 2 electron reactions at E = -0.8 V vs. S.C.E. in background electroyte on a copper electrode under air.*

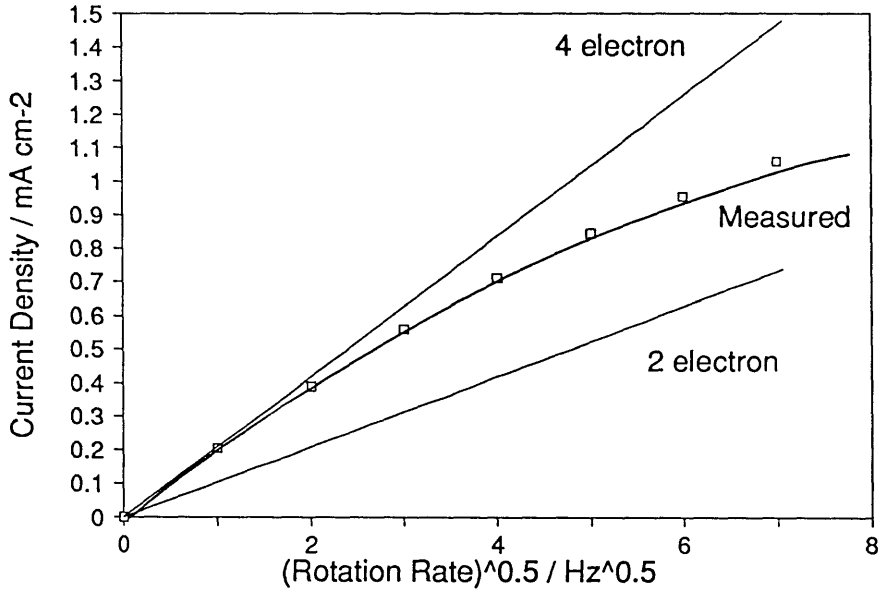

Figure 4.28.4. *Oxygen reduction current density vs. $\omega^{1/2}$ compared to the current given by the Levich equation for 4 and 2 electron reactions at E = -0.8 V vs. S.C.E. in background electrolyte with 2.1 g dm^{-3} gelatin on a copper electrode under air.*

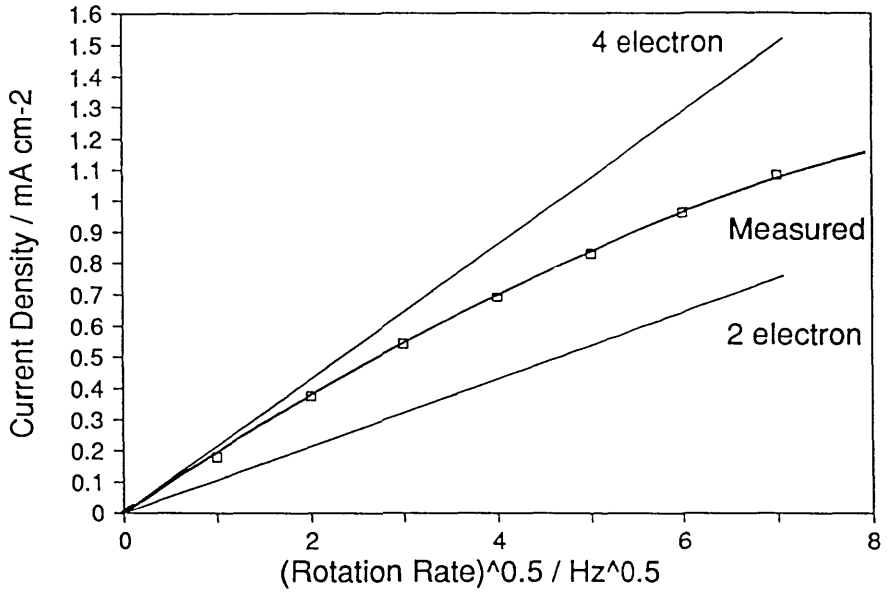

These diagrams indicate that O_2 was reduced initially by a 2*e* process to form a hydrogen peroxide intermediate:

$$O_2(g) + 2H^+ + 2e \Leftrightarrow H_2O_2 \qquad (1)$$

$$E^0 = 0.695 \text{ V}$$

which can be further reduced in another 2*e* process:

$$H_2O_2 + 2H^+ + 2e \Leftrightarrow 2H_2O \qquad (2)$$

$$E^0 = 1.763 \text{ V}$$

In order to detect the presence of the H_2O_2 intermediate, the ring potential was held at +0.8 V vs. S.C.E., to oxidise the H_2O_2 by the reverse of reaction (1). **Figure 4.28.5** shows the ring current obtained in solutions of background electrolyte with and without gelatin.

Figure 4.28.5. *Platinum ring current density vs. $\omega^{1/2}$ with disc potential at E = -0.8 V and ring potential at +0.8 V vs. S.C.E. in a) background electrolyte (■) and b) background electrolyte with 2.1 g dm^{-3} gelatin (+).*

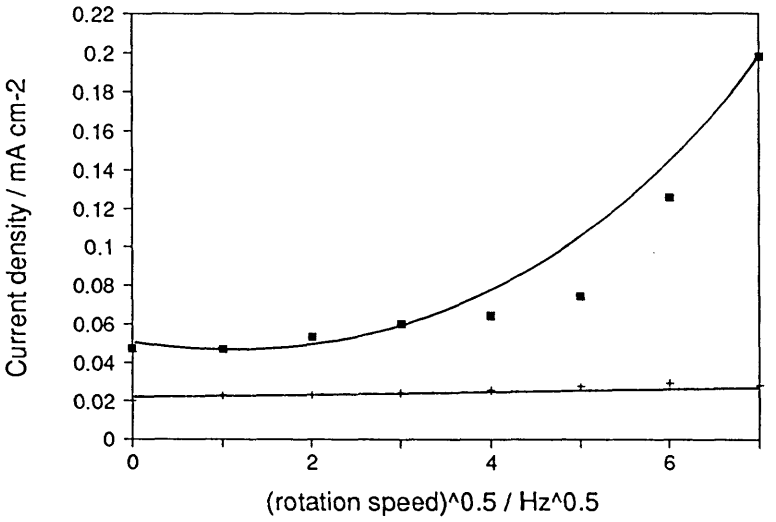

Both ring current plots indicate that as the rotation rate increased, an increased current was detected at the ring electrode as the H_2O_2 intermediate was swept away from the disc. Cyclic voltammograms of the Pt ring electrode in background electrolyte and the background electrolyte with 2.1 g dm^{-3} gelatin under air and nitrogen are shown in **Figures 4.28.6** and **4.28.7.**

Figure 4.28.6. *Cyclic voltammogram of background electrolyte at a platinum electrode under nitrogen and air. Sweep Rate = 100 mV s^{-1}.*

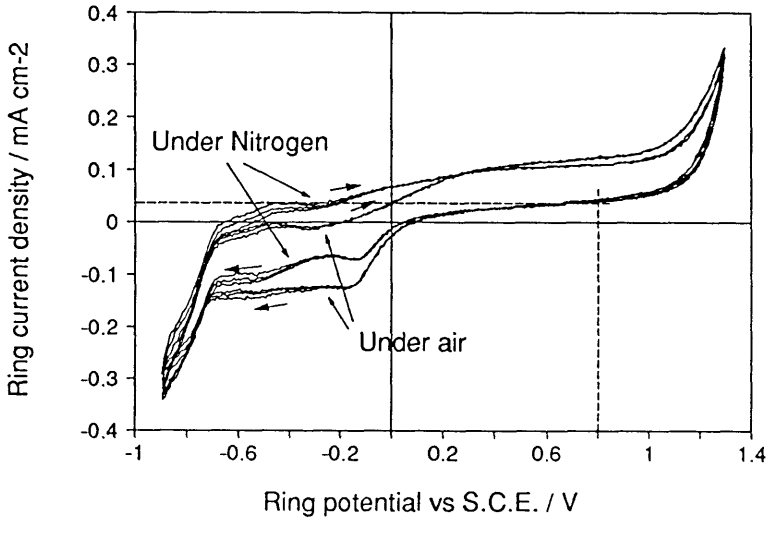

Figure 4.28.7. *Cyclic voltammogram of background electrolyte with 2.1 g dm^{-3} gelatin at a platinum electrode under nitrogen and air. Sweep Rate = 100 mV s^{-1}.*

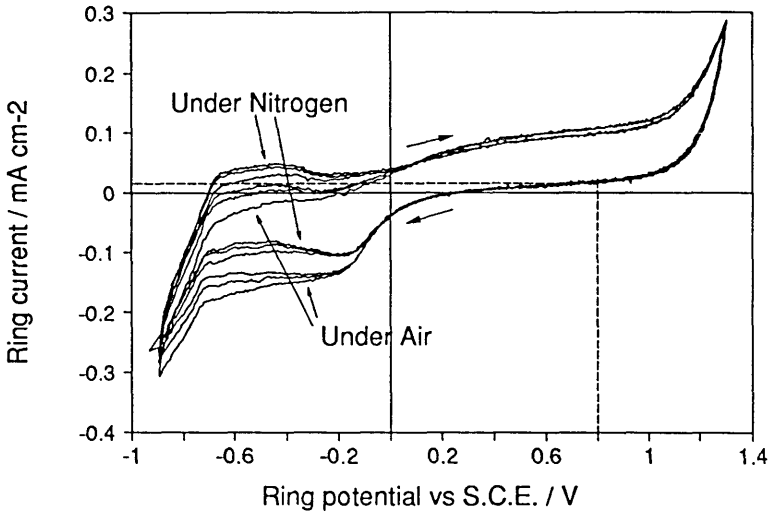

There was a slight difference in current densities due to oxygen reduction, but the oxidation current densities were very similar, indicating the current was due to the oxidation of Pt alone. The reduction currents with and without gelatin were similar. The negative-going potential produced "non-zero" oxidation currents at +0.8 V which were similar to the reduction current densities at zero rotation rate in **Figure 4.28.5**. This contribution to the total current was subtracted from the currents shown in **Figure 4.28.5** and the derived currents are shown in **Figure 4.28.8**.

Figure 4.28.8. *Platinum ring current (measured and predicted) vs. $\omega^{1/2}$ with disc potential at E = -0.8 V and ring potential at +0.8 V vs. S.C.E. in various solutions.*

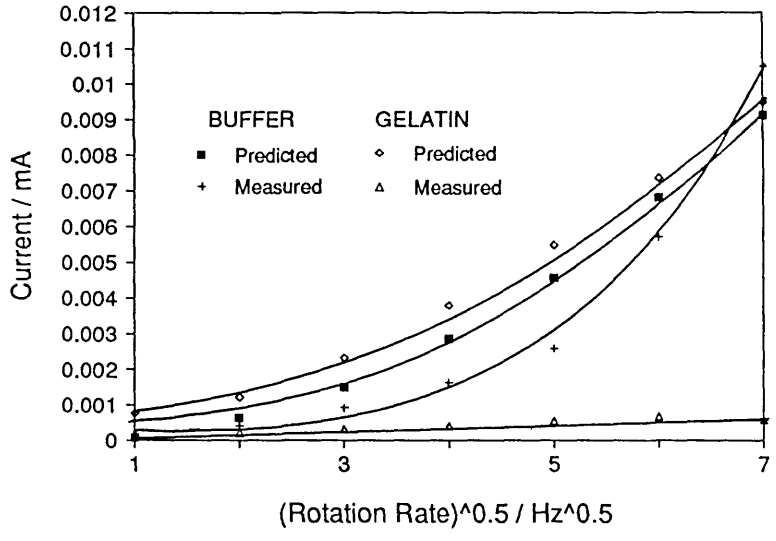

The predicted currents shown in **Figure 4.28.8** were obtained from **Figures 4.28.3** and **4.28.4**, by subtracting the measured current density from the 4 electron Levich line, δi, then using the disc area, A, to obtain the total H_2O_2 flux leaving the electrode, $2FA\,\delta i$. The collection efficiency of the ring was 0.11, calculated from tables [149] based on the relative ring and disc sizes, and so the predicted current at the ring was $0.11A\delta i$. The measured current in the background electrolyte solution was similar to the predicted current; however, the current in the background electrolyte solution with gelatin was much lower, indicating that H_2O_2 was consumed by the gelatin between the disc and the ring. This was possibly due to oxidation of the NH_2 groups on the gelatin. One likely reaction model of amino acid oxidation, and hence gelatin oxidation, is [150]:

$$H_2O_2 + 2H^+ + 2e \rightarrow 2H_2O$$

$$R - CH(NH)_2 - CO_2H \rightarrow R - CH(\dot{N}H_2^+) - CO_2H + e$$

$$R - CH(\dot{N}H_2^+) - CO_2H \rightarrow R - C = (\dot{N}H_2) - CO_2H + H^+$$

$$R - C = (\dot{N}H_2) - CO_2H \rightarrow R - C = (\dot{N}H_2^+) - CO_2H + e$$

$$R - C = (\dot{N}H_2^+) - CO_2H + 3H_2O \rightarrow R - CH = O + NH_4^+ + HCO_3^- + 3H^+$$

The oxidation of gelatin by H_2O_2 would account for the reason that the copper colloid was more stable when stored under nitrogen than under air. This reaction mechanism would also account for the buffering effect seen when excess gelatin was added.

It was reported by Gallop *et al.* [151] that hydrogen peroxide had the effect of breaking peptide bonds in collagen and forming units of 10,000 molar mass or less. Smejkal and Blazej [152] suggested the oxidative deamination of collagen was catalysed by cupric ions, which bind to the collagen to form a complex which reacts with atomic oxygen from hydrogen peroxide. The binding of copper to the peptide backbone of proteins to give a purple/blue complex is well known as part of the Biuret method. Kenchington [153] and Davis [154] carried out alkaline hypobromite oxidation of gelatin. This process removes amine and lowers the pI. Davis also notes that oxidation destroys the colloid stabilising properties of gelatin.

CHAPTER 5. CONCLUSIONS

5.1. Production of Copper Colloids using DMAB

5.1.1. DMAB oxidation

The oxidation of DMAB was investigated at a platinum electrode and a copper electrode using cyclic voltammetry. At the platinum electrode, a large peak was observed at +1.1 to 1.2 V corresponding to the oxidation of DMAB to dimethylamine and boric acid (**Figure 4.19.4**). A similar peak was observed by Sazonova and Gorbonova [38]. DMAB oxidation to boric acid was also suggested by Mallory [32] in the electroless plating of Ni. No further oxidation of dimethylamine was observed and this agrees with the findings of Sazonova and Gorbonova who compared the charge consumed with the degree of coverage at a Pt electrode. The cyclic voltammogram produced at a copper electrode showed a small reduction peak (**Figure 4.19.1**) that did not occur when DMAB was absent, suggesting the presence of a copper-DMAB complex. At slower sweep rates (**Figure 4.19.2**), two peaks occurred, which suggested that the complex was first adsorbed and then reduced. Ohno *et al.* [141] found that there was some dissolution of copper at pH 7.0 and 25 °C in a 2g dm^{-3} DMAB solution suggesting that DMAB was a ligand for Cu ions. Further indirect evidence of a Cu-DMAB complex came from the analysis of the dispersion medium of the colloids (**Section 4.11**) that showed that Cu(II) ions were present in the solution but were not complexed with water. DMAB oxidation/copper reduction was observed to be slow, but when Pd was present it acted as a catalyst and oxidation was fast. DMAB reduction of Pd(II) ions occurred immediately forming colloid particles that were below the detectable range of the particle sizing instruments used. These were the nuclei on which subsequent copper reduction could take place and Lelental [33] suggested a reaction scheme for the catalytic decomposition of DMAB on Pd that involved an adsorbed boron species. Subsequent copper growth on the Pd nuclei was still slow, however, as the method of mixing, i.e., addition rates, relative proportions of reactants, use of micromixing and sonication, appeared to have little effect on the reaction rate and size of particles obtained, which indicates that the process was reaction rate controlled. Attempts to obtain kinetic data were difficult due to the speed of the reaction and the opaqueness of the colloids obtained. At lower concentrations the reaction was much slower, indicating that the reaction was transport controlled. Kobayashi *et al.* [15] claim in a patent that copper colloids

can be formed using DMAB with no mention of a catalyst. The reduction takes place at 70 °C which may enhance the reaction kinetics slightly, but this would also have an adverse effect on the gelatin that is used as a stabiliser. No mention of reaction time is indicated, nor subsequent particle size or colloid life-span.

5.1.2. The nature of the colloidal copper particles formed by DMAB

Copper colloids formed by the reduction of Cu(II) ions with DMAB on Pd nuclei were found to exhibit a peak light absorption at about 590 nm. This corresponds to the theoretical Mie prediction λ_{MAX} of 586 nm for a 50 nm copper particle [27], indicating that the particles are unoxidised. These results are similar to the results of Hirai *et al.* [20], who found clear spectrophotometric absorbance peaks at 570 nm for copper colloid solutions, which they attributed to excitation of surface plasmons of copper particles. Papavassiliou and Kokkinakis [28] found a clear adsorption peak at 580 nm for the optical adsorption spectra of copper particles. On exposure of the colloid to air, there was a peak shift to longer wavelengths that was thought to be due to air oxidation of Cu^0 to Cu^{2+} ions. This shift was not as dramatic as the disappearance of the spectral peak (570 - 590 nm) observed by Savinova *et al.* [22] when their colloids stabilised by poly(vinyl pyrrolidone) were exposed to air and it is likely that there was only slight oxidation of the sample due to the protective action of gelatin. Further evidence for the existence of unoxidised metal copper particles was that potentials of gelatin-stabilised copper colloids, inferred from measurement of the potential of a macro copper electrode, were in the metal region of a copper/water potential-pH diagram (**Figure 4.18.1**).

5.2. Alternative means of Copper Colloid Production

5.2.1. Copper hydrous oxide colloids

A proposed alternative way of depositing copper onto a silica surface, other than using metallic copper colloids, is to adsorb positively charged copper hydrous oxide colloid particles on to the silica surface [96] followed by *in-situ* reduction. Silica has a pH_{pzc} of about 2 [97] and is negatively charged at higher pH values. The pzc of copper hydrous oxide is about 9 and so in the pH range 2-9, is available for the bonding to the silica surface by electrostatic adsorption. These colloids were prepared and had the same order of particle size as those prepared by McFayden and Matijevic [139]. However, to ensure monodispersity,

the ionic strengths of the solutions were very high, leading to instability, and the particle sizes were 200 times larger than colloids used as catalysts in the plating industry. Large particle sizes would be a possible source of non-uniform size coverage of hole surfaces. As the colloids prepared were not stable for more than a day, there was no further investigation of these colloids.

5.2.2. Regenerative Aqueous Reductants

One of the cheapest and easiest forms of reduction is by electrons that are obtained from non-chemical means. However, electrons transmitted to a solution via electrodes are only useful in homogeneous systems and are unable to produce highly dispersed colloids. This being the case, a regenerative chemical couple could act as an intermediary between electrode and copper colloid formation. To examine the effect of reduction using aqueous regenerative reductants, two were used, the V(II)/V(III) couple and the Cr(II)/Cr(III) couple. It was found that larger particles were formed than when DMAB was used and this could be due to coloumbic repulsion between the positively charged reductant ions and the Cu(II) ion that could cause slower electron transfer, hence a slower nucleation rate and larger particles. Savinova *et al.* also used V(II) ions as a reductant for the formation of copper colloids and found a similar effect when the particle sizes formed were compared to those of colloids formed using BH_4^- ions under the same conditions. The feasibility was demonstrated of metallising drill hole surfaces directly by using the Cr(II)/Cr(III). However, the oxidation of such a reductant on the copper surfaces of printed circuit boards would cause copper deposition both there as well as the drill hole surfaces.

5.3. Stabilisation of Copper Colloids using Gelatin

5.3.1. Electrostatic stabilisation of copper colloids

The stability of copper colloid systems was investigated by preparation of electrostatically stabilised dispersions of copper colloids to determine under what conditions stabilisation was achieved. **Figure 4.1.1** shows that even at low (5 mol m^{-3} Cu) concentrations, the colloid was unstable and agglomerated soon after reduction. Only addition of a highly charged, adsorbed counter ion, stabilised the colloid at this concentration. Despite this, the life-span of the colloid was about a week, which was most likely due to the destabilising effect of Ostwald ripening. This indicates that the presence

of gelatin in a copper colloid system acts not only as a stabiliser, but as a prevention against Ostwald ripening, due to the fact that gelatin inhibits copper ion diffusion. There is no mention in the literature of the effect of steric stabilisers on metal ion diffusion in metal colloid systems; and the effect was investigated further by electrode impedance spectroscopy (***Section 5.1.2***). There is also no mention of the use of electrostatically stabilised metal colloids, most dispersions rely on some form of steric stabiliser, however, the results have shown that it was possible to generate electrostatically stabilised colloids, at concentrations that would normally lead to agglomeration, which were stable for up to a week under non-optimised conditions. It is important to note the copper concentrations when comparing the life-span of colloids in **Appendix A**, as this is an significant factor in determining colloid stability, as indicated in **Figure 2.3.2.2.**

5.3.2. The effect of gelatin on copper ion diffusion

The effect of gelatin on copper ion diffusion and hence the limiting current density was evident from the cyclic voltammogram shown in **Figure 4.20.1.** The measured capacitance of the double-layer at a copper electrode without gelatin present was similar to that obtained by Wanner *et al.* [142]. When gelatin was present, there appeared to be two effects on the double layer: firstly, the increase in the effective diffusion coefficient led to an increase in the diffusion resistance, and secondly there was an increase in the double layer capacitance, which is further evidence for gelatin decreasing the concentration of Cu(II) ions in the diffuse layer, hence aiding stabilisation by preventing Ostwald ripening.

5.3.3. Gelatin stabilised copper colloids

Gelatin has been shown to be the most effective steric stabiliser of all those tested, providing not only stabilisation of the particles against agglomeration, but also against the destabilising effects of Ostwald ripening. As gelatin is a naturally occurring macromolecule, its structure and size can vary greatly, but for it to be effective it requires the same proportion of amide-groups as an acid-processed gelatin. This indicates that these groups provide enhanced repulsion by means of an electrostatic element; hence, gelatin can be considered an electrosteric stabiliser. The model envisaged is of carboxyl groups bonding to a positively charged copper surface and the amide groups providing the repulsion. The iep of the gelatin was 8.8, which was found to be the iep of the copper colloid system, **Figure 4.3.1**, indicating that the gelatin completely enveloped the copper particles and hence they responded in an electric field as gelatin particles. Further evidence

of gelatin enveloped copper particles came from observation of the particle size with changing pH (**Figure 4.3.2**), which showed that there was a large increase in average particle size at the iep. The iep is the point where gelatin strands contain a net zero charge and hence minimum swelling in water occurs. This allows closer approach of particles and hence the possibility of agglomeration. As there appeared to be a correlation between the particle size of the colloid and the difference between the pH of the colloid and the iep of gelatin, it would appear that pH is a major factor in determining the electrophoretic mobility and rate of agglomeration, and hence particle size.

5.3.4. The effect of oxygen on gelatin stabilised copper colloids

Although gelatin appeared to be an excellent stabiliser, gelatin stabilised copper colloids had the problem of having a life-span of only three months. Life-span in colloid terms refers to the point at which a supernatant solution became visible. Current practice is for the product to be shipped and stored in plastic drums. These are known to be permeable to air and hence oxygen was investigated as a possible source of destabilisation. Any quick method of assessing colloid stability, such as the thermal test mentioned in **Section 3.10** was found not to correlate with the actual life-span of colloids. This could be due to thermal effects on the gelatin structure. Copper colloids were observed to be stable for three to four times longer when kept under nitrogen than when kept under air (**Figure 4.5.1**). Rotating ring-disc voltammetry was used to investigate the mechanism of oxygen reduction at a copper electrode. A four electron transfer observed at low speeds was observed to change towards a two electron transfer at higher speeds (**Figure 4.28.3**). Oxygen was known to be reduced by various mechanisms, Balakrishnan and Venkatesan [145] found peaks on a cyclic voltammogram of a copper electrode in chloride and sulphate media that corresponded to the reduction of oxygen to a hydrogen peroxide intermediate before final reduction to water. However, in acid chloride and sulphate media, they detected no peroxide intermediate and suggested that direct reduction to water occurred involving splitting of the O-O bond. It is unlikely that no intermediates were formed as the reduction of oxygen to water involves the transfer of four electrons and four protons and there are many possible reaction pathways. Peroxide reduction at the ring electrode increased the ring current with increasing rotation rate (**Figure 4.28.5**), indicating that there was an intermediate formed. However, when gelatin was present there was very little current detected, despite the fact that peroxide was produced at the disc (**Figure 4.28.4**). Comparing the flux generated at the disc electrode and detected at the ring electrode indicated that there was only a minor decrease in current when gelatin was absent and a

major decrease when it was present (**Figure 4.28.8**). The minor decrease can be attributed to small losses such as the catalysis of peroxide reduction by cuprous ions [147]. The major loss was attributed to gelatin oxidation by peroxide and a possible reaction scheme was presented in **Section 4.28**, which shows the destruction of amide and carboxyl groups, vital for colloid stabilisation.

5.4. Alternative means of Copper Colloid Stabilisation

Many steric stabilisers were tested, a few of which had already been tried in the literature (**Appendix A**). It is difficult to judge the effectiveness of a steric stabiliser as there are several important factors that are not standard. The first is the concentration of the copper, which has two major effects: a) when copper is reduced from its ion (usually Cu(II)), there is a residual ion concentration in solution which affects the width of the double-layer and hence the closeness of particle approach, b) increasing the copper concentration increases the particle collision rate and hence the possibility of agglomeration. The second (and third) factor is the concentration of the stabiliser and its degree of polymerisation. Particle stabilisation by steric means can take many different forms (**Section 2.3.4**) and at certain concentrations and chain lengths, a polymer can cause the opposite effect and agglomerate particles by bridging flocculation. The final factor is the use of the term "stable" in the literature. For experimental requirements, a colloid which lasts for one day is considered stable, and yet for industrial requirements colloids are required to remain stable for greater than six months. As was shown in **Section 4.4**, the particle size of the colloid gradually increases with time due to agglomeration, and hence although the particle may appear "stable", i.e., no supernatant is visible, it no longer fulfils the specifications required for plating. On comparison of the results obtained using steric stabilisers in **Section 4.13** and those used by other workers, it is possible to see that gelatin is the most successful for the reasons outlined in **Section 5.3**.

APPENDIX A

The following table summarises the various attempts of workers to form copper colloids.

Workers	Copper Source	Reductant	Stabiliser	Technique	Result	Copper Concentration
Lea Ronal [5]	$CuSO_4.5H_2O$	Dimethylamino-borane, DMAB	Gelatin	Pd catalyst, addition at room temperature	100 nm particles stable for 3-4 months	5 g dm^{-3}
Kobayashi *et al.* [15]	$CuSO_4$	DMAB	Gelatin and poly(ethylene glycol), PEG	Addition at 70 °C	Stable colloid, unknown life	5 g dm^{-3}
Creighton *et al.* [16]	$CuSO_4$	$NaBH_4$	Trisodium citrate	Addition at high pH	Colloid stable for 24 hours	0.25 g dm^{-3}
Savinova *et al.* [22]	$CuSO_4.5H_2O$	$NaBH_4$	PVA, MM = 25000, charged molar ratio *ca.* 20	Addition at room temperature under argon	Colloid Size, nm : 3	0.005 g dm^{-3}
"	"	"	PVP, MM = 25000, charged molar ratio *ca.* 20	"	3	0.005 g dm^{-3}
"	"	"	PEG, MM = 2000	"	Copper precipitates	N/A
"	"	"	Poly(acryl amide), MM = 4×10^7	"	No reduction	N/A
"	"	$NaBH_4$	None	"	Black precipitate	N/A
"	"	Methylviologen radical, $MV^{+\cdot}$	None	"	Black precipitate	N/A
"	"	V^{2+}	None	"	Black precipitate	N/A
"	"	$[SiW_{12}O_{40}]^{5-}$	None	"	Black precipitate	N/A
"	"	Methylviologen cation radical, $MV^{+\cdot}$	PVA	"	Particle size: > 500 nm	N/A
"	"	V^{2+}	PVP	"	500 nm	N/A
"	"	$[SiW_{12}O_{40}]^{5-}$	PVP	"	8 - 25 nm	N/A
"	$Cu(HCOO)_2$	$NaBH_4$	PVP	"	4 - 100 nm	0.005 g dm^{-3}
"	$Cu(CH_3COO)_2$	$NaBH_4$	PVP	"	4 - 100 nm	0.005 g dm^{-3}
"	Cu-2,9-di-methyl-phenan throline complex, $Cu(DMP)_2Cl_2$	$NaBH_4$	PVP	"	3 nm	0.005 g dm^{-3}
"	Cu-ethylene-diamine complex, $Cu(en)_2SO4$	$NaBH_4$	PVP	"	5 nm	
Curtis *et al.* [21]	Copper(II) acetate monohydrate	Hydrazine hydrate	None	Reflux in methanol under nitrogen	Mean size 13.5 nm, in a range 3 - 30 nm	0.065 g dm^{-3}
Papavassiliou and Kokkinakis [28]	$CuSO_4.5H_2O$	Hydrazine	Gelatin	Addition at 80°C	Homogeneous solution achieved only after the removal of large particles by centrifugation	1 g dm^{-3}
Hirai *et al.* [17]	$CuSO_4.5H_2O$	Water soluble primary and secondary alcohols, and di-ethers	Vinyl polymers with a polar group	Refluxing	Reductants unable to reduce Cu(II)	N/A

Workers	Copper Source	Reductant	Stabiliser	Technique	Result	Copper Concentration
Hirai *et al.* [18][19]	$CuSO_4.5H_2O$	$NaBH_4$	Poly(vinyl pyrrolidone), PVP	Stabiliser added at 80 °C under nitrogen for 2 hours.	Stable colloid, unknown life or particle size	1.25 g dm^{-3}
Hirai *et al.* [20]	$CuSO_4.5H_2O$	$NaBH_4$	None	Addition at room temperature	Black precipitate	N/A
"	"	"	PVP, degree of polymerisation (DP):	Stabiliser added at 80 °C under nitrogen for 1 hour. Size (nm):	Stable colloid (> 3 months) under nitrogen, unstable on contact with air.	0.025 g dm^{-3}
"	"	"	3240	10	"	0.025 g dm^{-3}
"	"	"	1440	6	"	0.025 g dm^{-3}
"	"	"	90	5	"	0.025 g dm^{-3}
"	"	"	Poly(vinyl alcohol), PVA, DP: 1500	15	"	0.025 g dm^{-3}
"	"	"	Poly(potassium vinyl sulphate)	undetermined	"	0.025 g dm^{-3}
"	"	"	Dextrin	9	"	0.025 g dm^{-3}
"	"	"	Amylopectin	10	"	0.025 g dm^{-3}
"	"	"	Methylamylo-pectin	undetermined	"	0.025 g dm^{-3}
"	"	"	Methylcellulose, DP: 140	10	"	0.025 g dm^{-3}
"	"	"	Ethylcellulose	undetermined	"	0.025 g dm^{-3}
"	"	"	(2-Hydroxyethyl cellulose)	undetermined	"	0.025 g dm^{-3}
"	"	"	Poly(methyl vinyl ether), DP: 570	Stabiliser added at 25 °C under nitrogen for 1 hour.	"	0.025 g dm^{-3}
"	"	"	Poly(ethylene oxide)	Stabiliser added at 80 °C under nitrogen for 1 hour.	Aggregation and black precipitate	N/A
"	"	"	β-cyclodextrin	"	"	N/A
"	"	"	Poly(acrylic acid)	"	No reduction	N/A
"	"	"	Poly(2-acrylamido -2-methyl-1-pro-pane-sulphonic acid)	"	No reduction	N/A
"	"	"	Copolymer of methyl vinyl ether and maleic acid	"	No reduction	N/A
"	"	"	Poly(amino-ethylene)	"	Polymer insoluble	N/A
"	"	"	Soluble Nylon	"	Polymer insoluble	N/A
"	$CuCl_2$	"	PVP	"	Stable colloid, unknown life	0.025 g dm^{-3}
"	$Cu(CH_3O)$	"	PVP	"	"	0.025 g dm^{-3}
"	$CuNO_3$	"	PVP	"	Unstable colloid, even under nitrogen	0.025 g dm^{-3}
"	$CuSO_4$	Hydrogen (80 °C at 37 atm.)	PVP, DP: 3240	"	No reduction	0.025 g dm^{-3}
"	"	Ethanol	PVP, DP: 3240	"	No reduction	0.025 g dm^{-3}
"	"	Methanol/NaOH	PVP, DP: 3240	"	No reduction	0.025 g dm^{-3}
"	"	Formaldehyde	PVP, DP: 3240	"	Gelation	0.025 g dm^{-3}
"	"	Hydrazine	PVP, DP: 3240	" size: 20 to 160 nm	Stable colloid	0.025 g dm^{-3}

APPENDIX B

The θ-Point

In an osmotic pressure experiment, an additional pressure Π exerted on an organic solution results in the solvent polymer's chemical potential being rendered equal to that of the pure solvent at ambient pressure p:

$$\mu_1^{\ominus} = \mu_1 + \int_p^{p+\Pi} \left(\frac{\partial \mu_1}{\partial p}\right) \mathrm{d}p$$

$$= \mu_1 + \int_p^{p+\Pi} \overline{V}_1 \quad \mathrm{d}p$$

$$= \mu_1 + \Pi \overline{V}_1$$

so that

$$\Pi = -(\mu_1 - \mu_1^{\ominus})/\overline{V}_1$$

$$= -(RT/\overline{V}_1)\{\ln(1 - v_2) + (1 - 1/x)v_2 + \chi_1 v_2^2\}$$

Assuming v_2 is small, then

$$\Pi = (RT/\overline{V}_1)\left\{v_2/x + \left(\frac{1}{2} - \chi_1\right)v_2^2 + \ldots\right\}$$

x can be set equal to $\overline{V}_2/\overline{V}_1$ so that $\overline{xV}_1 = \overline{V}_2$. Also, $v_2 = c_2\overline{v}_2$, where c_2 = polymer concentration and $\overline{v}_2$ = partial specific volume, i.e., $\overline{v}_2 = \overline{V}_2/M_2$, where M_2 = molar mass of the polymer. These relationships result in $v_2/x\overline{V}_1 = c_2/M_2$. Therefore

$$\Pi/c_2 = RT\left\{1/M_2 + (\overline{v}_2^2/\overline{V}_1)\left(\frac{1}{2} - \chi_1\right)c_2 + \ldots\right\}$$

The first virial term in this power series is the van't Hoff infinite dilution expression for osmotic pressure. It is associated with the movement of the centres of mass of the solute molecule over the available volume. The second term is the two-body interaction term. According to this theory, the second virial coefficient B_2 in the expansion

$$\Pi/c_2 = RT\{B_1 + B_2 + b_3 c_2^2 + \ldots\}$$

must be such that

$$B_2 = (\overline{v}2^2/\overline{V}_1)\left(\frac{1}{2} - \chi_1\right)$$

When $\chi_1 = \frac{1}{2}$, $B_2 = 0$, this is called the θ-point.

In a poor solvent for a polymer, the polymer molecules are in dynamic association. Since osmotic pressure is a colligative property, any reduction in the effective number of discrete molecules reduces the osmotic pressure below the ideal van't Hoff limit. In a good solvent, the polymer segments are mutually repulsive since contact with solvent molecules are enthalpically favoured. This tends to cause the polymer chains to swell, a process that is counteracted by the loss of configurational entropy as the chains expand. The θ-point demarcates the region where the segmental interactions switch from being repulsive to attractive, and hence above the θ-point, steric stabilisation is achieved.

APPENDIX C

The Side-Chain Groups in Gelatin [155]

Amino Acid	Side-chain structure	Number occurring per 1000 residues	
		Acid Process Pork Skin	Alkali Process Ox Skin
Amide	$-NH_3$	40.8	7.5
Alanine	$-CH_3$	110.8	112.0
Glycine	-H	326	333
Valine	$-CH(CH_3)_2$	21.9	20.1
Leucine	$-CH_2CH(CH_3)_2$	23.7	23.1
Isoleucine	$-CH(CH_3)CH_2CH_3$	9.6	12.0
Proline	2-pyrrolidine-carboxylic acid	130.3	129.0
Phenylalanine	$-CH_2C_6H_5$	14.4	12.3
Tyrosine	$-CH_2C_6H_4OH$	3.2	1.5
Serine	$-CH_2OH$	36.5	36.5
Threonone	$-CH(OH)CH_3$	17.1	16.9
Arginine	$-(CH_2)_3NHC(NH)NH_2$	48.2	46.2
Histidine	imidazolylmethyl	6.0	4.5
Lysine	$-(CH_2)_4NH_2$	26.2	27.8
Aspartic acid	$-CH_2COOH$	46.8	46.0
Glutamic acid	$-(CH_2)_2COOH$	72.0	70.7
Hydroxyproline	4-hydroxy-2-pyrolidine carboxylic acid	95.5	97.6
Hydroxylsine	$-(CH_2)_3CH(OH)NH_2$	5.9	5.5
Methionine	$-CH_2CH_2SCH_3$	5.4	5.5

APPENDIX D

Thermodynamic data and equations used in the construction of potential-pH diagrams.

(Data from "Standard Potentials in Aqueous Solution" [156])

1. Boron/Water

SPECIES	FORMULA	B	H_2O	e	H^+	ΔG^0 / J mol^{-1}	PHASE
B	B	1	0	0	0	0	(s)
BO_2^-	$B+2H_2O-4H^+-3e$	1	2	-3	-4	-678900	(aq)
B_2O_3	$2B+3H_2O-6H^+-6e$	2	3	-6	-6	-1193700	(s)
$B_4O_7^{2-}$	$4B+7H_2O-14H^+-12e$	4	7	-12	-14	-2605000	(aq)
BH_4^-	$B+4H^++5e$	1	0	5	4	114270	(aq)
$B_{10}H_{14}$	$10B+14H^++14e$	10	0	14	14	192000	(s)
HBO_2 (monoclinic)	$B+2H_2O-3H^+-3e$	1	2	-3	-3	-723400	(s)
$H_2BO_3^-$	$B+3H_2O-4H^+-3e$	1	3	-3	-4	-910400	(aq)
H_3BO_3	$B+3H_2O-3H^+-3e$	1	3	-3	-3	-969010	(s)
H_3BO_3	$B+3H_2O-3H^+-3e$	1	3	-3	-3	-968850	(aq)
$B(OH)_4^-$	$B+4H_2O-4H^+-3e$	1	4	-3	-4	-1153320	(aq)
$H_2BO_3.H_2O_2^-$	$B+5H_2O-6H^+-5e$	1	5	-5	-6	-1057700	(aq)
$H_2BO_3.H_3BO_3.2H_2O_2^-$	$2B+10H_2O$ $-11H^+-10e$	2	10	-10	-11	-2161900	(aq)
$H_2B_4O_7^-$	$4B+7H_2O-12H^+-11e$	4	7	-11	-12	-2720000	(aq)
$HB_4O_7^-$	$4B+7H_2O-13H^+-12e$	4	7	-12	-13	-2685300	(aq)

2. Chromium/Water

SPECIES	FORMULA	Cr	H_2O	e	H^+	ΔG^0 / J mol^{-1}	PHASE
Cr	Cr	1	0	0	0	0	(s)
Cr_2O_3	$2Cr+3H_2O-6H^+-6e$	2	3	-6	-6	-1058000	(s)
$Cr(OH)_3$	$Cr+3H_2O-3H^+-3e$	1	3	-3	-3	-858000	(s)
CrO_2	$Cr+2H_2O-4H^+-4e$	1	2	-4	-4	-548000	(s)
CrO_3	$Cr+3H_2O-6H^+-6e$	1	3	-6	-6	-510000	(s)
Cr^{2+}	Cr-2e	1	0	-2	-2	-174000	(aq)
$Cr(H_2O)_6^{3+}$	$Cr+6H_2O-3e$	1	6	-3	0	-215000	(aq)
$Cr(OH)^{2+}$	$Cr+H_2O-H^+-3e$	1	1	-3	-1	-430000	(aq)
$Cr(OH)_2^+$	$Cr+2H_2O-2H^+-3e$	1	2	-3	-2	-653000	(aq)
$Cr(OH)_4^-$	$Cr+4H_2O-4H^+-3e$	1	4	-3	-4	-1013000	(aq)
CrO_4^{2-}	$Cr+4H_2O-8H^+-6e$	1	4	-6	-8	-727000	(aq)
$HCrO_4^-$	$Cr+4H_2O-7H^+-6e$	1	4	-6	-7	-764000	(aq)
H_2CrO_4	$Cr+4H_2O-6H^+-6e$	1	4	-6	-6	-760000	(aq)
$Cr_2O_7^{2-}$	$2Cr+7H_2O-14H^+-12e$	2	7	-12	-14	-1301000	(aq)
CrO_4^{3-}	$Cr+4H_2O-8H^+-5e$	1	4	-5	-8	-737000	(aq)

3. Copper/Water

SPECIES	FORMULA	Cu	H_2O	e	H^+	ΔG^0 / J mol^{-1}	PHASE
Cu	Cu	1	0	0	0	0	(s)
Cu^+	Cu-e	1	0	-1	0	50300	(aq)
Cu^{2+}	Cu-2e	1	0	-2	0	65700	(aq)
Cu_2O	$2Cu+H_2O-2H^+-2e$	2	1	-2	-2	-148100	(s)
CuO	$Cu+H_2O-2H^+-2e$	1	1	-2	-2	-134000	(s)
$Cu(OH)_2$	$Cu+2H_2O-2H^+-2e$	1	2	-2	-2	-359500	(s)
$HCuO_2^-$	$Cu+2H_2O-3H^+-2e$	1	2	-2	-3	-258900	(aq)
CuO_2^{2-}	$Cu+2H_2O-4H^+-2e$	1	2	-2	-4	-183900	(aq)

4. Nitrogen/Water

SPECIES	FORMULA	N_2	H_2O	e	H^+	ΔG^0 / J mol^{-1}	PHASE
N_2	N_2	1	0	0	0	0	(g)
HNO_3	$0.5N_2+3H_2O-5H^+-5e$	0.5	3	-5	-5	-111300	(aq)
NO_3^-	$0.5N_2+3H_2O-6H^+-5e$	0.5	3	-5	-6	-111300	(aq)
N_2O_5	$N_2+5H_2O-10H^+-10e$	1	5	-10	-10	114000	(s)
HNO_2	$0.5N_2+2H_2O-3H^+-3e$	0.5	2	-3	-3	-55600	(aq)
NO_2^-	$0.5N_2+2H_2O-4H^+-3e$	0.5	2	-3	-4	-37000	(aq)
$H_2N_2O_2$	$N_2+2H_2O-2H^+-2e$	1	2	-2	-2	36000	(aq)
$N_2O_2^{2-}$	$N_2+2H_2O-4H^+-2e$	1	2	-2	-4	139000	(aq)
$NH_2O_2^-$	$0.5N_2+2H_2O-2H^+-e$	0.5	2	-1	-2	76100	(aq)
HN_3	$1.5N_2+H^++e$	1.5	0	1	1	322000	(aq)
NH_4N_3	$2N_2+4H^++4e$	2	0	4	4	274000	(s)
$NH_2OH_2^+$	$0.5N_2+H_2O+2H^++e$	0.5	1	1	2	-56650	(aq)
NH_2OH	$0.5N_2+H_2O+H^++e$	0.5	1	1	1	23400	(aq)
$N_2H_5^+$	N_2+5H^++4e	1	0	4	5	82400	(aq)
N_2H_4	N_2+4H^++4e	1	0	4	4	128000	(aq)
$N_2H_4.H_2^{2+}$	N_2+6H^++4e	1	0	4	6	94140	(aq)
NH_4^+	$0.5N_2+4H^++3e$	0.5	0	3	4	-79370	(aq)
NH_3	$0.5N_2+3H^++3e$	0.5	0	3	3	-26600	(aq)
NH_4OH	$0.5N_2+H_2O+3H^++3e$	0.5	1	3	3	-263800	(aq)
NH_3	$0.5N_2+3H^++3e$	0.5	0	3	3	-16500	(g)
N_2H_4	N_2+4H^+-4e	1	0	4	4	159300	(g)
N_2O	$N_2+H_2O-2H^+-2e$	1	1	-2	-2	104200	(g)
NO	$0.5N_2+H_20-2H^+-2e$	0.5	1	-2	-2	86570	(g)
N_2O_3	$N_2+3H_2O-6H^+-6e$	1	3	-6	-6	139400	(g)
NO_2	$0.5N_2+2H_2O-4H^+-4e$	0.5	2	-4	-4	51300	(g)
N_2O_4	$N_2+4H_2O-8H^+-8e$	1	4	-8	-8	97820	(g)
HNO_3	$0.5N_2+3H_2O-5H^+-5e$	0.5	3	-5	-5	-74760	(g)

5. Vanadium/Water

SPECIES	FORMULA	V	H_2O	e	H^+	ΔG^0 / J mol^{-1}	PHASE
V	V	1	0	0	0	0	(s)
V^{2+}	V-2e	1	0	-2	0	-218000	(aq)
VO	V+H2O-2H-2e	1	1	-2	-2	-404200	(s)
V^{3+}	V-3e	1	0	-3	0	-251300	(aq)
V_2O_3	$2V+3H_2O-6H^+-6e$	2	3	-6	-6	-1139000	(s)
VO^+	$V+H_2O-2H^+-3e$	1	1	-3	-2	-451800	(aq)
VOH^{2+}	$V+H_2O-H^+-3e$	1	1	-3	-1	-4171900	(aq)
V_3O_5	$3V+5H_2O-10H^+-10e$	3	5	-10	-10	-1816000	(s)
V_4O_7	$4V+7H_2O-14H^+-14e$	4	7	-14	-14	-2473000	(s)
V_2O_4	$2V+4H_2O-8H^+-8e$	2	4	-8	-8	-1318600	(s)
VO^{2+}	$V+H_2O-2H^+-4e$	1	1	-4	-2	-446400	(aq)
$VOOH^+$	$V+2H_2O-3H^+-4e$	1	2	-4	-3	-657000	(aq)
$(VOOH)_2^{2+}$	$2V+4H_2O-6H^+-8e$	2	4	-8	-6	-1331000	(aq)
$V_4O_9^{2-}$	$4V+9H_2O-18H^+-16e$	4	9	-16	-18	-2784000	(aq)
V_6O_{13}	$6V+13H_2O-26H^+-26e$	6	13	-26	-26	-4109000	(s)
V_2O_5	$2V+5H_2O-10H^+-10e$	2	5	-10	-10	-1419400	(s)
$V_2O_5.H_2O$	$2V+6H_2O-10H^+-10e$	2	6	-10	-10	-1657000	(s)

Continued on next page.

SPECIES	FORMULA	V	H_2O	e	H^+	ΔG^0 / J mol^{-1}	PHASE
VO_2^+	$V+2H_2O-4H^+-5e$	1	2	-5	-4	-587000	(aq)
VO_3^-	$V+3H_2O-6H^+-5e$	1	3	-5	-6	-783700	(aq)
VO_4^{3-}	$V+4H_2O-8H^+-5e$	1	4	-5	-8	-899100	(aq)
HVO_4^{2-}	$V+4H_2O-7H^+-5e$	1	4	-5	-7	-974900	(aq)
$H_2VO_4^-$	$V+4H_2O-6H^+-5e$	1	4	-5	-6	-1020900	(aq)
H_3VO_4	$V+4H_2O-5H^+-5e$	1	4	-5	-5	-1040300	(aq)
$V_2O_7^{4-}$	$2V+7H_2O-14H^+-10e$	2	7	-10	-14	-1720000	(aq)
$HV_2O_7^{3-}$	$2V+7H_2O-13H^+-10e$	2	7	-10	-13	-1792000	(aq)
$H_3V_2O_7^-$	$2V+7H_2O-11H^+-10e$	2	7	-10	-11	-1864000	(aq)
$V_3O_9^{3-}$	$V+9H_2O-18H^+-15e$	1	9	-15	-18	-2356000	(aq)
$V_4O_{12}^{4-}$	$4V+12H_2O-24H^+-20e$	4	12	-20	-24	-3202000	(aq)
$V_{10}O_{28}^{6-}$	$10V+28H_2O-56H^+-50e$	10	28	-50	-56	-7675000	(aq)
$HV_{10}O_{28}^{5-}$	$10V+28H_2O-55H^+-50e$	10	28	-50	-55	-7708000	(aq)
$H_2V_{10}O_{28}^{4-}$	$10V+28H_2O-54H^+-50e$	10	28	-50	-54	-7729000	(aq)
$VO_2.H_2O_2^+$	$V+4H_2O-6H^+-7e$	1	4	-7	-5	-746400	(aq)
$VO.H_2O_2^{3+}$	$V+3H_2O-4H^+-7e$	1	3	-7	-5	-523400	(aq)

REFERENCES

1. H. Freundlich, *Colloid and Capillary Chemistry*, 589-593, Meuthen (1926).
2. W. Goldie, *"Metallic Coating of Plastics"*, Electrochemical Publication Ltd., Middlesex, England 1968.
3. C. F. Coombs, *Printed Circuits Handbook* (2nd Ed) McGraw-Hill (1979).
4. C. Lea and K. J. Whitlaw, *Trans. IMF*, **64**, 124 (1986).
5. W. R. Brasch, Lea Ronal, Inc. *United States Patent*, **4,681,630** (1987).
6. R. M. Lukes, *Plating*, **51**, 1066 (1964).
7. J. Th. G. Overbeek, *Colloid Sci.*, **1**, 287, Ed. Kruyt, H. R., Elsevier (1952).
8. R. H. Ottewill and R. F. Woodbridge, *J. Colloid Sci.*, **16**, 581 (1961).
9. W. R. Brasch, Lea Ronal Inc., *United States Patent*, **4,681,630** (1987).
10. J. Smidt, *Chem. Ind.*, **54**, 61 (1962).
11. K. Kobayashi, T. Sato and M. Shinichi, *Copper colloidal catalyst bath for electroless coating*, **Jpn. Kokai 23,764** (1986).
12. K. Kobayashi, T. Sato and M. Shinichi, *Copper colloidal catalyst for electroless coating*, **Jpn. Kokai 19,784** (1986).
13. T. Sato, K. Kobayashi and M. Shinichi, *Copper colloidal catalyst solutions for electroless coating*, **Jpn. Kokai 19,782, 23,765, 23,763, 23,762** (1986).
14. T. Sato, K. Kobayashi and M. Shinichi, *Copper colloidal catalyst solutions for electroless plating*, **Jpn. Kokai 19,783** (1986).
15. K. Kobayashi, T. Sato and M. Shinichi, *Colloidal-copper catalyst solution for electroless plating and manufacture thereof*, **Jpn. Kokai 263,972** (1986).
16. J. A. Creighton, M. S. Alvarez, D. A. Weltz, S. Garoff, and M. W. Kim, *J. Phys. Chem.*, **87**, 4793 (1983).
17. H., Hirai, Y. Nakao, and N. Toshima, *J. Macromol. Sci.-Chem.*, **A13(6)**, 727 (1979).
18. H. Hirai, H. Wakabayashi, and M. Komiyama, *Makromol. Chem., Rapid Commun.*, **4**, 1047 (1983).
19. H. Hirai, H. Wakabayashi, and M. Komiyama, *Makromol. Chem., Rapid Commun.*, **5**, 381 (1984).
20. H. Hirai, H. Wakabayashi, and M. Komiyama, *Bull. Chem. Soc. Jpn.*, **59**, 367 (1986).
21. A. C. Curtis, D. G. Duff, P. P. Edwards, D. A. Jefferson, B. F. G. Johnson, A. I. Kirkland and A. S. Wallace, *J. Phys. Chem.*, **92**, 2270 (1988).
22. E. R. Savinova, A. L. Chuvilin and V. N. Parmon, *J. Mol. Catal.*, **48**, 217 (1988).
23. F. Basolo and R. G. Pearson, *Mechanisms of Inorganic Reactions: A Study of Metal Complexes in Solution*, Wiley, New York (1967).

24. Lord Rayleigh, *Phil. Mag.*, **47**, 375 (1899).
25. G. Mie, *Ann. Physik*, **25**, 377 (1908).
26. M. Kerker, *The Scattering of Light and other Electromagnetic Radiation*, Academic Press, New York (1969).
27. I. S. Radchenko and M. E. Fonkich, *Opt. Spectrosc.*, **26**, 118 (1969).
28. G. C. Papavassiliou and Th. Kokkinakis, *J. Phys.*, **F.4**, L67 (1974).
29. W. J. Plieth, *J. Phys. Chem.*, **86**, 3166 (1982).
30. T. Berzins, *U. S. Patent* **3,045,334** (1962).
31. H. G. McLeod, *U. S. Patent* **3,045,334** (1962).
32. G. O. Mallory, *Plating*, **April**, 319 (1971).
33. M. Lelental, *J. Electrochem. Soc.*, **120 (12)**, 1650 (1973).
34. M. Lelental, *J. Catalysis*, **32**, 429 (1974).
35. R. E. McCoy and S. H. Bauer, *J. Amer. Chem. Soc.*, **78**, 2061 (1956).
36. G. E. Ryschkewitsch, *Advan. Chem. Ser.*, **42**, 71 (1964).
37. H. C. Kelly, F. R. Marchelli and M. B. Giusto, *Inorg. Chem.*, **3**, 431 (1964).
38. S. V. Sazonova and K. M. Gorbonova, *Elektrokhimiya*, **19(12)**, 1485 (1983).
39. F. London, *Z. Phys.*, **89,** 736 (1934).
40. H. C. Hamaker, *Physica*, **4,** 1058 (1937).
41. J. Gregory, *Adv. Colloid Interface Sci.*, **2,** 396 (1970).
42. D. Tabor and R. H. S. Winterton, *Proc. Roy. Soc., Ser. A*, **312,** 435 (1969).
43. J. Visser, *Adv. Colloid Interface Sci.*, **3,** 331 (1972).
44. V. A. Parsegian and B. W. Ninham, *J. Colloid Interface Sci.*, **37,** 332 (1971).
45. D. H. Everett and J. F. Stageman, *Faraday Disc. Chem. Soc.*, **65,** 230 (1978).
46. P. Debye and E. Hückel, *Physik. Z.*, **25,** 97 (1924).
47. D. C. Grahame, *Chem. Rev.*, **41,** 441 (1947).
48. D. J. Shaw, *Introduction to Colloid and Surface Chemistry*, 3rd. Ed., Butterworths (1980).
49. H. Reerink and J. Overbeek, *Disc. Faraday Soc.*, **18,** 74 (1954).
50. S. S. Dukhin and B. V. Derjaguin, *Surface and Colloid Science*, **7**, 49, E. Matijevic (Ed.), Wiley Interscience (1974).
51. M. von Smoluchowski, *Handbuch der Electrizität und des Magnetismus*, Graetz Vol II, pp. 366, Barth, Leipzig (1921).
52. D. C. Henry, *Proc. Roy. Soc. (London) Ser. A*, **133**, 106 (1931).
53. R. W. O'Brien and L. R. White, *J. Chem. Soc. Faraday Trans. 1*, **74**, 1607 (1978).

54. D. H. Napper, *Polymeric Stabilization of Colloidal Dispersions,* Academic Press (1983).
55. S. Asakura, and F. Oosawa, *J. Polymer Sci.*, **33,** 183, (1958).
56. S. Fukushima and S. Kumagai, *J. Colloid Interface Sci.*, **42(3)**, 539 (1973).
57. V. T. Crowl and M. A. Malati, *Trans. Farad. Soc.*, 301 (1966).
58. D. H. Napper, *J. Colloid Interface Sci.*, **32(1)**, 106 (1970).
59. P. J. Flory, *Principles of Polymer Chemistry*, Ch. 14, Cornell University Press, Ithaca, New York (1953).
60. D. H. Napper, *J. Colloid Interface Sci.*, **33(3)**, 384 (1970).
61. F. Hofmeister, *Arch. Exptl. Pathol. Pharmakol.*, **24**, 247 (1888).
62. H. S. Frank and W. Y. Wen, *Disc. Faraday Soc.*, **24**, 133 (1957).
63. H. Lyklema and T. Van Vliet, *Faraday Discuss.*, **65**, 25 (1978).
64. J. Klein, *Nature*, **288**, 248 (1980).
65. A. G. Ward and A. Courts, *The Science and Technology of Gelatin*, Academic Press (1977).
66. R. Zsigmondy, *Z. Analyt. Chem.*, **40**, 697 (1901).
67. A. M. Kragh and R. Peacock, *J. Photogr. Sci.*, **15**, 220 (1967).
68. A. M. Kragh and W. B. Langston, *J. Coll. Sci.*, **17**, 101 (1962).
69. J. H. De Boer, M. E. A. Hermans and J. M. Vleekens, *Proc. Kon. Ned. Akad. Van Weetns.*, **B60**, 45 (1957).
70. S. S. Baird, *Conference on clean surfaces,* New York Academy of Sciences 869 (1963).
71. V. J. Kulividze, *Kinetica i Kataliz,* **3,** 91 (1962).
72. K. R. Lange, *J. Colloid Sci.*, **20**, 231 (1965).
73. R. Lussow, *J. Electrochem. Soc.*, **115,** 660 (1968).
74. J. A. Hockey, *Chem. Ind.,* 57 (1965).
75. M. R. Basila, *J. Chem. Phys.*, **35**, 1151 (1961).
76. A. C. Zettlemoyer and J. J. Chessick, *J. Phys. Chem.*, **64**, 1131 (1960).
77. O. Groit and J. A. Kitchener, *Trans. Faraday Soc.*, **61,** 1026 (1965).
78. M. P. Aronson and H. M. Princen, *J. Colloid Interface Sci.*, **52,** 345 (1975).
79. B. V. Eremenko, B. E. Platonov, I. A. Uskov and I. N. Lyubchenko, *Colloid J.*, **36**, 218 (1974).
80. L. C. F. Blackman and R. Harrop, *J. Appl. Chem.*, **18**, 37 (1968).
81. H. H. Kellog, *Glass Sci. Bull.*, **2,** 58 (1945).
82. B. Tamamuski and K. Tamamaki, *Trans. Faraday Soc.*, **55,** 1013 (1959).

83. V. I. Lygin and A. V. Kiselev, *Kolloid Zh.*, **23,** 299 (1961).
84. R. K. Iler, C. C. Ballard, R. C. Broge, D. S. St. John and J. R. McWhorter, *J. Phys. Chem.*, **65**, 20 (1961).
85. V. I. Lygin, *Russ. J. Phys. Chem.*, **23,** 250 (1961).
86. C. S. Brookes, *J. Colloid Sci.*, **13,** 522 (1958).
87. A. V. Kiselev, Y. A. Koutetski and I. Clizkek, *Dokl. Akad. Nauk., SSSR*, **137**, 638 (1961).
88. O. Beek, A. E. Smith and W. Wheeler, *Proc. Roy. Soc.*, **A177**, 62 (1940).
89. K. Kimoto, Y. Kamiya, M. Nonoyama and R. Uyeda, *Jap. J. Appl. Phys.*, **2(11)**, 702 (1963).
90. N. Wada, *Jap. J. Appl. Phys.*, **8**, 551 (1969).
91. S. Iwama, E. Shichi and T. Sahashi, *Jap. J. Appl. Phys.*, **12(10)**, 1531 (1973).
92. S. Yatsuya, Y. Tsukaki, K. Mihama and R. Uyeda, *J. Crystal Growth*, **45**, 490 (1978).
93. A. H. Pfund, *J. Opt. Soc. Amer.*, **23**, 375 (1933).
94. H. Akoh, Y. Tsukasaki, S. Yatsuya and A. Tasaki, *J. Crystal Growth*, **45**, 495 (1978).
95. J. L. Marignier, J. Belloni, M. O. Delcourt and J. P. Chevalier, *Nature*, **317**, 344 (1985).
96. J. B. Melville and E. Matijevic, *Foams,* 199-216, Academic Press (1977).
97. D. J. O'Conner and A. S. Buchanan, *Trans. Faraday Soc.*, **52,** 397 (1956).
98. M. C. Fuerstenau and B. R. Palmer, *Flotation - A. M. Gaudin memorial volume,* 148-196, AIME.
99. R. O. James and T. W. Healy, *J. Colloid Interface Sci.*, **40,** 42 (1972).
100. C. I. House and H. L. Shergold, *Trans. IMM,* **93,** C19 (1984).
101. J. O'M. Bockris and A. K. N. Reddy, *Modern Electrochemistry,* 155-158, Macdonald (1970).
102. R. L. Cohen and R. L. Meek, *J. Colloid Interface Sci.*, **55**, 156 (1976).
103. J. Kim, S. H. Wen, D. Y. Jung and R. W. Johnson, *IBM J. Res. Develop.*, **28**, 697 (1984).
104. R. L. Jackson, *J. Electrochem. Soc.*, **135 (12)**, 3172 (1988).
105. Lea Ronal, *Lea Ronal Ronamet*, **Bulletin No. 306000** (1988).
106. R. C. Weast, (Ed.), *CRC Handbook of Chemistry and Physics, 66th Ed.*, D151-158, The Chemical Rubber Co. (1985).
107. U. Bertocci and D. R. Turner in *Encyclopedia of Electrochemistry of the Elements, Vol. II*, A. J. Bard (Ed.), p. 383, Marcel Dekker, New York (1977).
108. S. S. Donovan, *Ph.D Thesis*, Case Western University (1969).

109. P. J. Elving and B. Zemel, *Can. J. Chem.*, **37**, 247 (1959).
110. F. A. Cotton and G. Wilkinson, *Advanced Inorganic Chemistry 3rd Ed.*, Interscience, New York (1972).
111. G. K. Johnson and E. O. Schlemper, *J. Am. Chem. Soc.*, **100**, 3645 (1978).
112. K. Niki and H. Mizota, *J. Electroanal. Chem.*, **72**, 307 (1976).
113. K. Post and R. G. Robins, *Electrochim. Acta*, **21**, 401 (1976).
114. B. Lutz and H. Wendt, *Ber. Bun. Phys. Chem.*, **74(4)**, 372 (1970).
115. J. O. Hill, I. G. Worsley and L. G. Helper, *Chem. Rev.*, **71(1)**, 127 (1971).
116. C. S. Rohrer, O. E. Lanford and S. J. Kiehl, *J. Am. Chem. Soc.*, **64**, 2810 (1942).
117. N. A. Daugherty and T. W. Newton, *J. Phys. Chem.*, **68(3)**, 612 (1964).
118. F. C. Anson and D. M. King, *Anal. Chem.*, **34**, 362 (1962).
119. F. J. Miller and H. E. Zittel, *Anal. Chem.*, **35**, 321 (1963).
120. F. J. Miller and H. E. Zittel, *J. Electroanal. Chem.*, **7**, 116 (1964).
121. D. Cozzi, G. Ciantelli and G. Raspi, *Ric. Sci. Rend.*, **7**, 589 (1964).
122. Y. Israel and L. Meites, *Encyclopedia of Electrochemistry of the Elements, Vol. VII*, Marcel Dekker, New York (1977).
123. Y. Israel and L. Meites, *J. Electroanal. Chem.*, **8**, 99 (1964).
124. W. J. Hamer, M. S. Malmberg and J. Rubin, *J. Electrochem. Soc.*, **103**, 8 (1956).
125. W. J. Bierman and W. K. Wong, *Can. J. Chem.*, **41**, 2510 (1963).
126. T. W. Newton, and F. B. Baker, *J. Phys. Chem.*, **68(2)**, 228 (1964).
127. T. W. Newton, and F. B. Baker, *Inorg. Chem.*, **3(4)**, 569 (1964).
128. J. W. Janus, A. W. Kenchington and A. G. Ward, *Research, Lond.* **4**, 247 (1951).
129. J. E. Eastoe and A. Courts, *Practical Analytical Methods for Connective Proteins*, Ch.6, Spon., London (1963).
130. Malvern, *Zetasizer IIc User Manual*, (1988).
131. E. Matijevic, *Acc. Chem. Res.*, **14**, 22 (1981).
132. D. T. Sawyer, *Experimental Electrochemistry for Chemists*, John Wiley and Sons (1976).
133. R. V. Bucur and L. Stoicovici, *J. Electroanal. Chem.*, **25**, 342 (1970).
134. S. Levine and G. H. Neale, *J. Colloid Interface Sci.*, **47**, 520 (1974).
135. I. S. Radchenko and M. E. Fonkich, *Opt. Spectrosc.*, **26**, 118 (1969).
136. E. G. Shafrin and W. A. Zisman, *Monomolecular Layers*, Washington D. C., A. A. A. Symposium Publications (1954).
137. V. K. LaMer and R. Dinegar, *J. Am. Chem. Soc.*, **72**, 4847 (1950).
138. V. K. LaMer, *Ind. Eng. Chem.*, **44**, 1270 (1952).

139. P. McFayden and E. Matijevic, *J. Inorg. Nuc. Chem.*, **35(6)**, 1883 (1973).
140. L. O. Basil, *Chem. Brit.*, **87**, 210 (1987).
141. I. Ohno, O. Wakabayashi and S. Haruyama, *J. Electrochem. Soc.*, **123**, 2323 (1985).
142. M. Wanner, H. Wiese and K. G. Weil, *Ber. Bunsenges. Phys. Chem.*, **92**, 736 (1988).
143. E. Matijevic, A. M. Poskanzer and P. Zuman, *Plating*, **62**, 958 (1975).
144. W. H. Bauer and E. A. Collins in *Rheology*, Vol. 4, p.423, F. R. Eirich (Ed.), Academic Press (1967).
145. K. Balakrishnan and V. K. Venkatesan, *Electrochim. Acta*, **24**, 131 (1979).
146. S. M. Abd El Haleem and B. G. Ateya, *J. Electroanal. Chem. Interfacial Electrochem.*, **117**, 309 (1981).
147. J. F. Skinner, A. Glasel, L. Hsu and B. L. Funt, *J. Electrochem. Soc.*, **127(2)**, 315 (1980).
148. A. J. Bard and L. R. Faulkner, *Electrochemical Methods, Fundamentals and Applications*, Wiley, New York (1980).
149. W. Albery and M. L. Hitchman, *Ring Disc Electrodes*, Clarendon Press, Oxford (1971).
150. V. D. Parker in *Organic Electrochemistry*, M. M. Baizer (Ed.), p.509, Marcel Dekker, New York (1973).
151. P. M. Gallop, S. Seifter and E. Meilman, *Recent Advances Gelatin and Glue Research*, Ed. G. Stainsby, p.82, Pergamon Press, London (1958).
152. P. Smejkal and P. Blazej, *Kosartsvi*, **19**, 180 (1969).
153. A. W. Kenchington, *Biochem. J.*, **68(3)**, 458 (1958).
154. P. Davis, *Recent Advances in Gelatin and Glue Research*, Ed. Stainsby, G., p.225, Pergamon Press, London.
155. J. E. Eastoe, *Biochem. J.*, **61**, 589 (1955).
156. A. J. Bard, R. Parsons and J. Jordan (Eds.), *Standard Potentials in Aqueous Solution*, IUPAC, Marcel Dekker, Inc., N. Y. and Basel (1985).